USAAMRDL-TR-76-17

(12)

ENGINE EVALUATION OF ADVANCED TECHNOLOGY CONTROL COMPONENTS

Colt Industries Inc.
Chandler Evans Control System Division
West Hartford, Conn. 06101

August 1976

Final Report for Period 7 March 1974 - 1 February 1976

Prepared for

EUSTIS DIRECTORATE
U. S. ARMY AIR MOBILITY RESEARCH AND DEVELOPMENT LABORATORY
Fort Eustis, Va. 23604

EUSTIS DIRECTORATE POSITION STATEMENT

This report contains detailed information on the design and testing of a full-authority electronic control system for turboshaft engines. The information contained in the report and the findings and conclusions cited are considered to be accurate and appropriate to the work conducted. The results of this work will be considered in the planning of any future work related to gas turbine engine control systems.

Roger C. Furgurson of the Propulsion Technical Area, Technology Applications Division served as Project Engineer for this effort.

DISCLAIMERS

The findings in this report are not to be construed as an official Department of the Army position unless so designated by other authorized documents.

When Government drawings, specifications, or other data are used for any purpose other than in connection with a definitely related Government procurement operation, the United States Government thereby incurs no responsibility nor any obligation whatsoever; and the fact that the Government may have formulated, furnished, or in any way supplied the said drawings, specifications, or other data is not to be regarded by implication or otherwise as in any manner licensing the holder or any other person or corporation, or conveying any rights or permission, to manufacture, use, or sell any patented invention that may in any way be related thereto.

Trade names cited in this report do not constitute an official endorsement or approval of the use of such commercial hardware or software.

DISPOSITION INSTRUCTIONS

Destroy this report when no longer needed. Do not return it to the originator.

Unclassified

SECURITY CLASSIFICATION OF THIS PAGE (When Data Entered)

REPORT DOCUMENTATION PAGE

READ INSTRUCTIONS BEFORE COMPLETING FORM

1. REPORT NUMBER: USAAMRDL-TR-76-17	2. GOVT ACCESSION NO.
3. RECIPIENT'S CATALOG NUMBER	
4. TITLE (and Subtitle): ENGINE EVALUATION OF ADVANCED TECHNOLOGY CONTROL COMPONENTS.	5. TYPE OF REPORT & PERIOD COVERED: Final 7 March 1974 - 1 Feb 1976
	6. PERFORMING ORG. REPORT NUMBER
7. AUTHOR(s): T. Morrison, A. H. White	8. CONTRACT OR GRANT NUMBER(s): DAAJ02-74-C-0020
9. PERFORMING ORGANIZATION NAME AND ADDRESS: Colt Industries Inc. Chandler Evans Control System Division West Hartford, Connecticut 06101	10. PROGRAM ELEMENT, PROJECT, TASK AREA & WORK UNIT NUMBERS: 62209A 1F262209AH76 00 024 EK
11. CONTROLLING OFFICE NAME AND ADDRESS: Eustis Directorate U.S. Army Air Mobility Research and Development Laboratory Fort Eustis, Virginia 23604	12. REPORT DATE: Aug 1976 — 179 p.
	13. NUMBER OF PAGES: 178
14. MONITORING AGENCY NAME & ADDRESS (if different from Controlling Office): DA-1-F-2622Ø9-AH-76	15. SECURITY CLASS. (of this report): Unclassified
	15a. DECLASSIFICATION/DOWNGRADING SCHEDULE

16. DISTRIBUTION STATEMENT (of this Report)

Approved for public release; distribution unlimited.

1-F-2622Ø9-AH-76ØØ

17. DISTRIBUTION STATEMENT (of the abstract entered in Block 20, if different from Report)

18. SUPPLEMENTARY NOTES

19. KEY WORDS (Continue on reverse side if necessary and identify by block number)

Engine Electronic Controls, Pumps, Temperature Sensors

20. ABSTRACT (Continue on reverse side if necessary and identify by block number)

This report describes the results of a design, fabrication, bench test, and evaluation of an engine-mounted advanced technology gas turbine engine control system on which development was started under previous Army contracts. The control system comprises a full-authority electronic computer module, a fuel

DD FORM 1 JAN 73 1473 EDITION OF 1 NOV 65 IS OBSOLETE

Unclassified 408 372

SECURITY CLASSIFICATION OF THIS PAGE (When Data Entered)

metering and inlet guide vane actuator module, a high-speed fuel pump and alternator module, a radiation pyrometer for blade temperature limiting, and other required sensors.

The control modules were evaluated on an experimental Army gas turbine engine (STAGG) which was under development at Pratt & Whitney Florida Research and Development Corporation. Tests of the engine-mounted system were conducted in two phases. An environmental phase allowed the control components to be debugged and evaluated over the full power range of the engine while the engine was being controlled by a test stand control system. The second phase of testing demonstrated active control of the engine. All of the engine-mounted control testing was conducted in accordance with the planned engine test schedule on a noninterference basis.

The goal of the control system evaluation program was to accumulate 50 hours of engine-mounted testing. Approximately 44 hours* were accumulated, and about 8.6 of these hours included active engine control. During this testing, all of the control modules were successfully evaluated including the control of engine accelerations, decelerations, speed governing, inlet guide vane scheduling and ignition. Operation of the radiation pyrometer blade temperature limiter was successfully evaluated, but active blade temperature limiting was not demonstrated because the STAGG engine test program ended before this test could be accomplished.

* of engine-mounted testing

PREFACE

The program was conducted under the technical direction of Mr. Roger G. Furgurson, Eustis Directorate, U. S. Army Air Mobility Research and Development Laboratory, Fort Eustis, Virginia. The work was conducted by Colt Industries, Inc., Chandler Evans Control System Division. A. H. White was Program Manager; D. G. Burnell, R. J. Hearn, K. Jankowski, T. Morrison, and R. D. Zagranski were the principal engineers. Mr. D. L. Kitts coordinated the technical activity at Pratt and Whitney Aircraft, Florida Research and Development Center.

TABLE OF CONTENTS

TABLE OF CONTENTS (Cont)

LIST OF ILLUSTRATIONS

LIST OF ILLUSTRATIONS (Cont)

LIST OF ILLUSTRATIONS (Cont)

LIST OF ILLUSTRATIONS (Cont)

LIST OF ILLUSTRATIONS (Cont)

LIST OF ILLUSTRATIONS (Cont)

LIST OF TABLES

INTRODUCTION

During the past several years, Eustis Directorate of the U. S. Army Air Mobility Research and Development Laboratory (AMRDL) has sponsored programs to design, develop and evaluate advanced technology control system components for potential use on future Army free turbine helicopter engines. The goal of the programs was to develop control system technology which offers high potential to alleviate the problems associated with present-day hydromechanical control systems and to have this technology available to reduce the required development during any subsequent full-scale engine development program.

PREVIOUS WORK

Previous research and development work on the program was conducted under Contracts DAAJ02-70-C-0002 and DAAJ02-72-C-C-0084. This effort included the design, fabrication, and bench test of all of the components for a small turboshaft engine based on a twin-engine helicopter application. The work was directed toward developing a complete engine control system including a full-authority electronic computer, a fuel metering system, an inlet guide vane actuator, a high-speed centrifugal fuel pump, a high-speed permanent magnet alternator for supplying control and ignition power, a radiation pyrometer for turbine blade temperature limiting, and other required sensors.

The development work under these contracts successfully demonstrated the capability of the electronic control system and high-speed pump technologies in a simulated engine environment. The work included a complete redesign of the electronic computer to incorporate emerging new technology components, and increasing pump speed for improved efficiency from the initial 37,500 rpm design to a 65,000 rpm configuration. Also, comprehensive evaluation of sensing, actuation and fuel metering concepts were conducted in arriving at the fuel control system component designs.

DESIGN MOTIVATIONS

The full-authority electronic control system concept was selected because it offers the well publicized advantages of lower cost and weight, ease of self-test for improved maintainability, and programming flexibility for rapidly changing engine fuel and geometry schedules to cater to engine development and growth. The high-speed pump and alternator provide minimum weight and size and allow for direct engine drive to eliminate or reduce the size of the engine gearbox. The radiation pyrometer provides for precise temperature limiting control of the gas producer turbine rotor blades. This is a very desirable control feature, because protecting turbine blades from overtemperature is particularly critical to long engine life on advanced, highly stressed, high-temperature gas turbines.

PROGRAM OBJECTIVE AND CONTROL REQUIREMENTS

The objective of the program described in this report was to build a control system based on the technology developed under the previous contracts and to test the system mounted on an engine. The Small Turbine Advanced Gas Generator (STAGG) which was being developed at Pratt and Whitney Aircraft, Florida Research and Development Center (FRDC), under AMRDL contract was chosen for the demonstration testing to minimize the cost of engine operating time. The overall requirements of the control system for operating the STAGG are outlined below. Although the control system demonstration tests on the STAGG were limited to sea level ambient conditions, the control requirements were established based on a modified UTTAS flight envelope, and the control was designed to meet these requirements.

Control Functions	Accuracy
Proportional Gas Generator Speed Governing	$\pm$ 1%
W_f/P_b Start, Acceleration, Deceleration	Start - $\pm$ 2 pph Accel - $\pm$ 4% Decel - $\pm$ 7.5%
Inlet Guide Vane Scheduling (30° full stroke)	$\pm$ 1/2°

Gas Generator Turbine Blade Temperature Limiting	±30°F
Fuel Shutoff	
Minimum and Maximum Fuel Flow Adjustments	
Independent Idle and Maximum Speed Adjustments	
Electronic Power for Control and Ignition	
Fault Isolation	
Fuel Pumping	

Environmental Conditions	Requirement
Engine Inlet Temperature (T_{t2})	-65°F to 165°F
Control System Ambient Temperature	-65°F to 180°F
Vibration in Radial Plane	.001 in., 20 to 1050 Hz (50 g's)
Vibration in Axial Plane	.0001 in., 20 to 1050 Hz
Fuel Contamination	MIL-E-5007C
Fuel Inlet Temperature	-65°F to 135°F
Altitude	0 to 20,000 ft
Inlet Ram Pressure Ratio	1.0 to 1.2

ACCURACY REQUIREMENTS

Control system accuracy requirements were obtained from a survey of engine and airframe manufacturers and reflect requirements of advanced engines presently under development.

The 4% W_f/P_b acceleration limits are based on limiting turbine inlet temperature variation to approximately 100°F consistent with meeting acceleration time requirements and providing adequate surge margin. The deceleration operating limits provide for preventing engine blowout and meeting rapid deceleration time requirements to prevent excessive overspeed when the engine load is suddenly removed. The starting fuel flow limits are required to prevent hot starts or engine hang-ups. The accuracy specified for inlet guide vane scheduling relates to optimizing specific fuel consumption. The limits given are the highest of the accuracy requirements specified by the engine manufacturers that were surveyed. The gas producer governing speed accuracy was based on present-day general practice. The ±30°F turbine blade temperature limits evolved from calculation of the accuracies we could expect to obtain using a radiation pyrometer temperature limiter control mode coupled with the fact that this overall accuracy matched the accuracy of exhaust gas temperature thermocouples (±30°F at 2000°F) which are an indirect method of limiting blade temperature. Therefore, limiting blade temperature to ±30°F offered a significant improvement in protecting the engine from overtemperature.

DESIGN RATIONALE

The selected design concepts were arrived at based on evaluation studies and bench tests which were conducted under previous contracts. A brief summary of the main reasons for choosing the various design concepts and the more critical system components is outlined below.

Fuel Pump

A detail trade-off study was conducted to evaluate gear, vane and centrifugal pumps. The prime motivations for selecting the centrifugal pump were its inherent simplicity, which offers low cost, and its capability to operate at very high speeds and to handle contaminated fuel. This type of pumping system is made possible because the electronic computer eliminates the need for high-pressure servo (servo flow for the IGV actuator is not required below idle speed) flow at starting conditions,

and there was no dry lift requirement because future Army aircraft will have a suction fuel pump system. The disadvantages of the centrifugal pumping system is low efficiency at high turndown flows. But the efficiency improvements made during these programs have made it a viable pumping scheme, and with continued development effort, more improvements may be possible.

Fuel Metering System

The main design considerations in the fuel metering system were in the selection of the main fuel metering valve configuration and the electromechanical interfaces. The sliding plate metering valve was selected because of its capability to handle contaminated fuel and because it is leak free, which is important in metering the small fuel flows required with small gas turbine engines. The contaminant resistant feature of the sliding plate valve is inherent in its wiping action, which keeps metering surfaces dirt free to eliminate wear.

The stepper motor was selected for actuating the metering valve primarily because it can be designed to fail-fixed (i.e., in its last position) if power is lost, and it eliminates the need for a hydraulic servo which would be required for any reasonably sized torque motor or solenoid-operated metering valve. The fail-fixed feature is particularly attractive for flight safety and in considering the implementation of a backup control.

For sensing metering valve position, the resolver was selected because it meets the high accuracy that is required. Also, it is easier to provide the electronic interface with a resolver than an LVDT or digital encoder when operating temperature range is considered. Because of contact wear problems, using a potentiometer is not feasible.

IGV Actuator

Several IGV actuator concepts were evaluated in arriving at the selected electrohydromechanical design concept.

Pneumatic systems were eliminated because bleeding compressor air severely degrades engine performance, and the bleed air is

hot and dirty, which complicates the actuator design. Also, pneumatic systems are bigger than their hydraulic counterpart. Although the pneumatic system has advantages in consideration of vulnerability, working with hot, dirty compressor air degrades reliability.

Electric actuators have the advantage of low cost but were eliminated because of high weight and high electrical power consumption.

The selected IGV actuator design uses a stepper motor and feedback resolver for the same reasons as they were chosen for use in the fuel metering system. Also, the selected design concept offers a simple, almost inherent hydromechanical backup control mode using a pressure speed signal from the centrifugal pump.

Electronic Computer

The concept of providing a special-purpose hybrid computer with all of the scheduling functions implemented with digital technique was selected because it offered the desired flexibility of easily changing schedules by replacing programmable memories, and it makes it possible to use digital and analog techniques where they have advantages. Total analog computer concepts were not feasible because of the difficulty of implementing bivariant functions with analog circuits. A programmable digital computer was considered to be too costly and too sophisticated for the relatively small amount of computation required for a small gas turbine engine control system, since the major portions of the computer are sensing and actuation interfaces.

The electronic computer packaging concept of vibration isolating the PCB's inside the computer housing was selected over external vibration isolation. This was done on the premise that the computer housing would have to be hard mounted to the engine for providing good thermal conduction and because of the hard line connection to the burner pressure sensor.

Pressure Transducers

During the course of the program, several commercially available pressure transducers were evaluated. For the initial system hardware design, a variable capacitor type pressure transducer was selected because at the time, it offered the best promise of meeting accuracy requirements and cost goals, and it easily interfaced with the digital circuits. However, during the development of the STAGG rig demonstration control hardware, a strain gage pressure transducer capable of meeting accuracy and vibration requirements was evaluated. This transducer was selected for the demonstrator control because it was immediately available; whereas work had to be done to package the electronics in the variable capacitance pressure transducer to withstand the specified 50g environment, which was substantially higher than original requirements for which it was designed.

Temperature Sensors

The radiation pyrometer was selected for development because it offered the fastest, most accurate and direct method of sensing the most critical components in the engine hot section. By limiting gas producer turbine blade temperature, the engine is protected from overtemperature due to excessive fuel flow or failure of the turbine blade cooling air due to blockage, etc. Turbine engine temperature limiting concepts using thermocouples or fluidic temperature sensors provide only an indirect method of limiting turbine inlet temperature, and they will not protect against the loss of turbine cooling air.

The compressor inlet temperature thermistor/resistor network probe was selected because it combines a low-cost sensor with a simple means of generating $\sqrt{\theta}$, which is required in some of the engine control modes. The probe generates a variable resistance proportional to the $\sqrt{\theta}$ which conveniently interfaces with the electronic computer.

SYSTEM DESCRIPTION

As indicated in Figure 1, the overall control system includes an electronic computer, a fuel metering/inlet guide vane (IGV) actuator, a 65,000-rpm fuel pump/alternator package, a radiation pyrometer for sensing gas generator turbine blade temperature, a compressor inlet temperature (T_{t2}) sensor, a strain gage type burner pressure (P_b) sensor, a speed sensor which operates from one of the alternator windings, and the associated interconnecting cables. The selected modular configuration was chosen to optimize the installation of the control system on the STAGG and to best implement a possible production configuration. A functional block diagram of the system is shown in Figure 2, and a description of the salient features of each control component is outlined below.

ELECTRONIC COMPUTER

Figures 3 through 6 are photographs of the electronic computer at various stages of assembly. The computer is a hybrid design wherein all of the scheduling functions are implemented using digital circuits to provide the required accuracy and programming capabilities for flexibility in providing scheduling changes. Plug-in 256 eight bit word programmable read only memories (PROM) are secured to the top PCB with metal straps. This provides for ease and speed in changing fuel flow and ITG schedules.

Only a few hours are required to change a PROM program using fairly simple portable programming equipment. There are three PROMs in the control. One contains the acceleration schedule, one contains the IGV schedule, and one stores data used for fault isolation. The fault isolation system operates during each engine start prior to engine light-off by checking the operation of each control loop. One of the lines in the test cable carries the fault indication signal for external display.

The electronic package houses the strain gage pressure transducer and the photovoltaic radiation pyrometer detector. The computer includes three main multilayer printed circuit boards (PCB) and a much smaller double-sided board which contains the

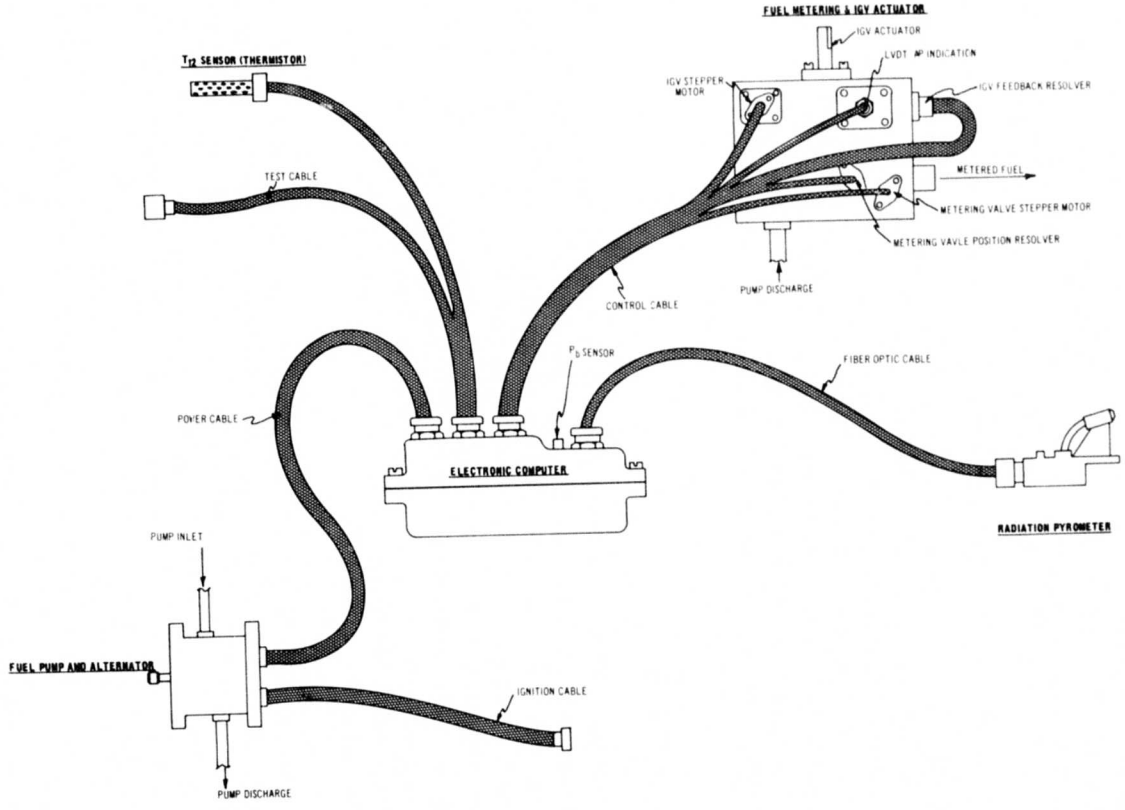

Figure 1. Control System Components

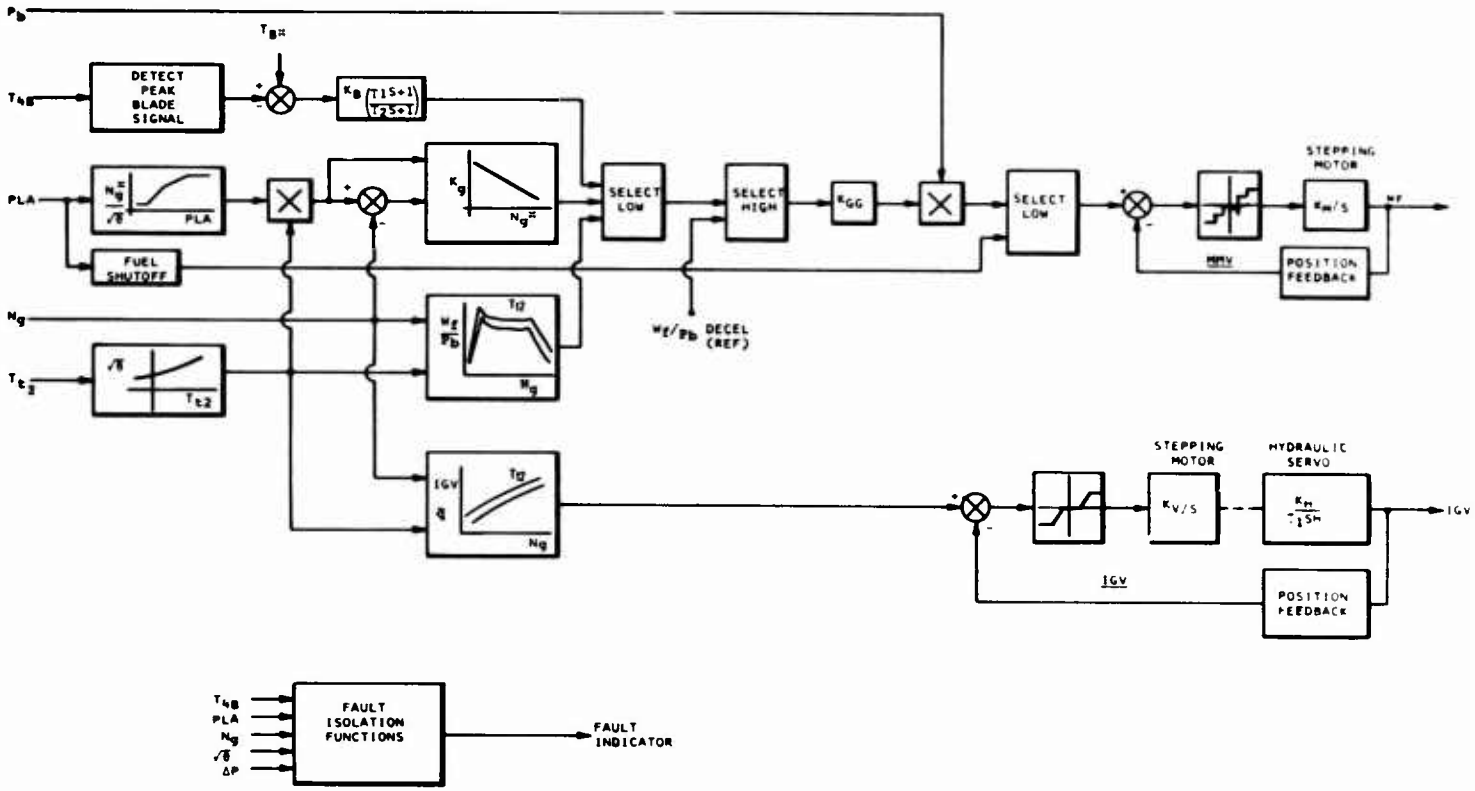

Figure 2. Control System Functional Block Diagram

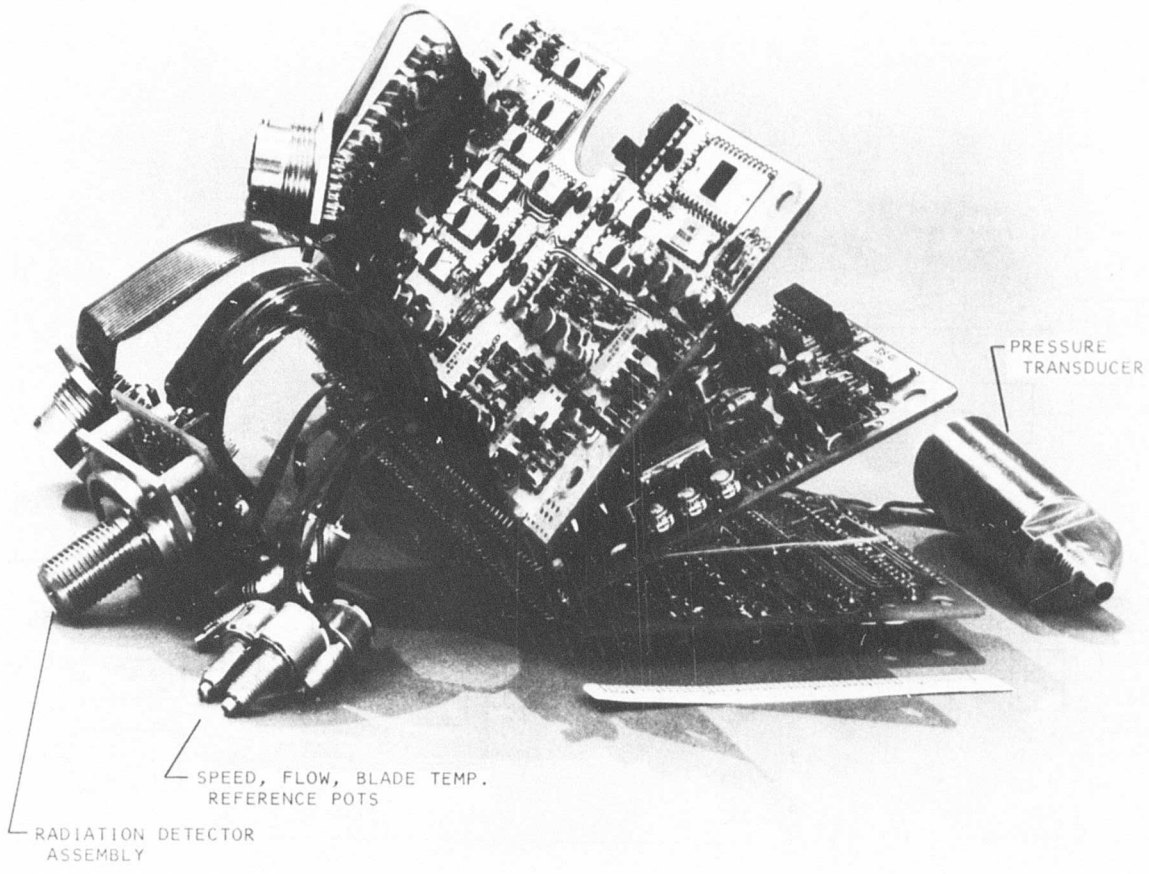

Figure 3. Electronic Computer Disassembled

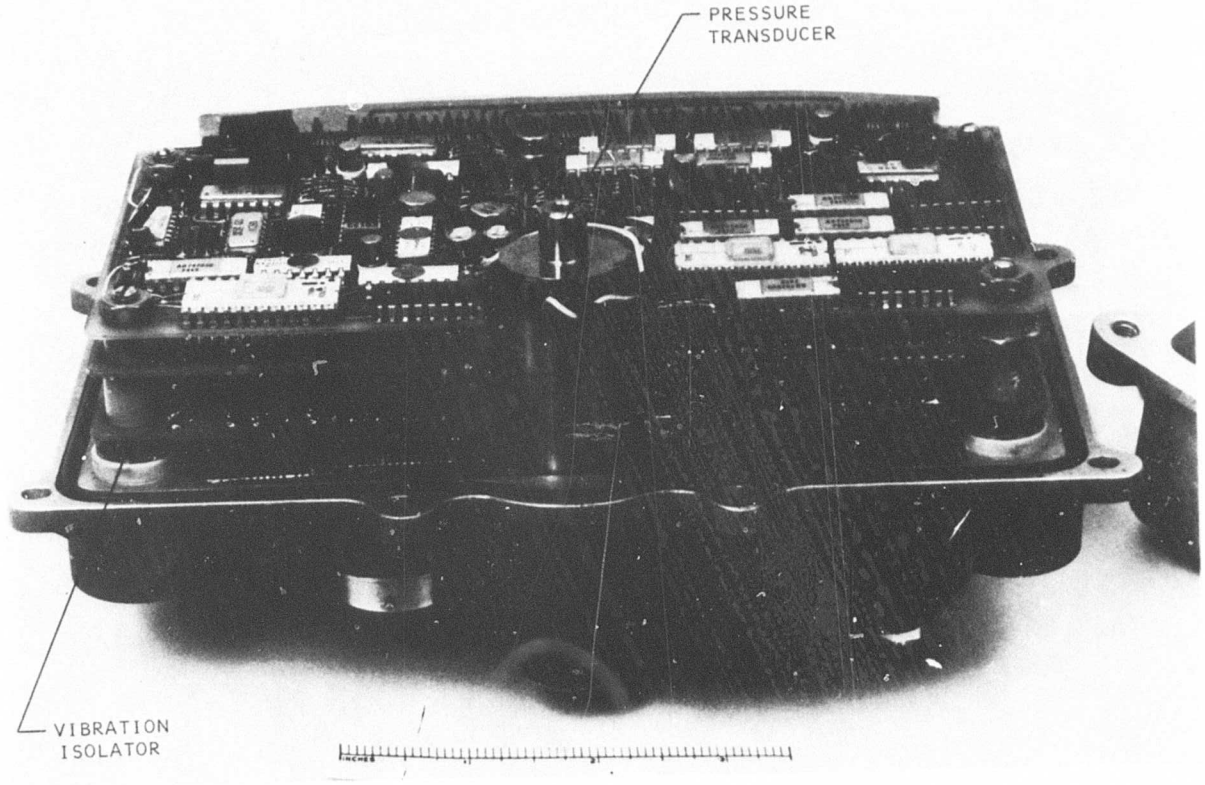

Figure 4. Electronic Computer Assembly (Side View)

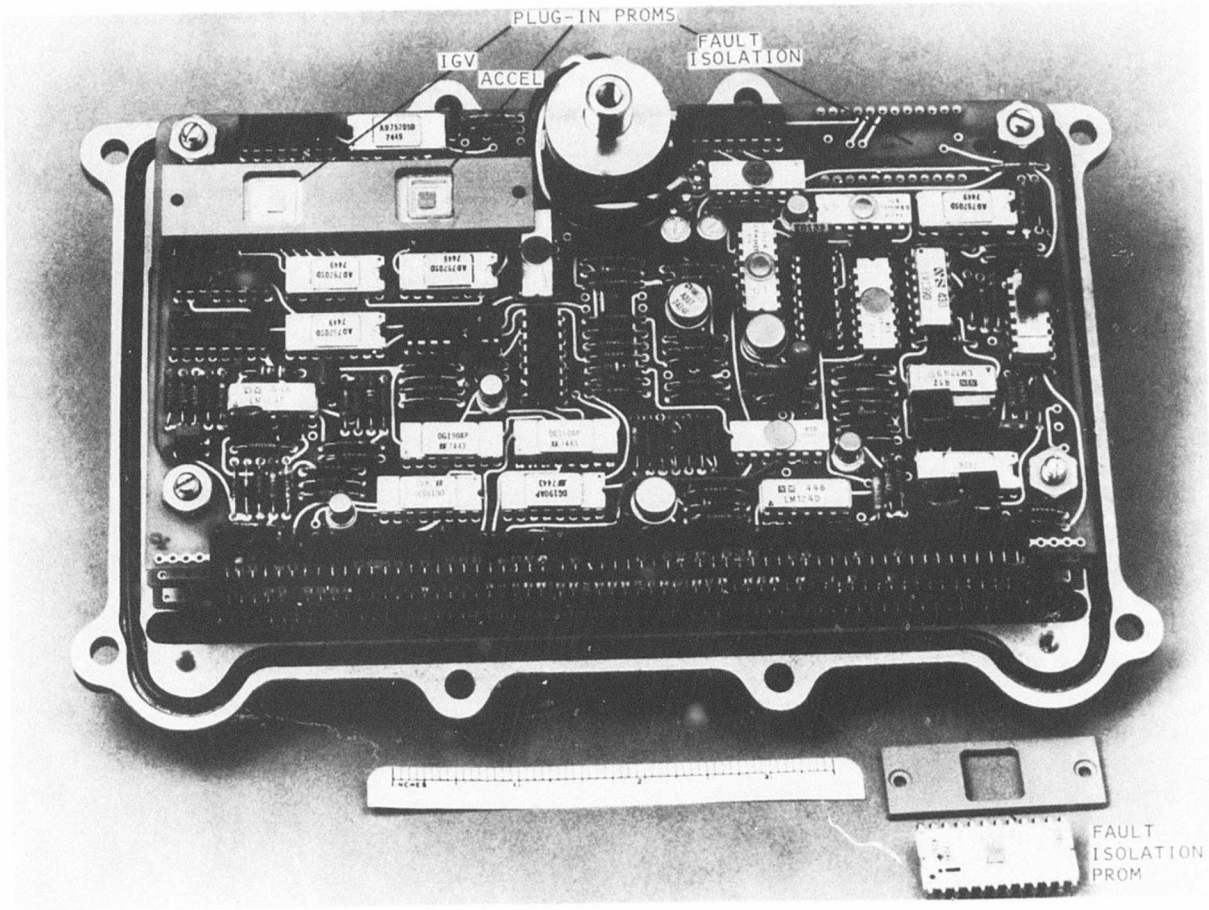

Figure 5. Electronic Computer Assembly (Top View)

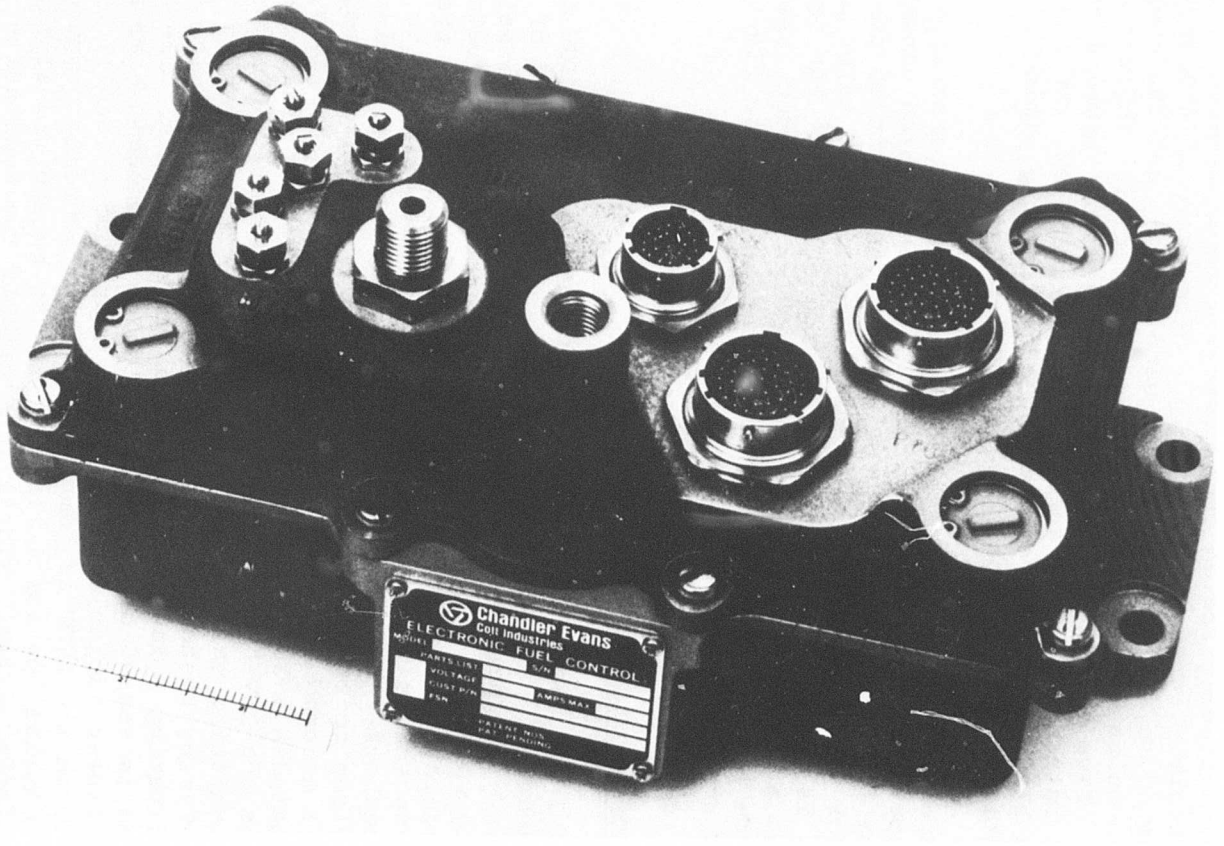

Figure 6. Electronic Computer Module

radiation detector and preamplifier circuits. The PCB and three hermetically sealed connectors are interconnected with two flexible printed circuit cables. The three main boards are mounted on four studs, one at each corner, and the complete computer bolts to the computer housing cover via vibration isolators. Five external potentiometer adjustments provide for setting idle and maximum speed, minimum fuel flow, and maximum turbine blade temperature, and for adjusting the timing of preignition fuel flow for charging fuel lines.

To maintain the electronics at low operating temperature without resorting to fuel cooling techniques, the design concept provides for installation of the computer on the inlet particle separator where ambient temperature is minimum and inlet air cooling is available. Also, the outside surface of the PCBs contains a copper thermal plane which helps to conduct the heat from hot components to the computer housing via flexible braided straps.

FUEL METERING/IGV ACUTATOR

Figures 7 and 8 are photographs of the fuel metering/IGV actuator hardware. The fuel metering section is comprised of a four-phase stepper motor which drives the rotary plate main metering valve, a diaphragm-activated throttling type metering head regulator which maintains an essentially constant pressure drop across the metering valve, and a metering valve position feedback resolver. The electronic computer maintains closed-loop control of metering valve position and thereby controls metered fuel to the engine. The fuel metering system also includes a 3μ barrier flow filter to supply clean servo flow for the IGV hydraulic servo and for washing the metering head regulating valve/sleeve clearance. Fault isolating the fuel metering system is accomplished by sensing metering head and indicating a fault if it exceeds preset limits. The metering head is sensed using a spring-loaded diaphragm which actuates a linear variable differential transformer (LVDT). The signal from the LVDT is compared to the electronic computer to preset nominal operating limits. If the sensed signal exceeds these limits, a fault signal is available for externally indicating that a problem exists in the fuel metering system or the fuel pump.

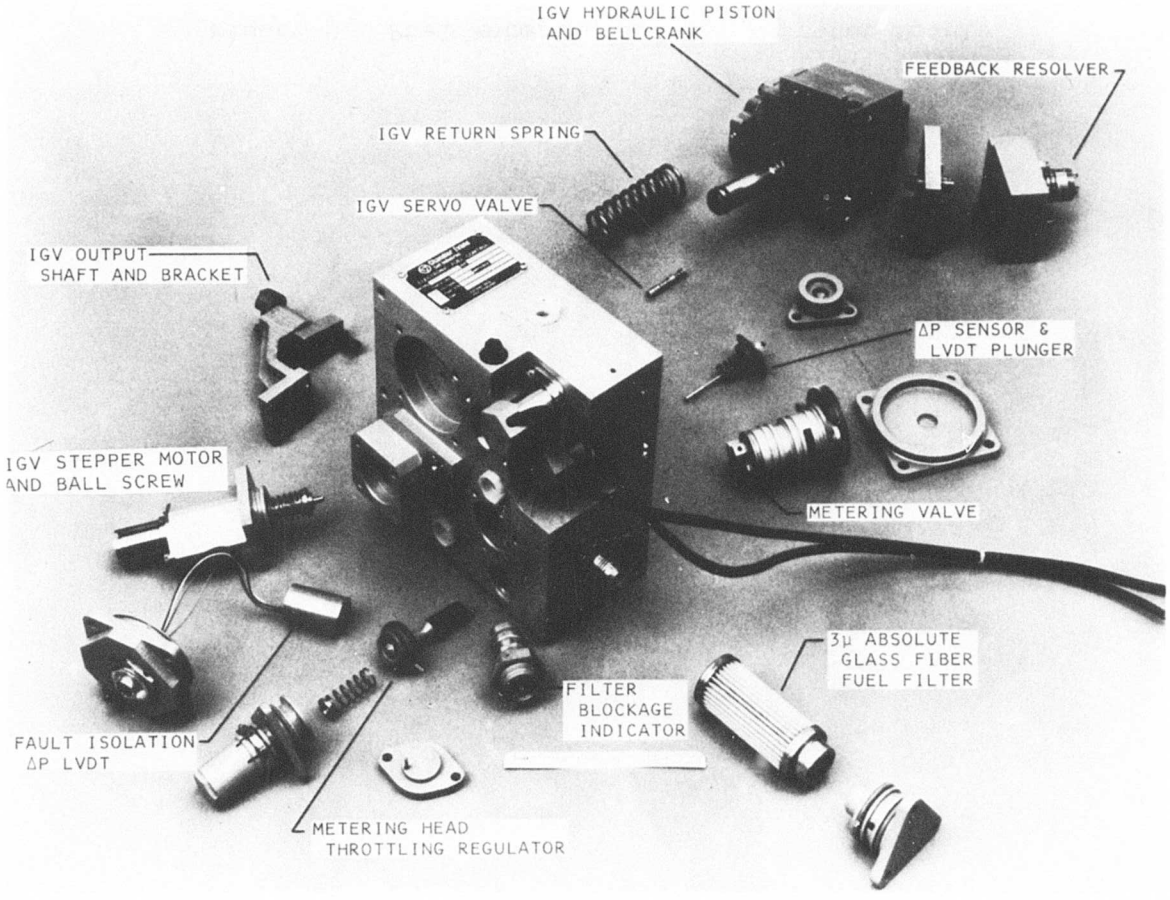

Figure 7. Fuel Metering and IGV Actuator Module Disassembled

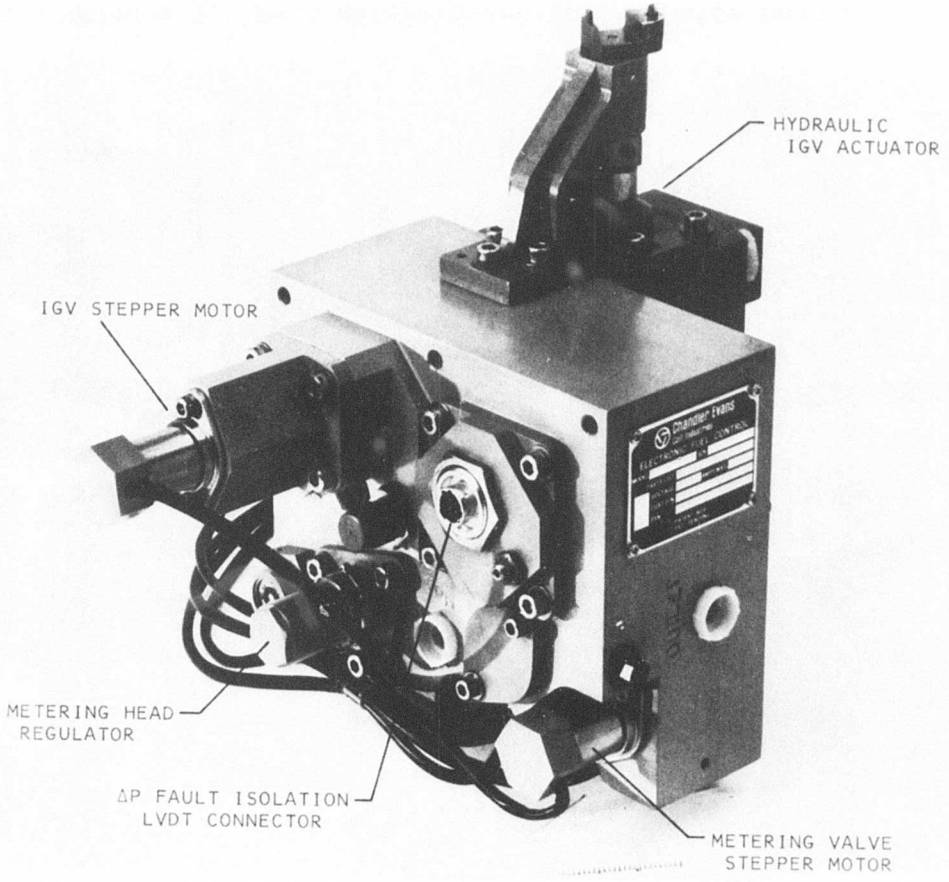

Figure 8. Fuel Metering and IGV Actuator Module

The IGV actuator is comprised of a four-phase rotary stepper motor which operates through a ball screw to translate the hydraulic three-way servo valve. The servo valve controls flow to the unsymmetrical area follow-up piston which rotates the IGVs through a ballcrank. IGV position is fed back to the electronic computer via the resolver for closed-loop control. IGV position is scheduled as a function of N_g and T_{t2}.

FUEL PUMP/ALTERNATOR

Figures 9 and 10 are photographs of the fuel pump/alternator system. The pumping system consists of a centrifugal main stage and a centrifugal boost stage operating back to back on a common drive shaft that is direct driven through the alternator rotor shaft. The main stage is an open impeller design consisting of 14 straight radial vanes. The boost element is a conical inducer and gives the pumping system a .45 V/L capability. The pumping system provides fuel pressurization over the complete engine operating envelope. Elimination of both the dry lift requirement (future Army helicopters will require a separate suction pump) and the need for hydraulic computer flow at engine starting conditions by electronic computation makes this simple dynamic pumping machine possible. The penalty of this simple design is lower overall efficiency as compared to a positive-displacement pump. The payoff is low cost, low sensitivity to fuel contamination, increased reliability, and high speed which makes it possible to eliminate the need for step-down gearing. This particular design operates at engine speed (65,000 rpm).

The alternator rotor utilizes samarium cobalt permanent magnets which, for structural integrity in the high centrifugal g field, are enclosed in a steel hub and an inconel hoop. The rotor runs in a dry cavity to eliminate viscous shear forces which would dissipate several horsepower at design speeds if the rotor were submerged in fuel. Carbon face seals are used to isolate the rotor. The alternator and pump are supported on journal bearings. The bearing and the carbon face seal on the pump of the alternator shaft are fuel lubricated. The bearing and the face seal on the engine side of the alternator are lubricated with engine oil. The alternator stator has six

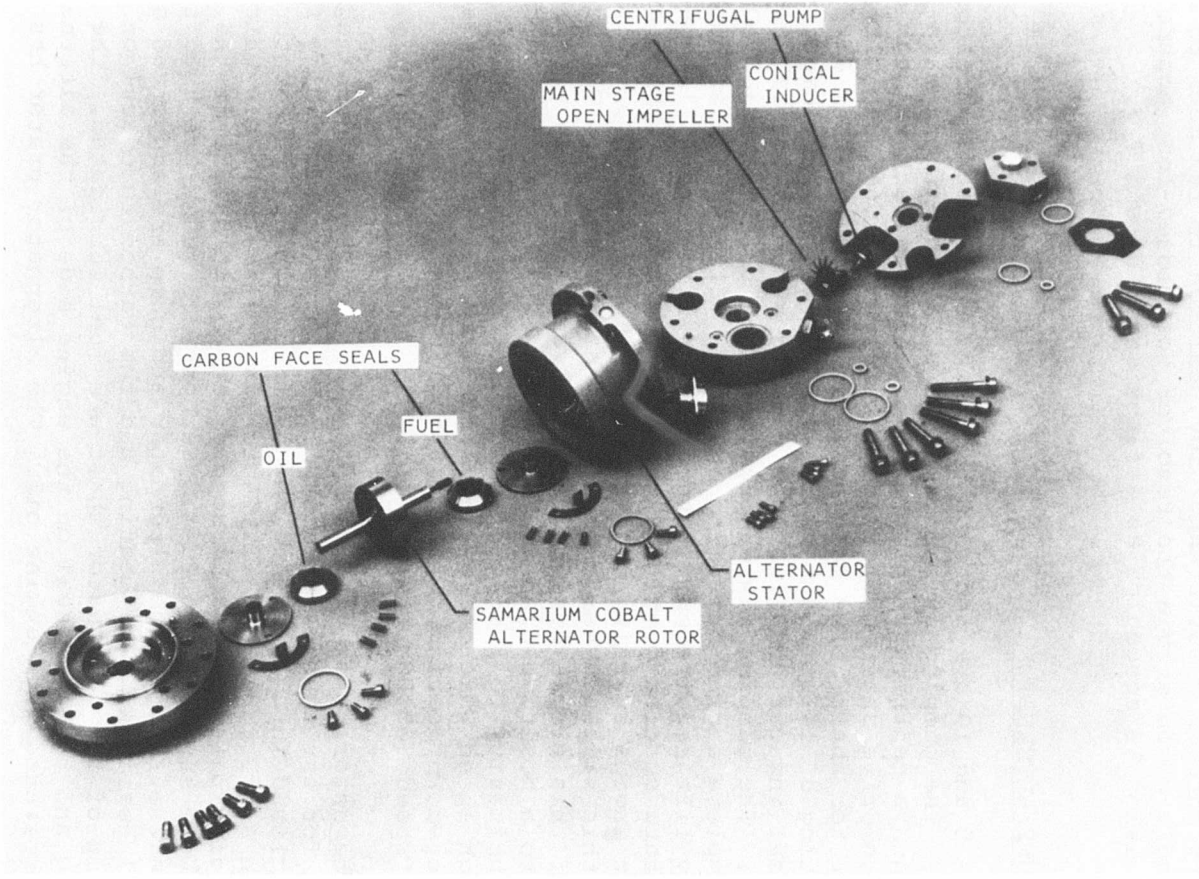

Figure 9. Centrifugal Pump and Alternator Disassembled

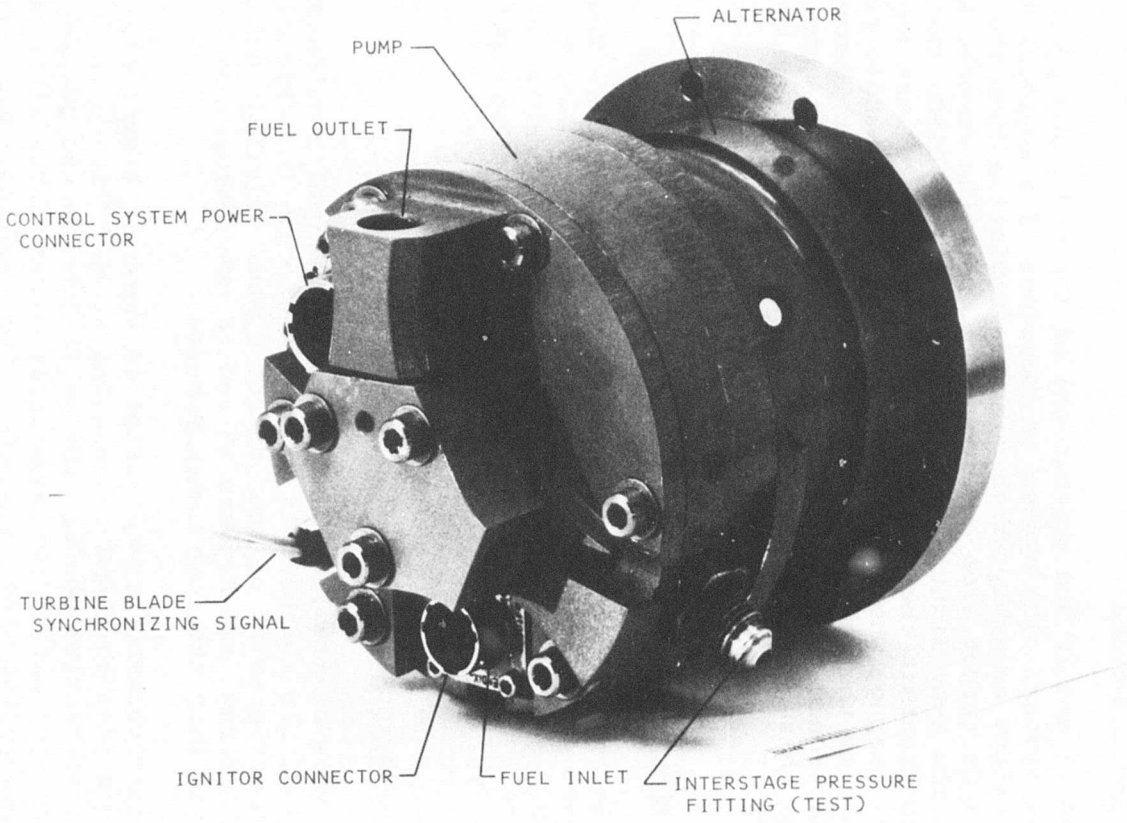

Figure 10. Centrifugal Pump and Alternator Assembly

separate windings, one each for the positive and negative power supply, one each for the two stepper motors, and two for powering the ignition exciters.

RADIATION PYROMETER

Figures 11 and 12 are photographs of the radiation pyrometer optical system. The system is comprised of a sapphire lens and aperture assembly which collects radiation from the turbine blade target area and focuses it onto the armored light pipe. The bent light pipe is required on the STAGG installation to transmit the radiation to the outside of the engine turbine casing, where the flexible fiber-optic bundle picks up and carries the radiation to the silicon detector located in the electronic computer. Purge and cooling air is channeled through passages between the optical elements and the outer shrouds.

INLET TEMPERATURE SENSOR

The inlet temperature sensor is shown in Figure 13. The unit comprises a shrouded thermistor/resistor network which, in conjunction with an electronic operational amplifier in the electronic computer, provides an output voltage proportional to the $\sqrt{\theta}$.

ENGINE INSTALLATION

An overview of the installation of the control modules on the FRDC STAGG rig is shown in Figure 14 through 16. Figure 14 is a schematic drawing of the control system installation on the FRDC STAGG rig, and Figures 15 and 16 are photographs of the STAGG rig with the components mounted.

The pump/alternator installation is shown in Figure 17. The drive provides threaded connections at both the engine shaft and the alternator shaft. The split line in the pump/alternator housing allows for separately mounting the alternator and screwing the shaft into the drive coupling. This arrangement minimizes radial loading at the alternator bearings and eliminates small splines which are difficult to oil-lubricate.

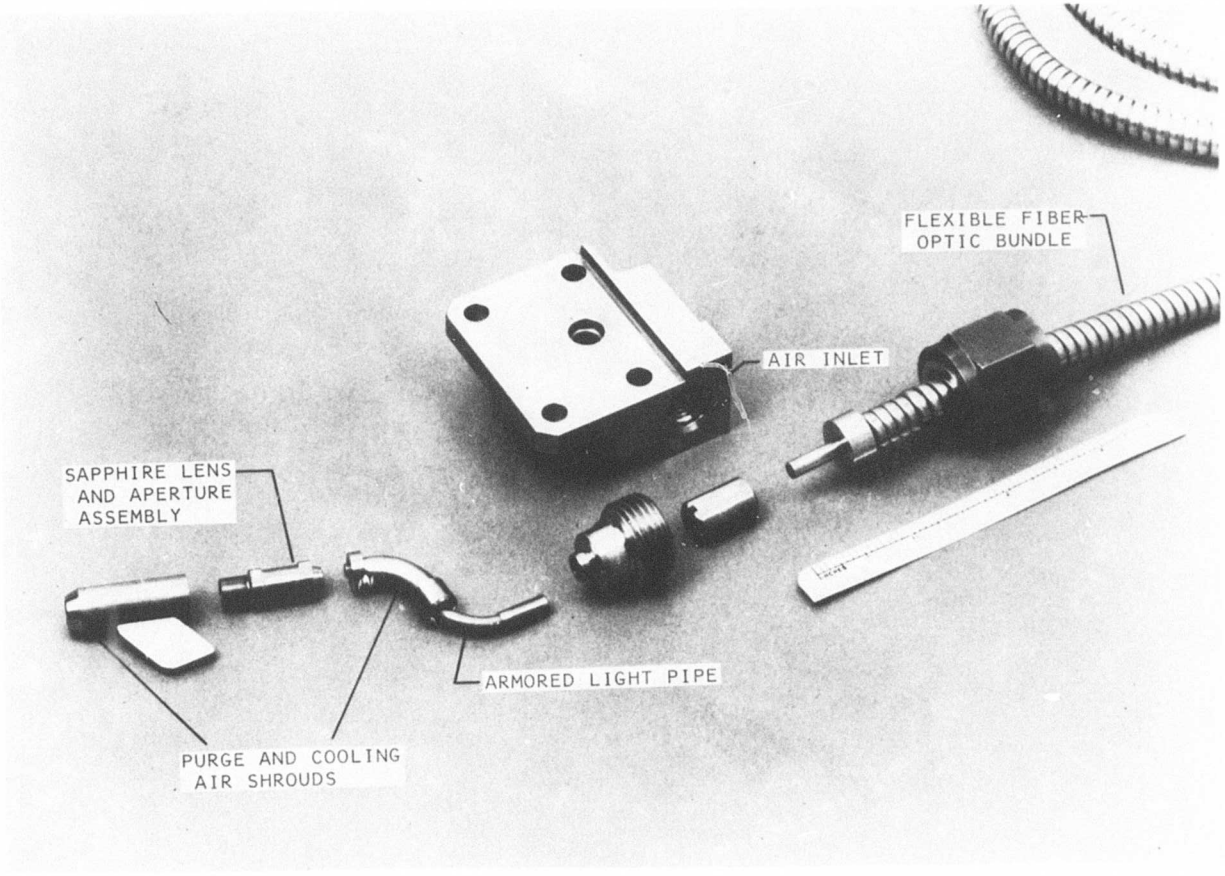

Figure 11. Radiation Pyrometer Optical System Disassembled

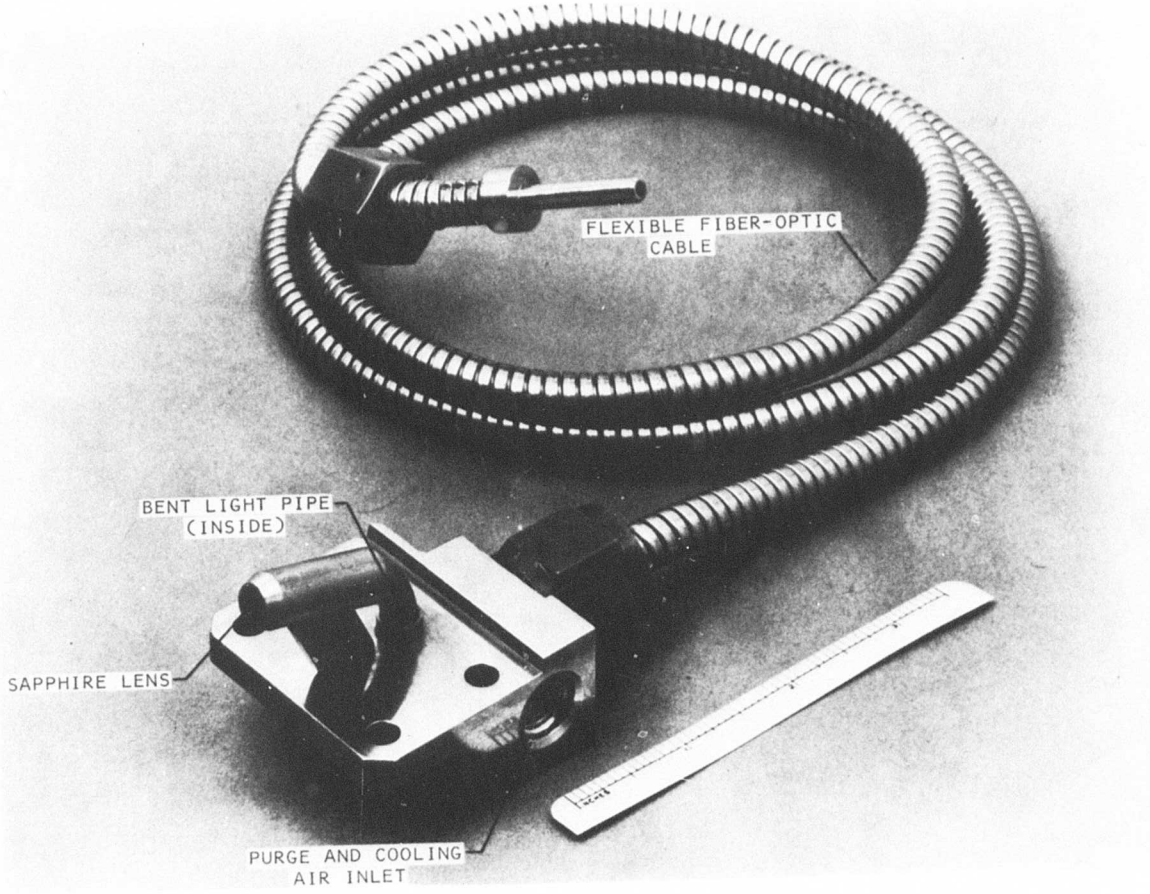

Figure 12. Radiation Pyrometer Optical System

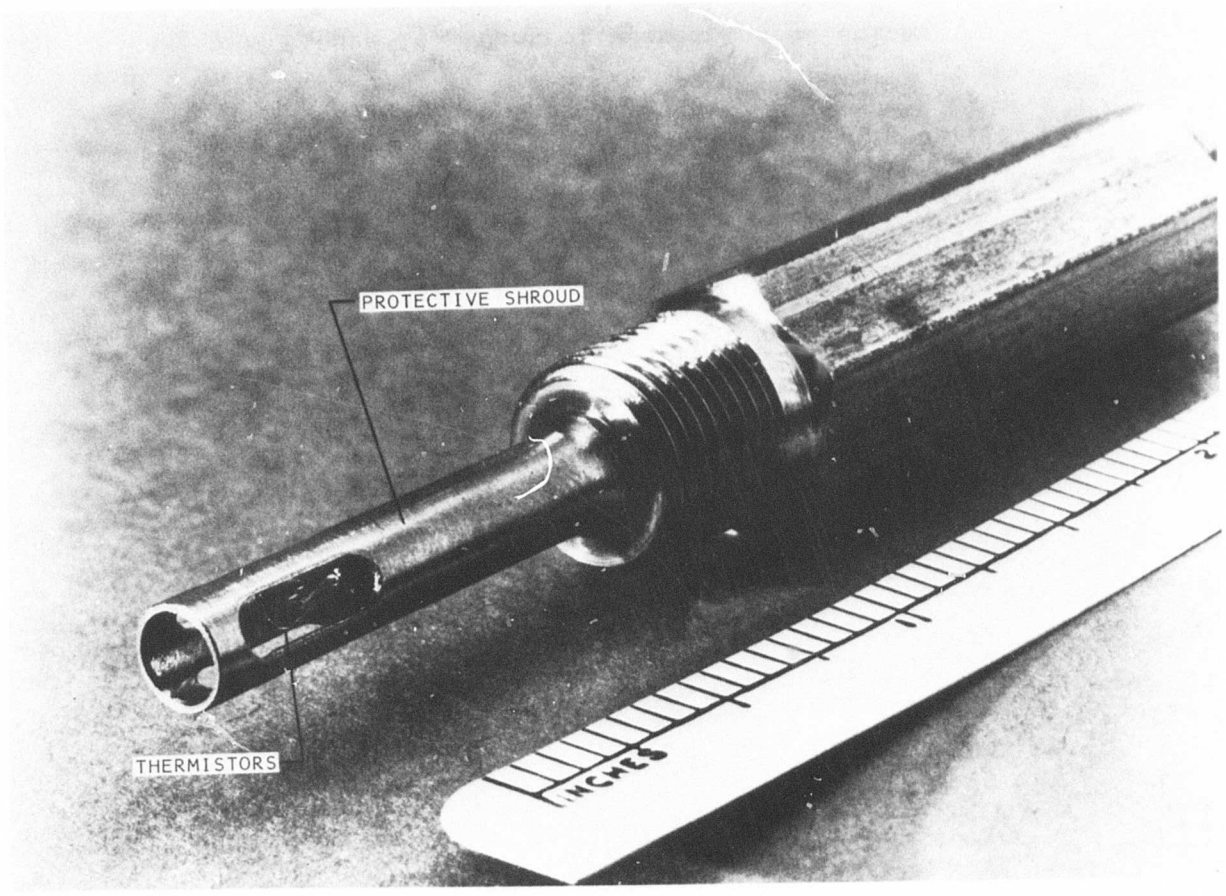

Figure 13. Compressor Inlet Temperature Sensor

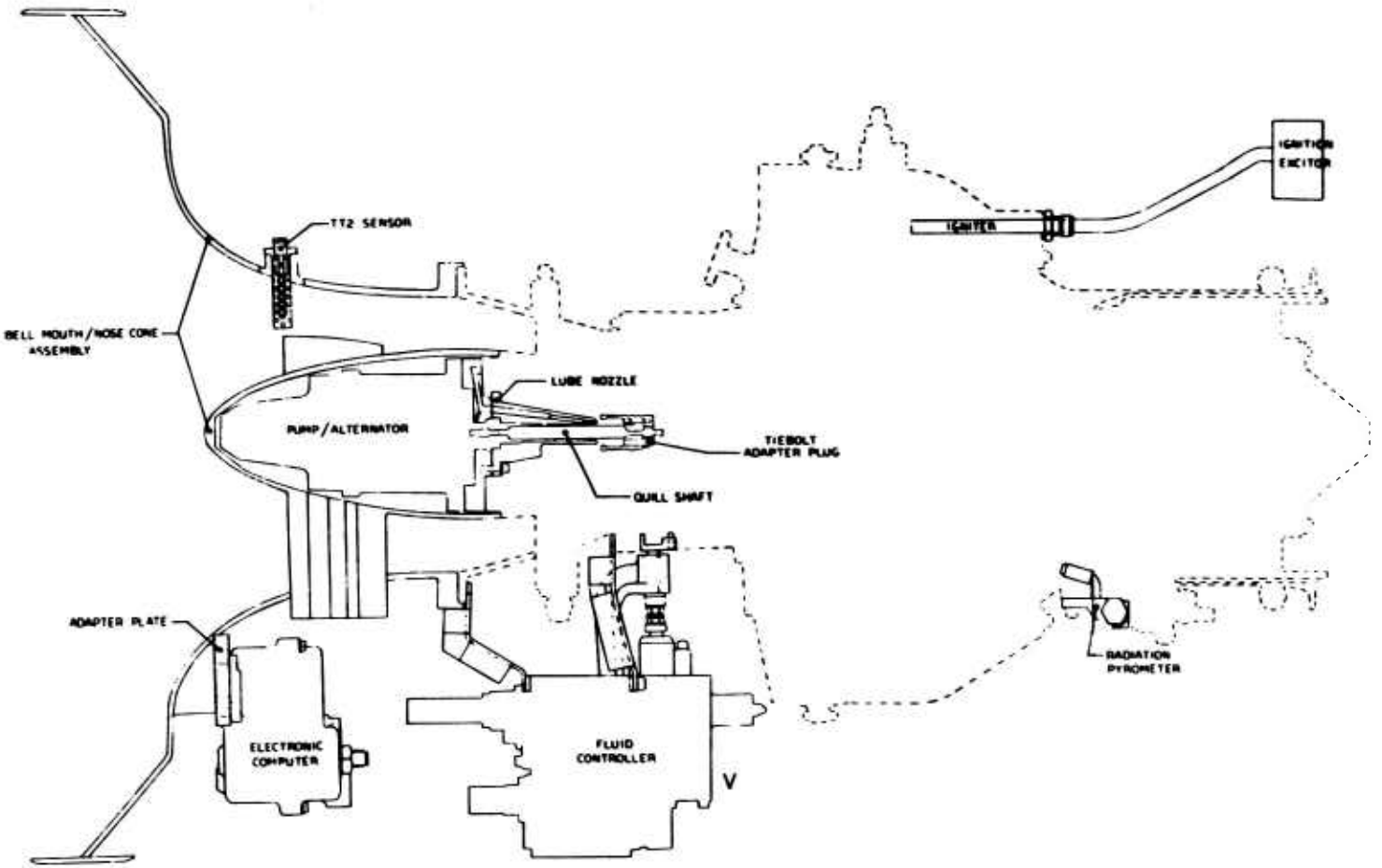

Figure 14. Control System Installation

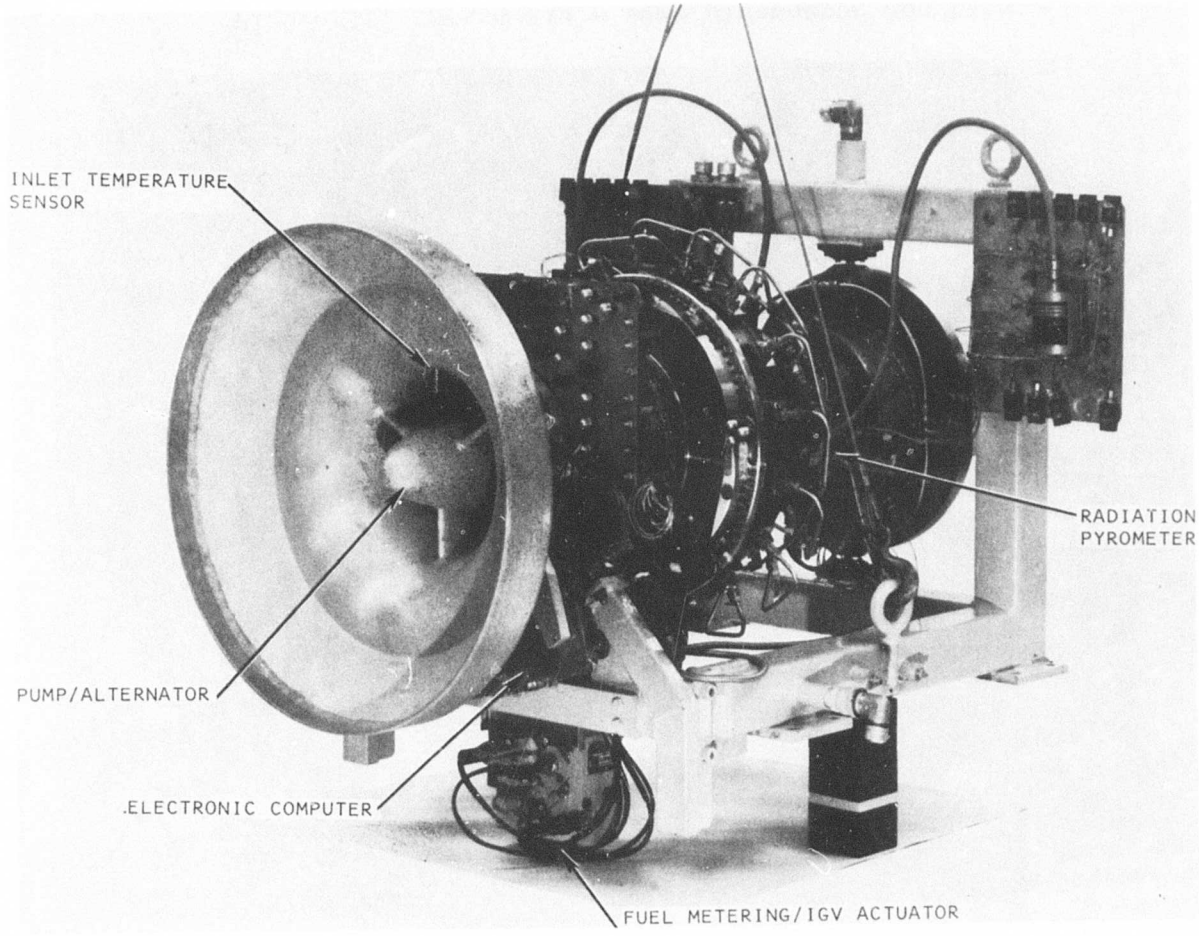

Figure 15. STAGG Rig - Control Mounting

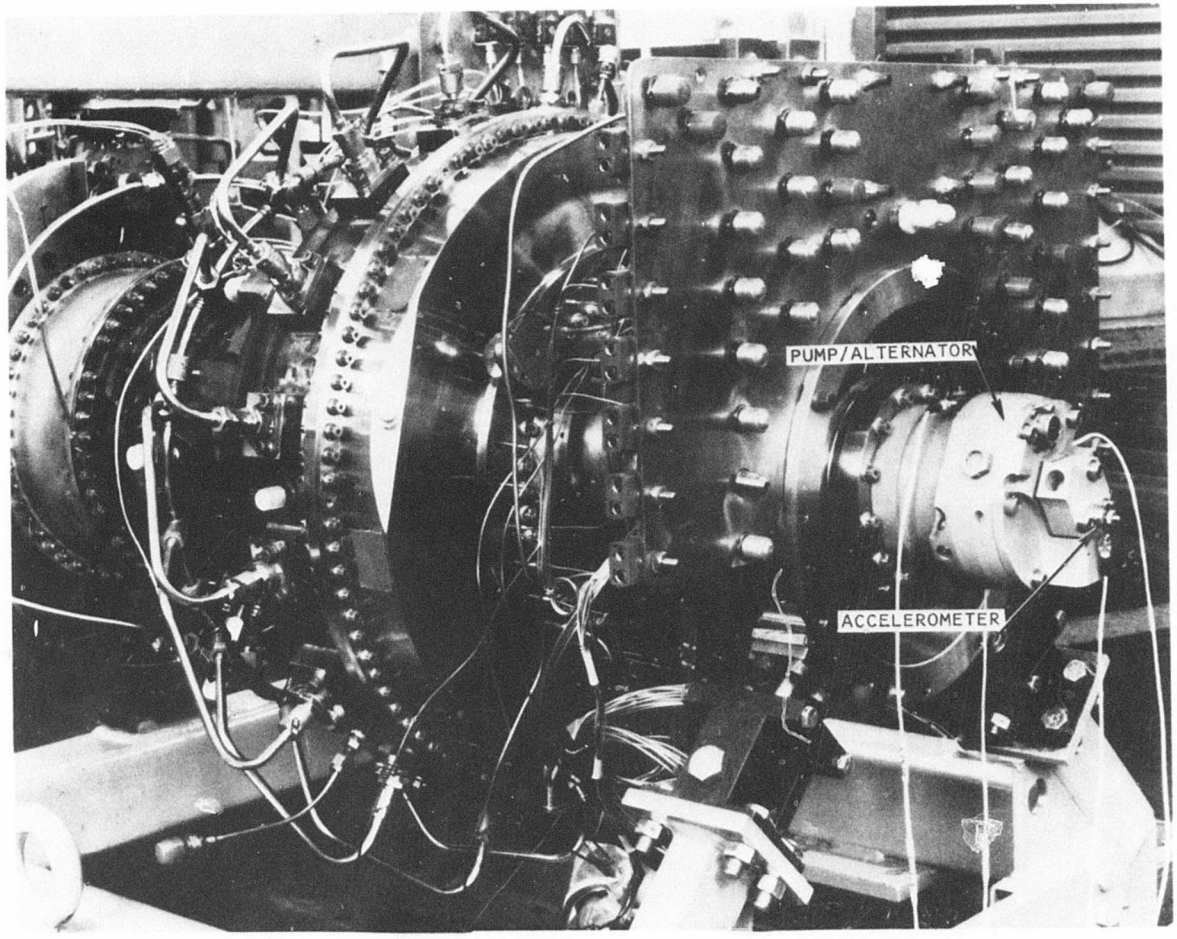

Figure 16. STAGG Rig - Pump/Alternator Mounting

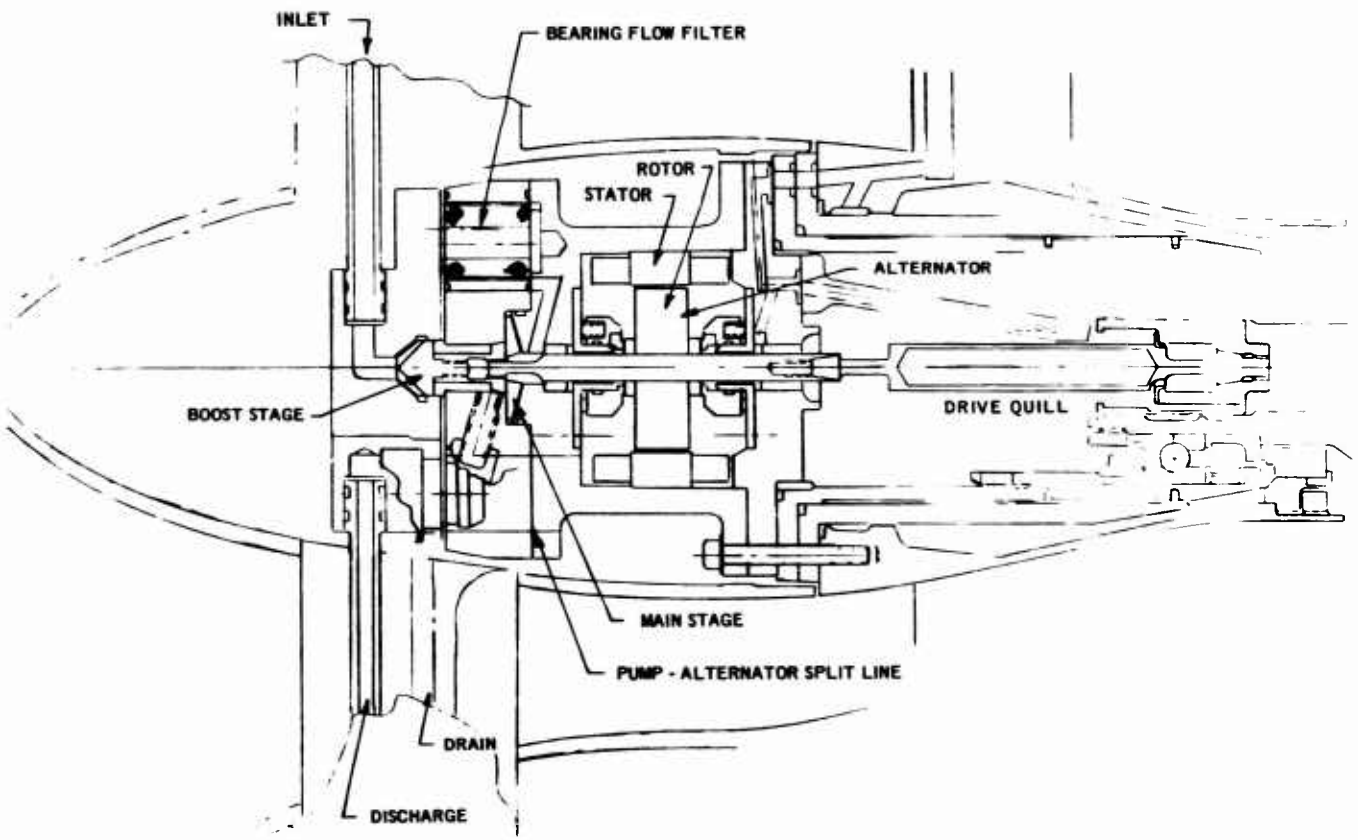

Figure 17. Pump/Alternator - Installation

Fuel lines and electrical cables are brought out through the bell mouth struts. The fuel lines include pump inlet, pump discharge, and overboard drain line. The electrical lines include control system power, ignition, and instrumentation. The electric cable connectors were wired with the cables in the struts, because the connectors are too large to pass through the struts.

The fuel metering/IGV actuator module is mounted on two separate brackets attached to flanges on the STAGG casing. The guide vane drive shaft has been made detachable so that the control may be checked out with the engine and guide vanes being controlled by test bed controls.

To align the axis of the geometry actuator with the axis of the engine actuator drive shaft, shims were used to move the fuel control forward and backward, and clearance bolt holes provided for adjustment in the horizontal plane. A datum adjustment is provided between the actuator and engine guide vane drive to align the fork and pin drive mechanism.

The electronic computer was mounted on an adapter plate which bolted to the bellmouth. The computer was oriented so that the plane of the PCB was in the plane of highest vibration levels. The mounting location reflects what would be recommended for a production installation to take advantage of the lower ambient temperature in the inlet region.

The inlet temperature sensor mounts in a protective shroud as indicated in Figure 14.

Installation of the pyrometer optical system is shown in Figure 18. As indicated, the bent light pipe is required to snake through the engine casing for a clear view of the turbine blade. The thermocouple was used to monitor the temperature of the hood to insure that sufficient cooling air was provided since the unit was located in the hot turbine exhaust area.

ENGINE TEST PROGRAM

The test of the engine-mounted control system was planned and conducted in two phases. For the first phase, which comprised the environmental tests, the control was engine-mounted and operational, but the engine was controlled by a test stand control system. During these tests, the bugs were worked out of the system, and a comprehensive evaluation of each control module, including vibration and temperature monitoring over the full power operating range of the engine, was conducted. The second phase of testing was the active mode wherein the control components were in control of the engine. In both the environmental and active test modes, the control was subjected to engine testing in accordance with the program planned for STAGG evaluation.

During the environmental testing, the IGV actuator was disconnected from the IGV's, and metered fuel flow was returned to the test stand supply system through a pressurizing valve which simulated the backpressure that the control would experience during active testing. For active mode tests, metered fuel flow was ported to the gas generator through the test stand shutoff and dump valve. Provisions in the test stand included the automatic shutting off of the fuel flow dump valve if measured flow exceeded allowable limits or electrical power to the test stand was interrupted. Also, manual fuel shutoff was provided by either power lever or by separate switch closure.

The objective of the engine-mounted control system testing was to accumulate 50 hours of operation to demonstrate the performance and endurance capability of the advanced control components. Approximately 44 hours of testing out of 58 hours of available engine running time was completed with most or all of the components engine mounted. About 8.6 of these hours included active control of engine fuel flow and IGV. Table I summarizes the engine-mounted control system test time that was accumulated during the program. All of this testing was conducted during a 6-week period.

TABLE 1. ENGINE TEST SUMMARY

Bld 3 Run #	Configuration	Controls Time (Hr)	Pump/Alt. Time (Hr)	Comments
Environmental Tests				
36	Controls only	1.61	0	Alternator stator was being replaced because windings were damaged during installation of accelerometers. Diode in test interface box was blown by electrical interference with recording equipment, and this disabled fuel metering control. Performance of fuel metering system was good before diode blew, and electronic computer was good during all tests.
37	Controls only	0.72	0	
38	Controls only	2.35	0	
39	Controls only	0.15	0	
40	Controls only	1.33	0	
41	At CECO	0	0	Control was at CECO for system bench testing with new alternator stator installed.
42	At CECO	0	0	
43	At CECO	0	0	
44	At CECO	0	0	
45	All components installed	4.21	4.21	Fuel pump seals failed due to overheating from cavitation caused primarily by malfunction of IGV actuator servo valve which short circuited the pump. Except for actuator control system malperformance, operation of control system was very good.
46	All components installed	3.79	3.79	
47	At CECO	0	0	Fuel pump seal was replaced and the IGV actuator servo valve was trapped in its sleeve to prevent short circuiting pump.
48	At CECO	0	0	
49	All components installed	5.83	5.83	Performance of control system was very good except that IGV actuator operation was erratic. Analysis of data indicated actuator servo valve was hanging up.
50	All components installed	2.93	2.93	
51	All components installed	1.55	1.55	
52	All components installed	10.80	10.80	Servo valve problem was resolved by wire connecting the servo valve and ball screw. Operation of overall system was very good during the entire run.
		35.27	29.11	
Active Tests				
53	All components installed	8.6	8.6	Active tests successfully demonstrated acceleration/deceleration governing and IGV scheduling. Test data indicated some sticking of metering head regulator. Engine testing was concluded with this run; therefore, closed-loop blade temperature limiting was not demonstrated. However, sufficient open-loop test data was recorded to demonstrate the successful operation of the radiation pyrometer and control system electronic circuits.
	TOTAL	43.87	37.71	

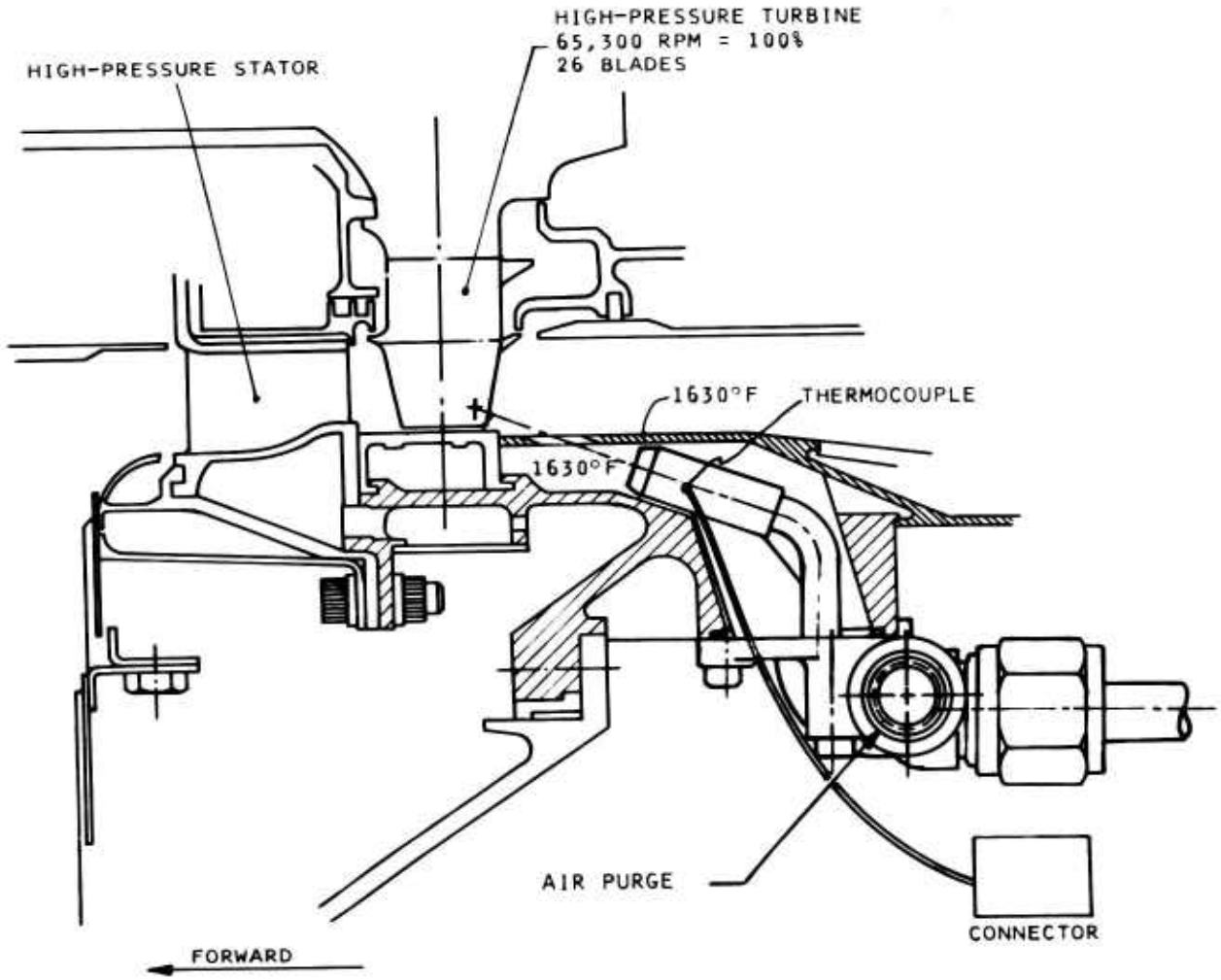

Figure 18. Pyrometer Installation

TEST SETUP AND INSTRUMENTATION

To obtain a comprehensive evaluation of the control system, the components were instrumented as indicated in Figure 19. The test interface box provides for interfacing various control signals for recording and display. The control and test signals available via the test interface box are defined by the test box control panel schematic shown in Figure 20. The control panel outputs the following functions.

DC Readout Select Switch

Enables one of the following control signals to be switched to a common voltage readout.

1.	Computed fuel flow	WCT
2.	The square root of the corrected compressor inlet temperature	$\sqrt{\theta}$
3.	Metering valve resolver position	WAT
4.	Fuel flow pressure ratio computer from the N_g governor	W/PNT
5.	Engine speed	N_gT
6.	Alternator voltage	VAT
7.	Fuel flow pressure ratio computed from the turbine blade temperature limit	W/PTBT
8.	Fuel flow pressure ratio computed from the acceleration limit	W/PAT
9.	Fuel flow pressure ratio selected for control	W/PT

LOCATION	DESCRIPTION
1	PUMP INLET PRESSURE
2	PUMP INLET TEMPERATURE
3	PUMP OUTLET PRESSURE
4	PUMP OUTLET TEMPERATURE
5	PUMP VIBRATION V-AXIS
6	PUMP VIBRATION A-AXIS
7	PUMP VIBRATION H-AXIS
8	PYROMETER SENSOR TEMPERATURE
9	ELECTRONIC COMPUTER VIBRATION (V,A, & H AXIS)
10	FLUID CONTROLLER VIBRATION (V,A, & H AXIS)
11	FUEL FLOW
12	DC VOLTMETER
13	OHMMETER
14	FREQUENCY READOUT
15	X-Y PLOTTER
16	8-CHANNEL "O" GRAPH
17	2-CHANNEL STRIP CHART RECORDER
19	NOSE CONE COMPARTMENT TEMP.
20	ELECTRONIC COMPUTER TEMP.
20	FLUID CONTROLLER TEMP.
21	OSCILLOSCOPE

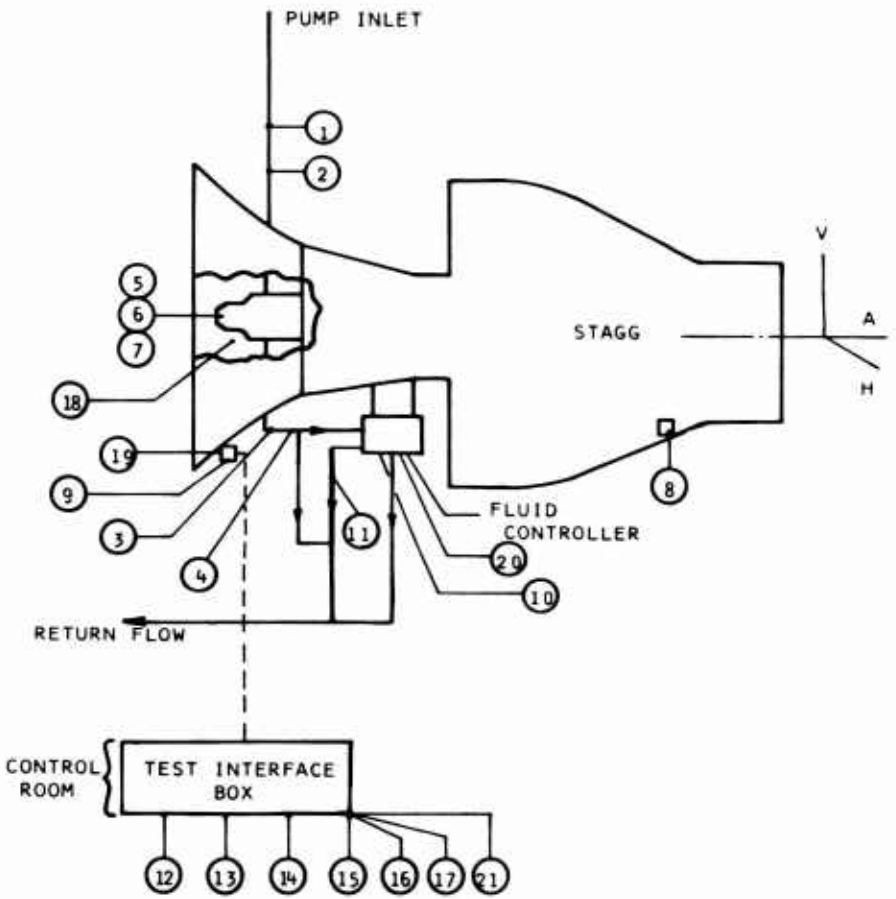

Figure 19. Instrumentation Locations

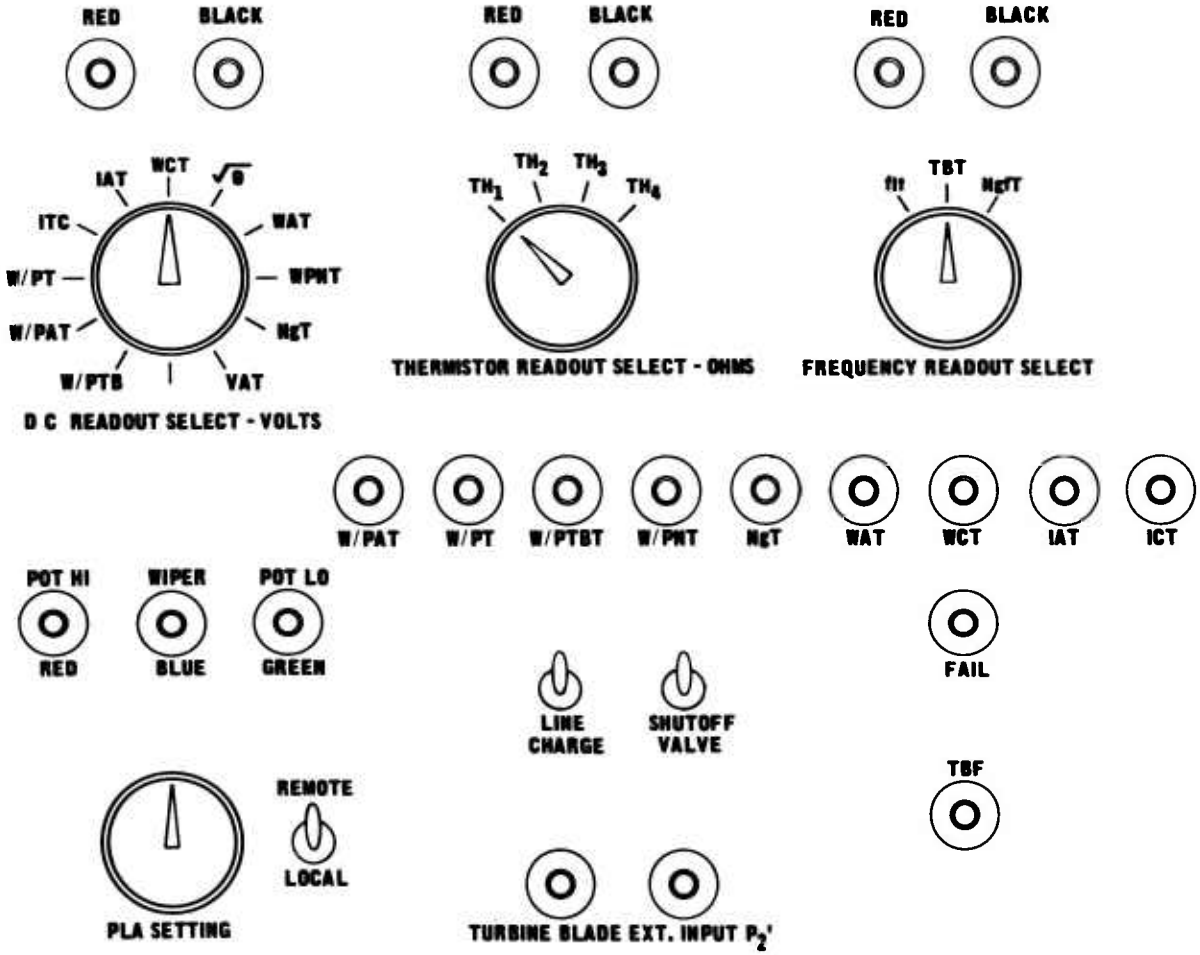

Figure 20. Test Interface Box

10. IGV position computed ICT

11. IGV position from resolver IAT

Thermistor Readout Switch

Enables one of four thermistor outputs to be read on an ohmmeter for monitoring internal temperatures in the electronic control.

Frequency Readout Select Switch

Either the reference crystal oscillator, the turbine blade, or the speed frequency signal can be monitored on the output.

PLA Setting

A single-turn 10KΩ potentiometer located in the test box or the STAGG PLA can be used during demonstration testing. The switch adjacent to the test box PLA provides for the selection of either signal.

Line Charge Switch

When switched to the ON position, the line charge switch will signal the electronic control to open the fuel metering valve for a fixed time interval to allow the fuel lines to be filled.

Shutoff Valve Switch

When switched to the ON position, the shutoff valve switch will actuate the fuel metering valve to the fuel shutoff position. Also, the control will shut off fuel when the PLA is moved to the shutoff position.

Failure Indicator Lamp

The failure indicator lamp will indicate a fault during the fault-isolation test sequence.

TBT Indicator Lamp

The TBT indicator lamp will indicate a loss of signal (frequency) from the radiation pyrometer.

Recording Terminals

Signals available at the DC readout switch are also terminated for monitoring on recording equipment.

ENGINE TEST RESULTS

Evaluation of the control components during all engine testing was based on data readout from the electronic test box together with appropriate measuring and recording equipment. In addition, a turbine flowmeter and a bonded strain gage transducer were used for accurate fuel flow and burner pressure readouts, respectively, and for computing actual fuel flow ratio units (W_f/P_b). Pressure, temperature and vibration instrumentation, located as shown in Figure 19, was used for on-line monitoring of the control components.

Environmental Performance Data

Acceleration/Deceleration

For the environmental phase of testing, although metered fuel returned to the tank, engine burner pressure P_b, engine speed N_g, turbine blade temperature T_{4b}, and inlet temperature T_{t2} were sensed by the control for computing fuel flow and IGV schedules.

All of the fuel flow data during environmental testing was taken with the engine operating at a constant speed. This was done because the fuel supply for the control was also used for the engine test stand control; and during initial testing, inlet pressure fluctuations were recorded when both controls simultaneously requested acceleration fuel flow. Using the test box PLA pot to set the

various fuel flow conditions during engine steady state, did not affect the test stand fuel control system. Therefore, it was possible to simulate acceleration and deceleration commands to the control while the engine remained in a steady-state condition.

Data recorded during various engine runs is shown plotted against the desired schedules in Figure 21. The maximum acceleration error was 0.06 ratio units or 3.3% of point error. This compares to the specified limit of $\pm$4.0%. Figure 22 is the electronic computer fuel flow ratio signal commanded for the same conditions. The maximum error is only 0.5% of point, indicating that the majority of error is in the metering section of the control unit. This is apparent from test data showing metering valve position recorded against fuel flow for the same engine runs as plotted in Figure 23. The deviation from the ideal calibration curve shown (fuel flows of 85 pph to 145 pph) accounts for the indicated acceleration errors of Figure 21. The shift was attributed to a sticky metering valve pressure regulator and substantiated on the bench after engine testing was completed. The sticking was caused by pressure forces squeezing the valve sleeve. The deceleration data, also plotted in Figure 21, showed a maximum error of 5.0%. The specified tolerance for decelerations is $\pm$7.5% of point.

Turbine Blade Temperature Limiting

In an actual application, blade temperature limiting would be set at about 1850°F. However, for demonstration purposes, the limit was set to 1550°F to ensure that the limiting temperature would be exceeded at a nominal engine operating condition. Also, the loop gain was set relatively low to insure that the system would be stable when active modes tests were started. It should be noted that at the lower limiting temperature, the control gain is nonlinear. This is due to the characteristic of the radiation pyrometer detector output.

Figures 24 and 25 show test data recorded during these different engine runs. Figure 24 shows the raw test data plot of fuel flow ratio units versus engine speed and turbine blade temperature. Figure 25 is a replot of this

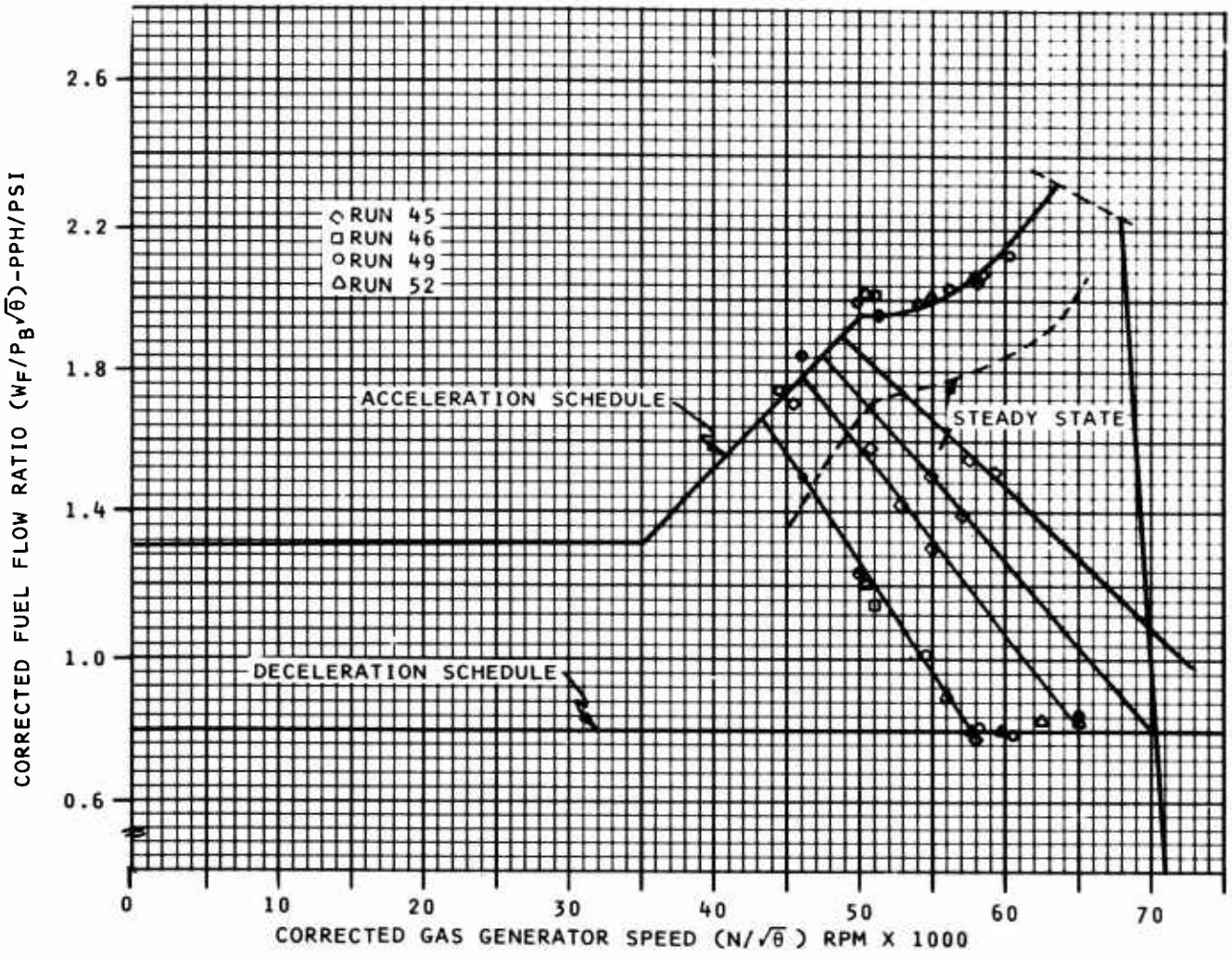

Figure 21. Acceleration/Deceleration Test Data - Environmental Mode

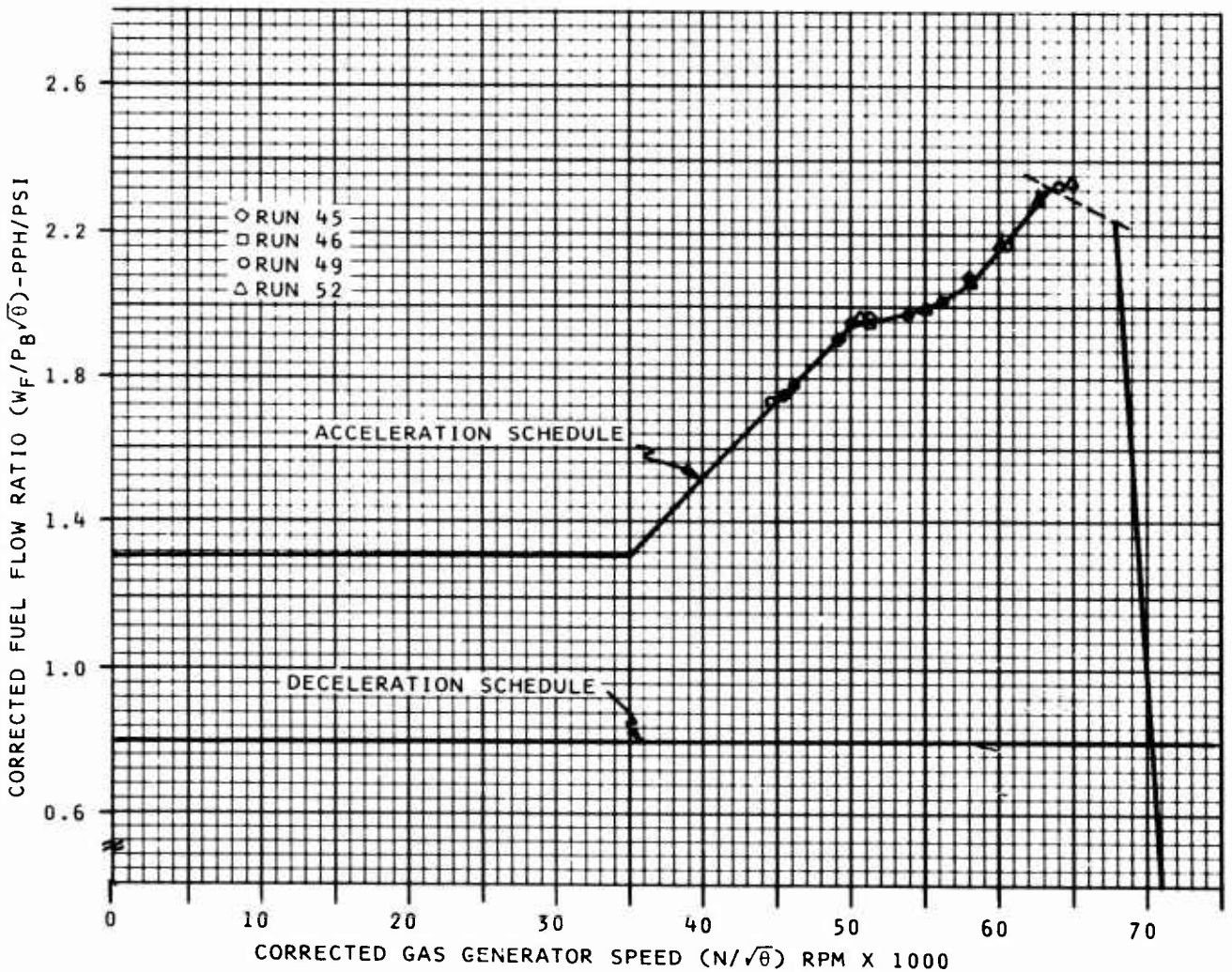

Figure 22. Acceleration Test Data - Electronic Signal - Environmental Mode

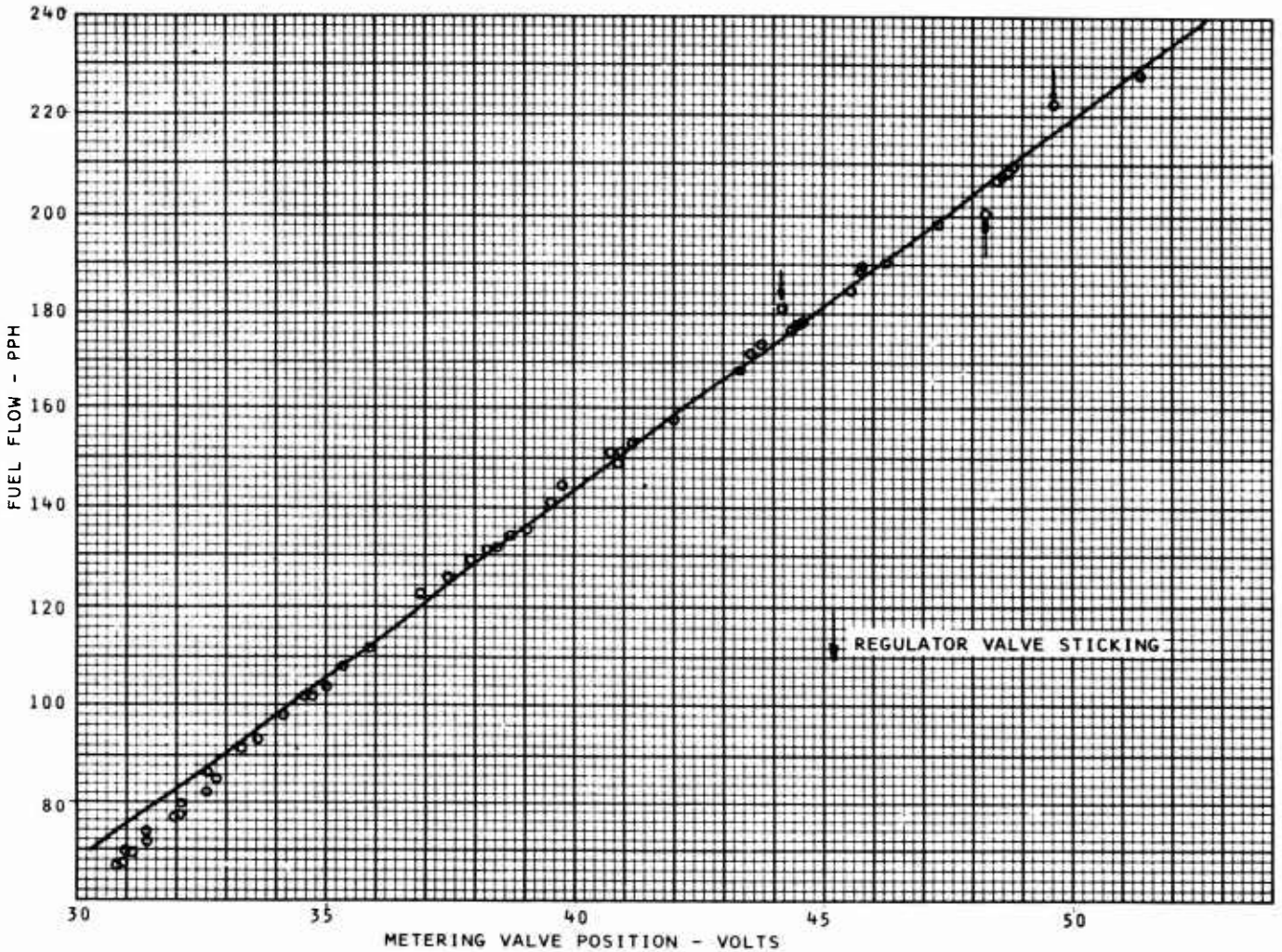

Figure 23. Metering Valve Flow Test Data - Environmental Mode

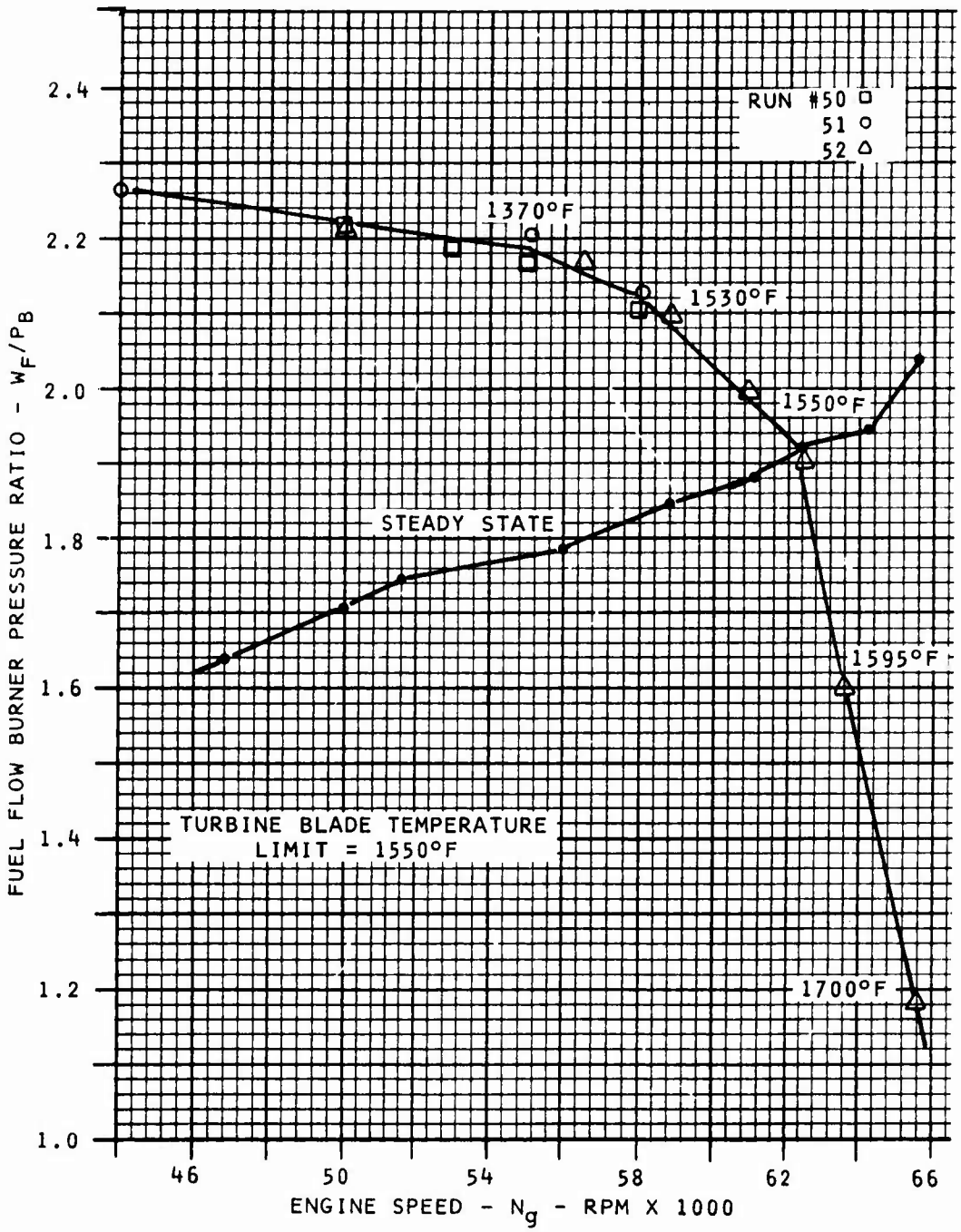

Figure 24. Turbine Blade Temperature Limiting Test Data - Environmental Mode

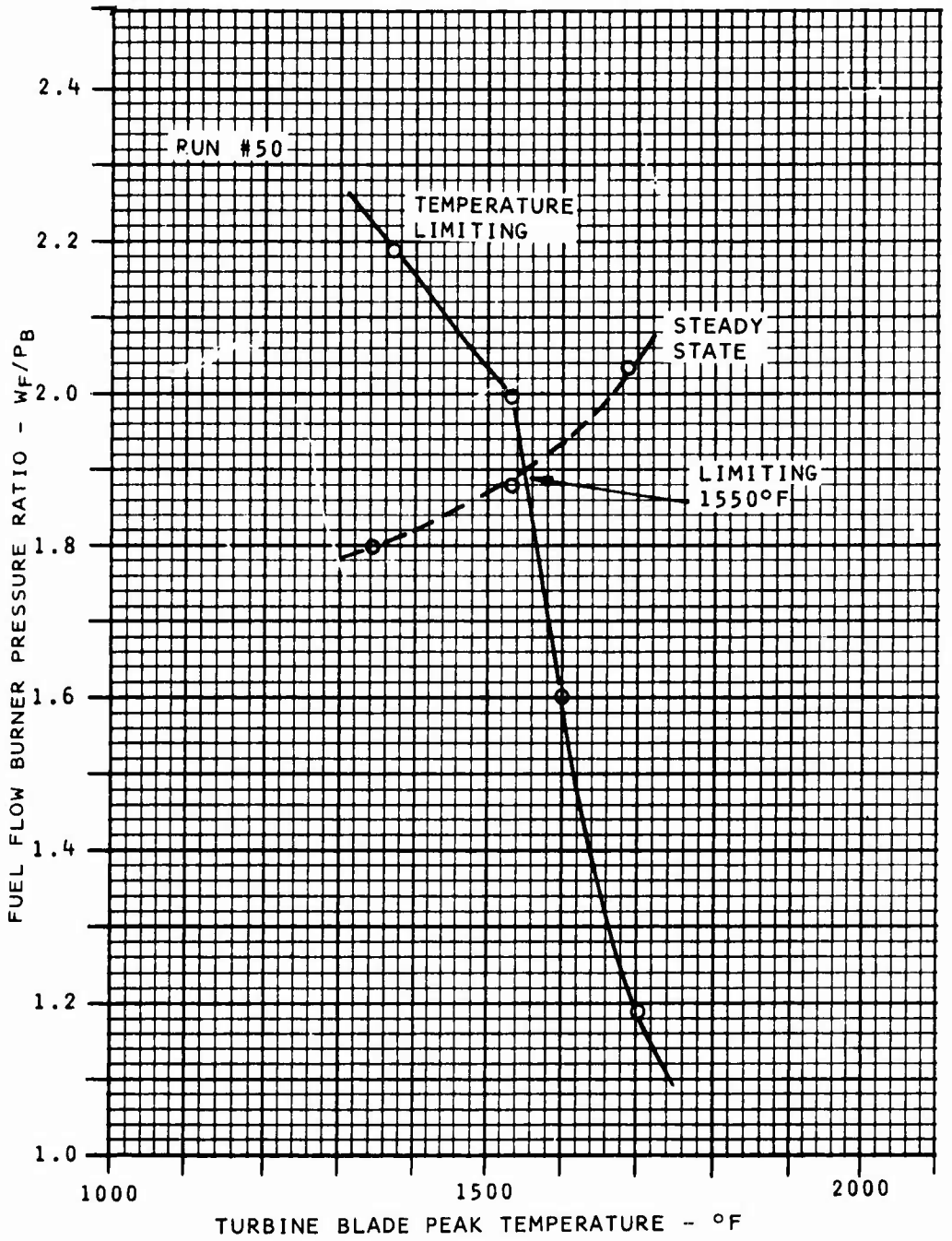

Figure 25. Turbine Blade Temperature Limiting Droop - Environmental Mode

data showing fuel flow ratio versus turbine blade temperature. This data defines the temperature droop characteristics of the blade temperature limiter and duplicates bench test data.

Inlet Guide Vane Control

Initial problems with the inlet guide vane actuator were resolved for the final two engine runs. The results of these runs are shown in the steady-state performance data of Figure 26. Run 52 was a 10-hour demonstration cycle in which the control was in the environmental setup. Thus, the actuator was not connected to the guide vanes. For Run 53 (8-1/2 hours active), the actuator was mechanically coupled to the inlet guide vanes. This data was taken at constant engine speed and is included herein because of the limited environmental data available. The data shown indicates good agreement with the schedule. The largest deviations occur at the slope break points and are primarily due to the error inherent in the digital computation of the function.

Speed Governor

Variations in the engine operating line from original estimates resulted in the variation from the planned power lever schedule shown in Figure 27. However, as this did not deter or limit the use of the power lever in controlling the engine, no attempt was made to compensate in the electronics. The electronic section of the fuel control contains a variable two-segment PLA schedule which can be adjusted to fit the required characteristics. The speed governor droops are shown in Figure 21. As indicated, the control provided a variable gain droop, and engine-mounted test data followed theoretical and bench test performance.

Vibration Requirements

To determine the vibration environment of each control module over the full power range of the engine, accelerometers were mounted as shown in Figure 28. These measurements were made to provide an indication of the vibration levels to expect on future small, high-speed

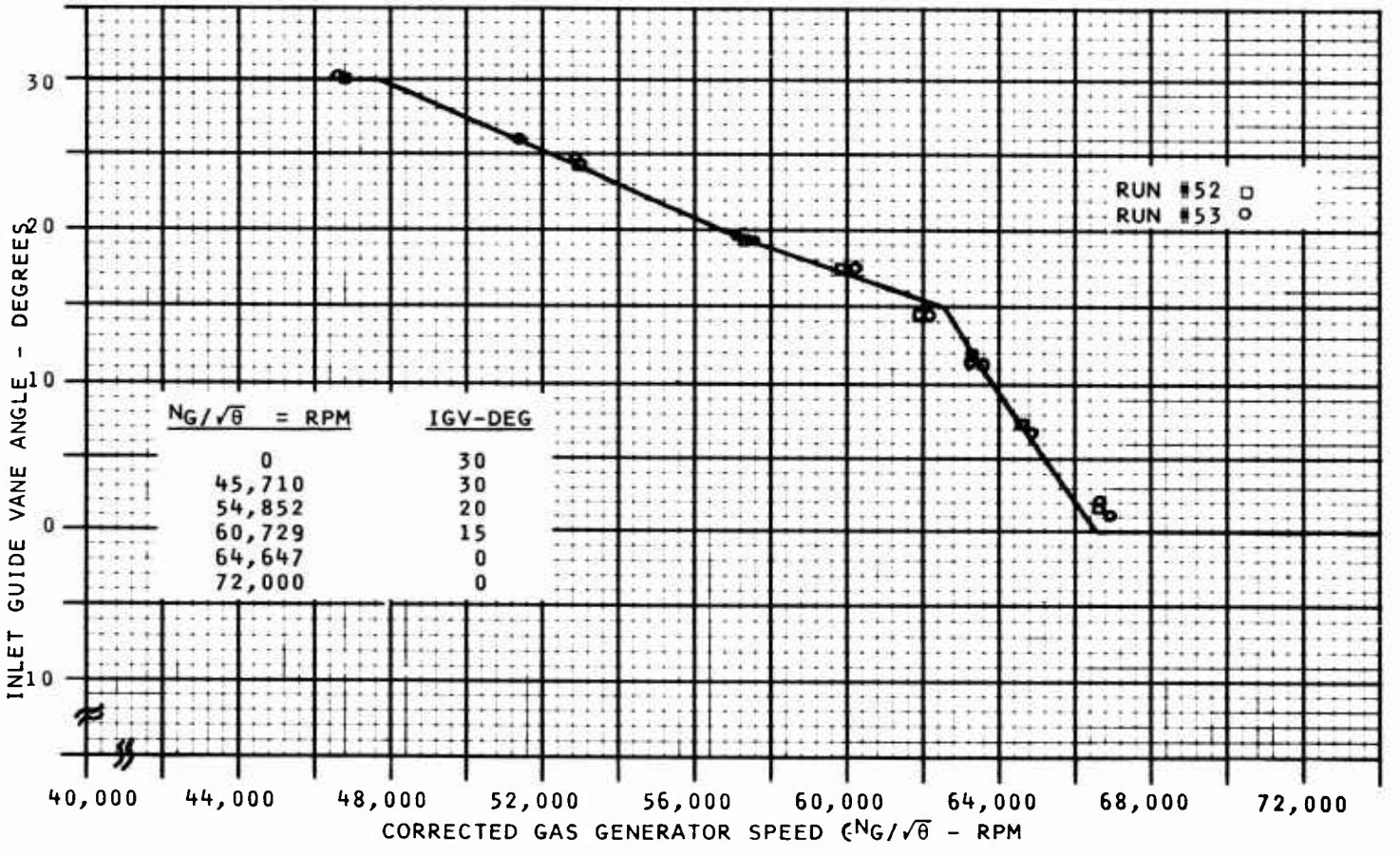

Figure 26. Inlet Guide Vane Test Data - Engine-Mounted Test

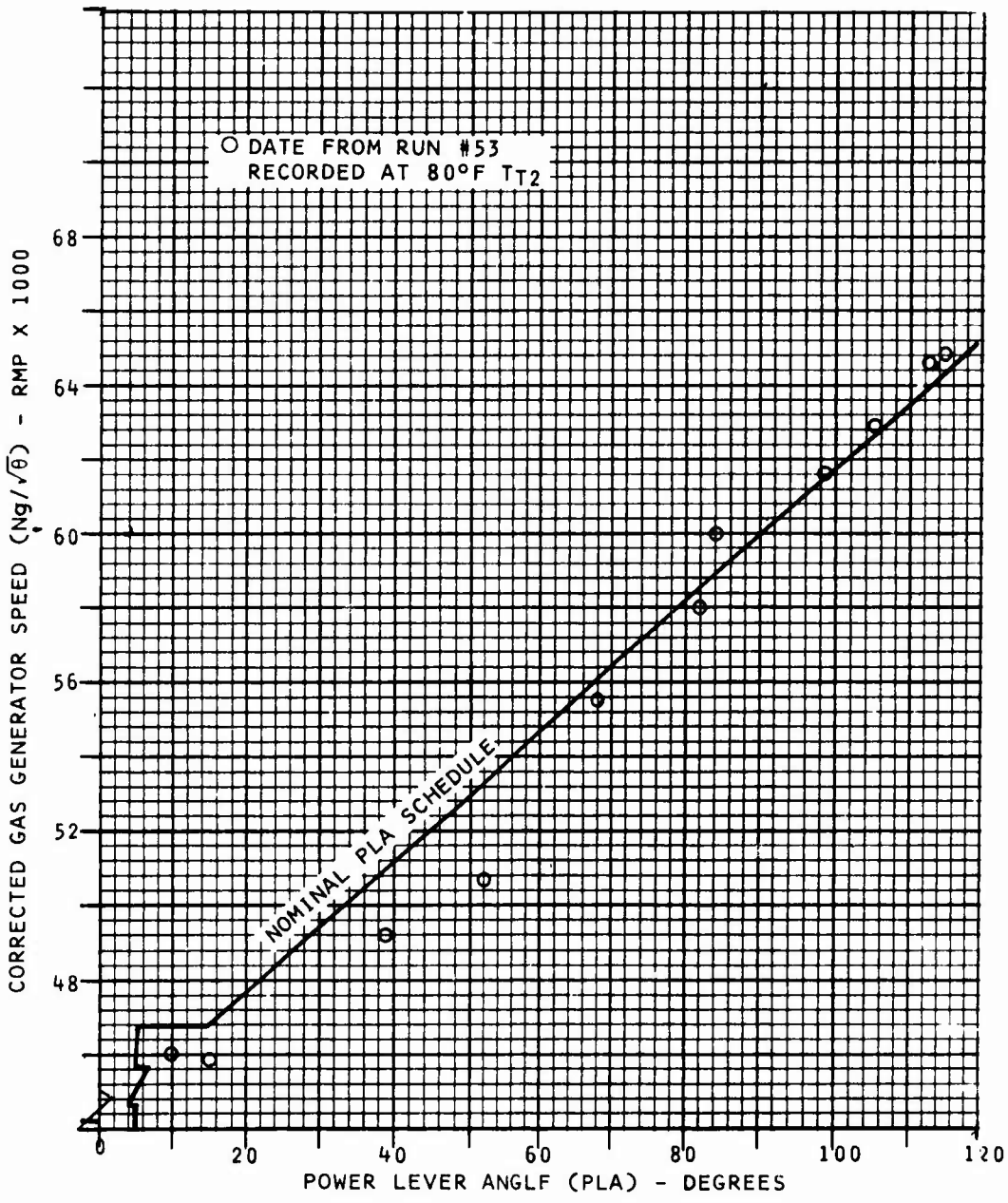

Figure 27. PLA Schedule Test Data

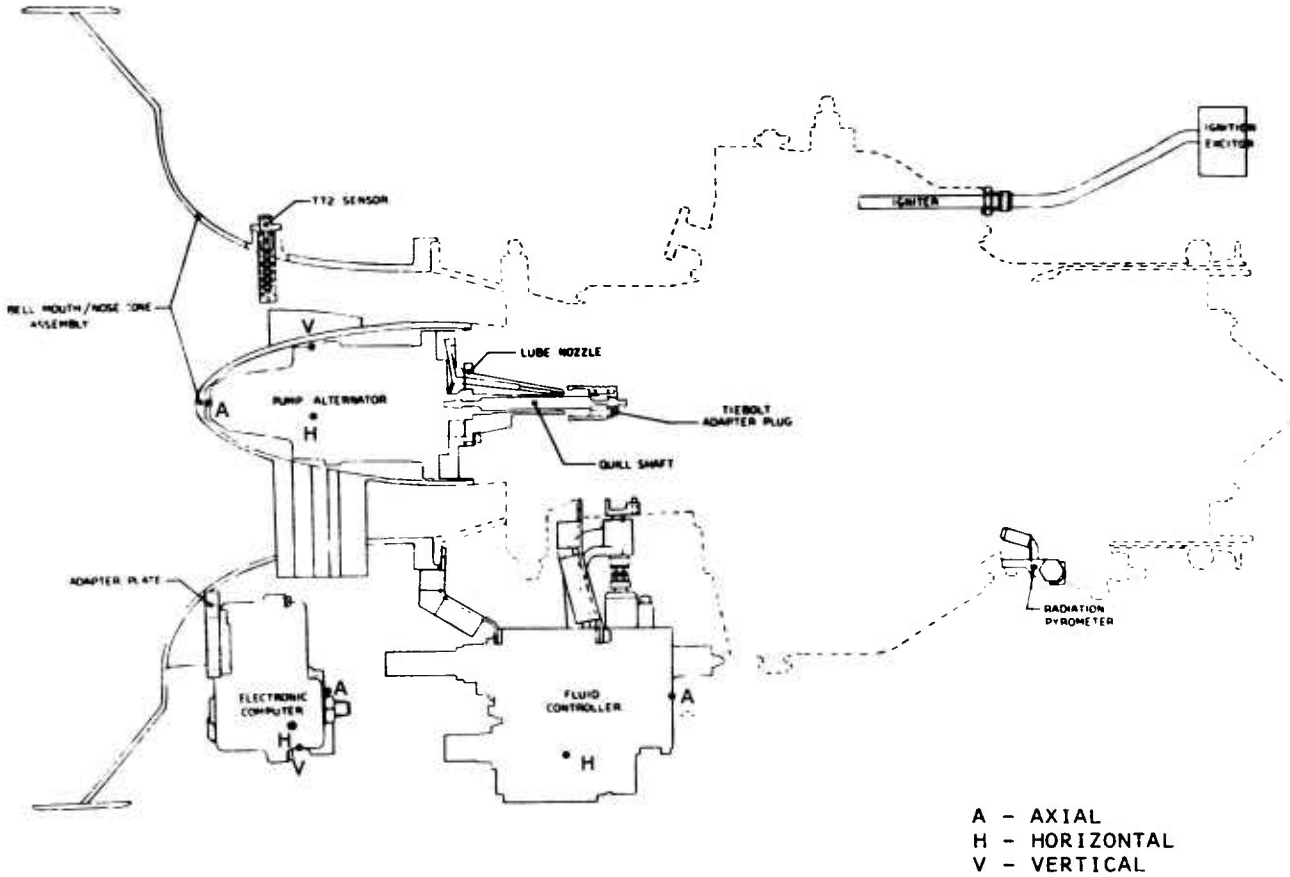

Figure 28. Vibration Sensor Locations

engines and for possible correlation of vibration levels to any failures or faults that might occur in the control system. High resonant vibration of the electronic control at 55,400 rpm was observed early in the test program. The electronic control housing vibration levels observed on the stand meters at this speed were 35, 54 and 43 g's in the vertical, horizontal and axial directions, respectively. The maximum vibration level of the gas generator rotor at this speed was 28 g's at the front bearing compartment. The maximum vibration level on the bellmouth was 10 g's in the vertical plane. Vibration data recorded on the computer, but not available as a stand readout, showed that the top PCB experienced an axial resonance of 97 g's (Figure 29). A spectral plot at this maximum g point showed a displacement of 1.25 mils and a dominant frequency of 930 Hz, as illustrated in Figure 30, which coincided with the 1E gas generator rotor frequency at this speed. Although some housing resonance was observed in earlier bench testing, near this frequency, the circuit board resonance was unexpected and may have been related to the cantilevered mounting. With priority on immediately isolating these high vibration levels so as not to lose out on the limited available engine running time, a vibration isolation padding was placed between the electronic control and the mount bracket adapter plate. Teflon tubing was used to encase the mounting bolts to provide a measure of damping between the bolts and the control housing. Typical vibration data following the addition of the damping material is shown in Figure 31. This fix maintained vibration below 5 g's during all additional engine testing. Although the electronic control was subjected to 6.16 hours of engine running at the higher vibration levels, there was no evidence of any deteriation in either its mechanical integrity or its electronic computational performance.

The fluid control module maintained relatively low vibration levels throughout the testing. This data is summarized in Figure 31. The measured pump/alternator vibration levels increased with engine running time and, during the final two engine runs, reached a maximum of 35 g's as shown in Figure 32.

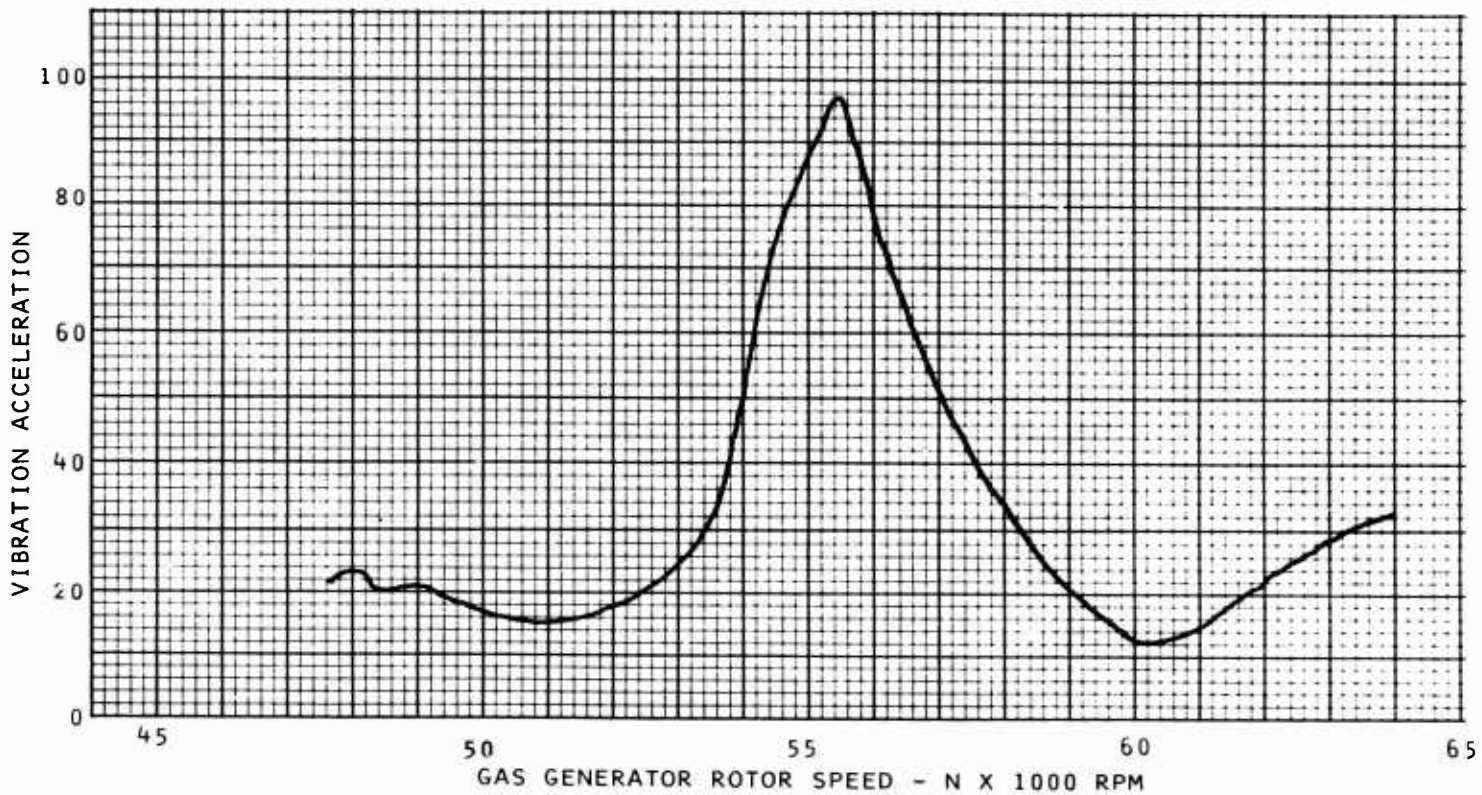

Figure 29. Electronic Control PCB Vibration

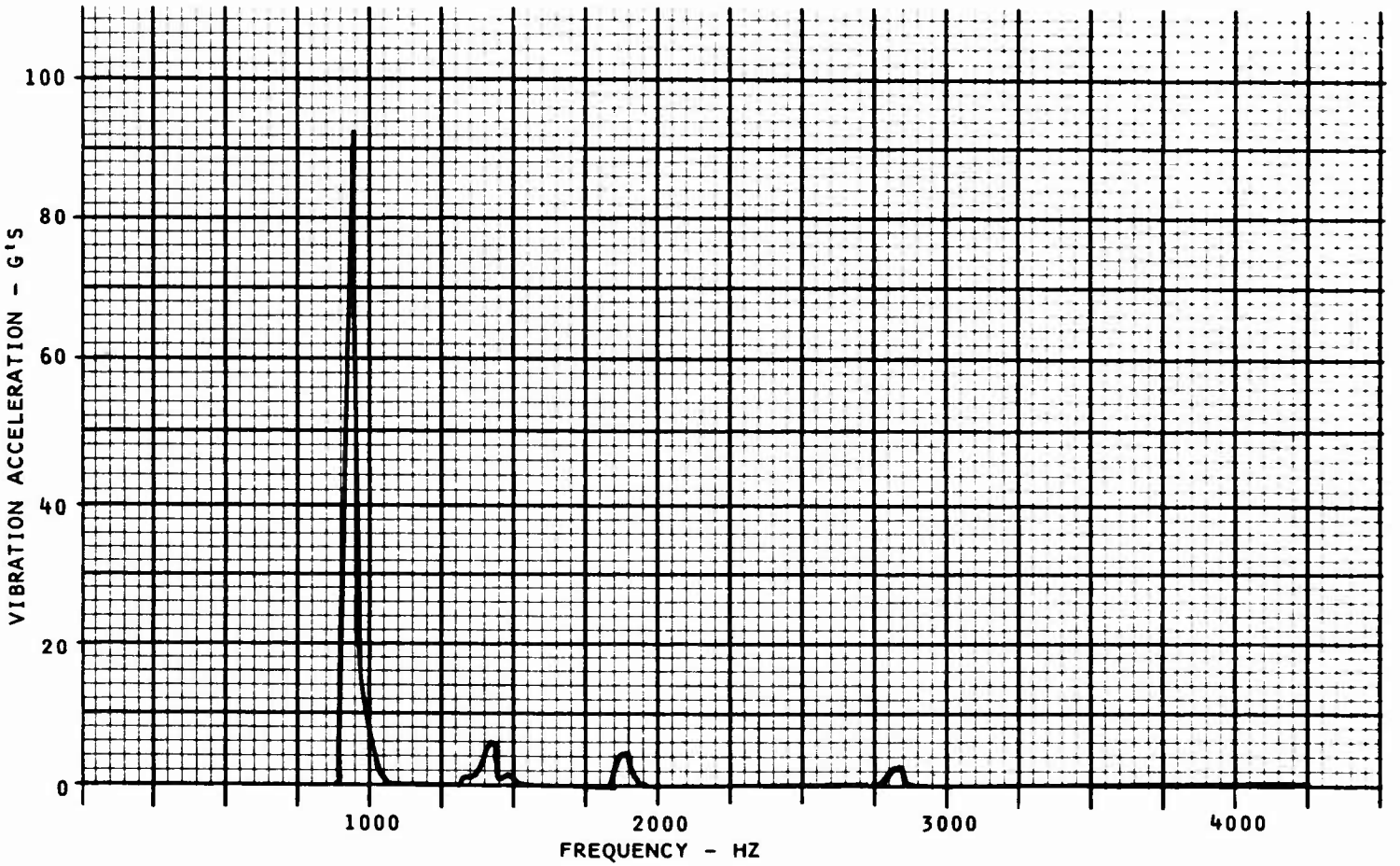

Figure 30. Electronic Control PCB Frequency Spectral Plot

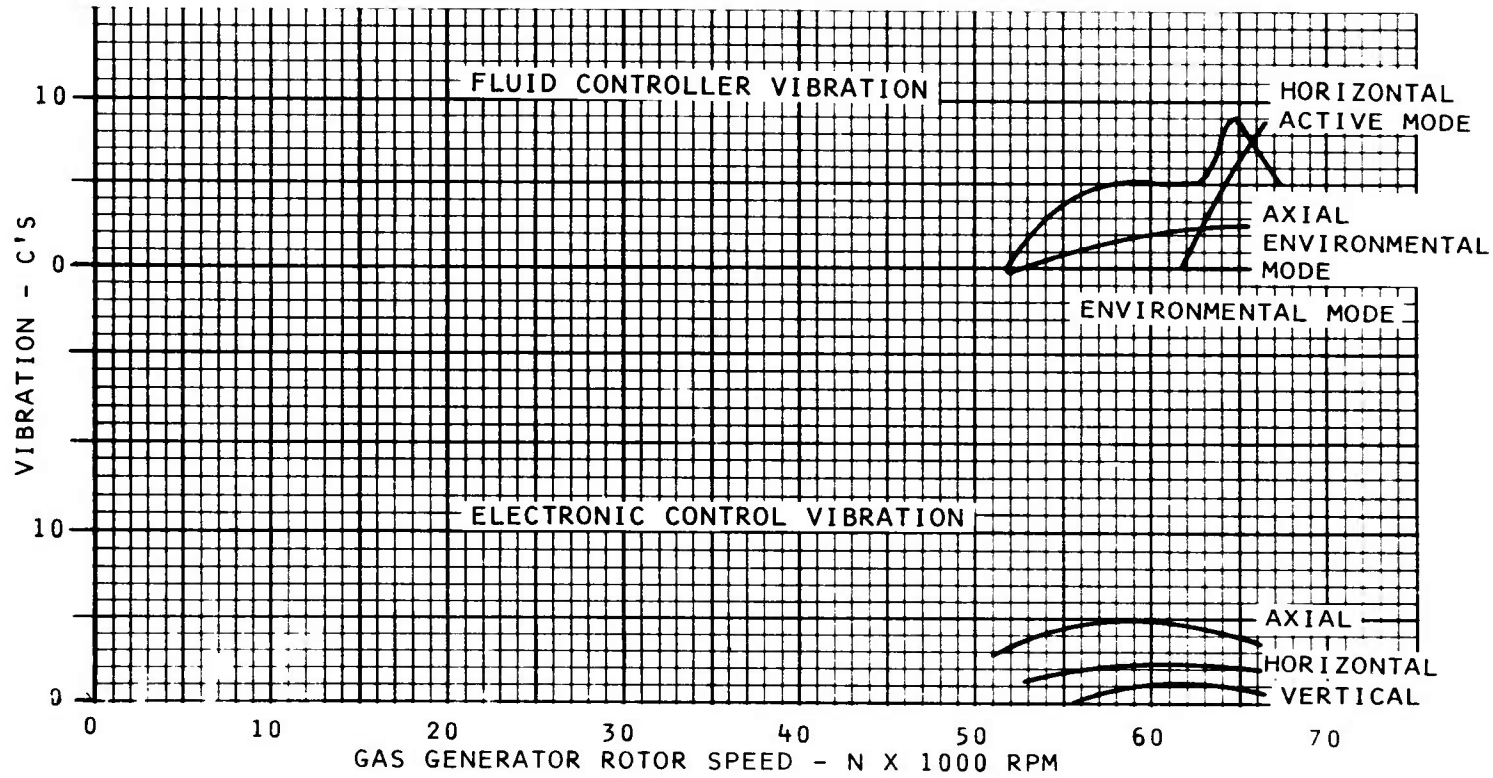

Figure 31. Electronic Computer and Fluid Controller Vibration

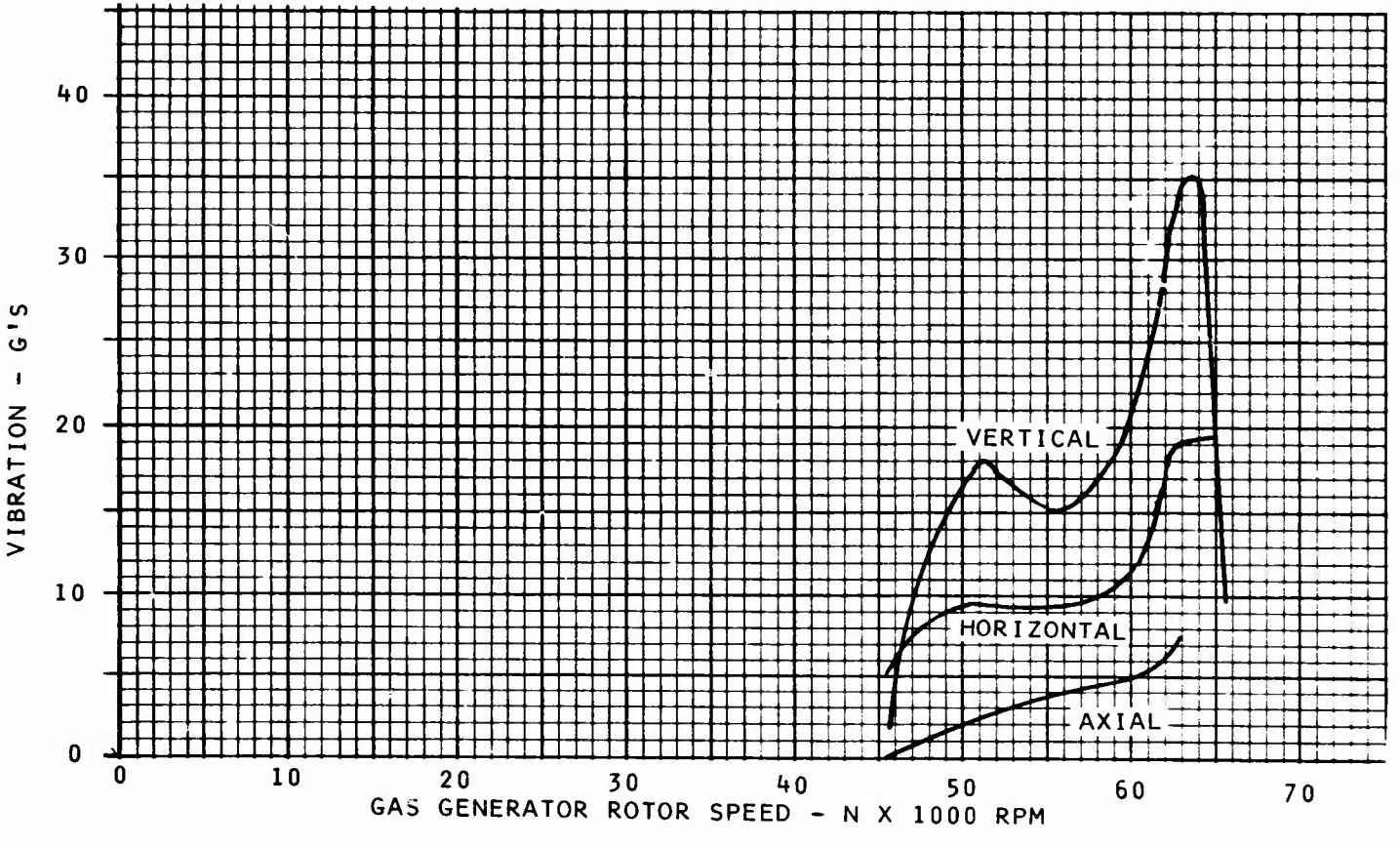

Figure 32. Pump/Alternator Vibration

Inspection of the pump after engine tests showed a small (.0005 inch) amount of journal bearing wear. It is not known, however, if this is the cause for the vibration or the effect. On initial engine runs, pump vibrations were in the 25 g range.

Temperature

The test program objectives included the performance evaluation of the fluid control and electronic control modules when heated externally to an ambient of 180°F. However, because of delays created by the various problems encountered, particularly the inadvertent damaging of the alternator and the termination of engine running, this objective was not met. The data presented in Table 2 summarizes the component temperature when operating from 20 to 100% engine power for an ambient temperature of 75° to 90°F. In all cases, these component temperatures were considered to be acceptable and well within the specified limits. For comparison, during previous bench tests, the case temperature of the hottest component was 211°F for a 180°F ambient and 116°F for a 70°F ambient.

Active Control Tests

As shown in Table 1, the active control demonstration testing was conducted during Run 53, accumulating 8.67 hours of operation. During this run, the gas generator was performance calibrated from idle to design temperature, and then a full acceleration/deceleration cycle between idle and design temperature was demonstrated. The engine testing was continued and included one of the 5-hour demonstration test cycles shown in Figure 33, which consisted of 4-1/2 hours of steady-state operation and 6 additional acceleration/deceleration cycles. A summary of the control performance through the active test follows:

Acceleration/Deceleration

Figure 34 is data plotted from one of the seven acceleration/deceleration cycles. A detailed review of the data from the other cycles showed that this typified all the

TABLE 2. COMPONENT TEMPERATURES DURING ENGINE RUN

Time (hr into run)	Operation Condition Of Control	Engine Speed (rpm)	Component Temperature (°F)								
			TH1	TH2	TH3	TH4	TC1	TC2	TC3	TC4	TC6
.2	Accel	46,000	149	133	163	122	100	100	100	124	132
.3	Decel	50,000	156	142	171	129	106	106	106	128	140
.47	Accel	52,000	161	145	176	132	106	108	106	128	126
.80	Gov.	54,000	162	147	177	133	109	109	109	126	132
1.50	Gov.	56,200	163	149	178	136	112	111	111	130	137
1.70	Gov.	59,160	167	151	181	138	112	113	113	130	136

TH1 - MC1507 on Top PCB
TH2 - Stepper Motor Darlington on Bottom PCB
TH3 - Power Transistor ±V Supply on Middle PCB
TH4 - Fault ISQ PROM

TC1, TC2, TC3 - Electronic Control Housing
TC4 - Fluid Controller
TC6 - Pump Discharge

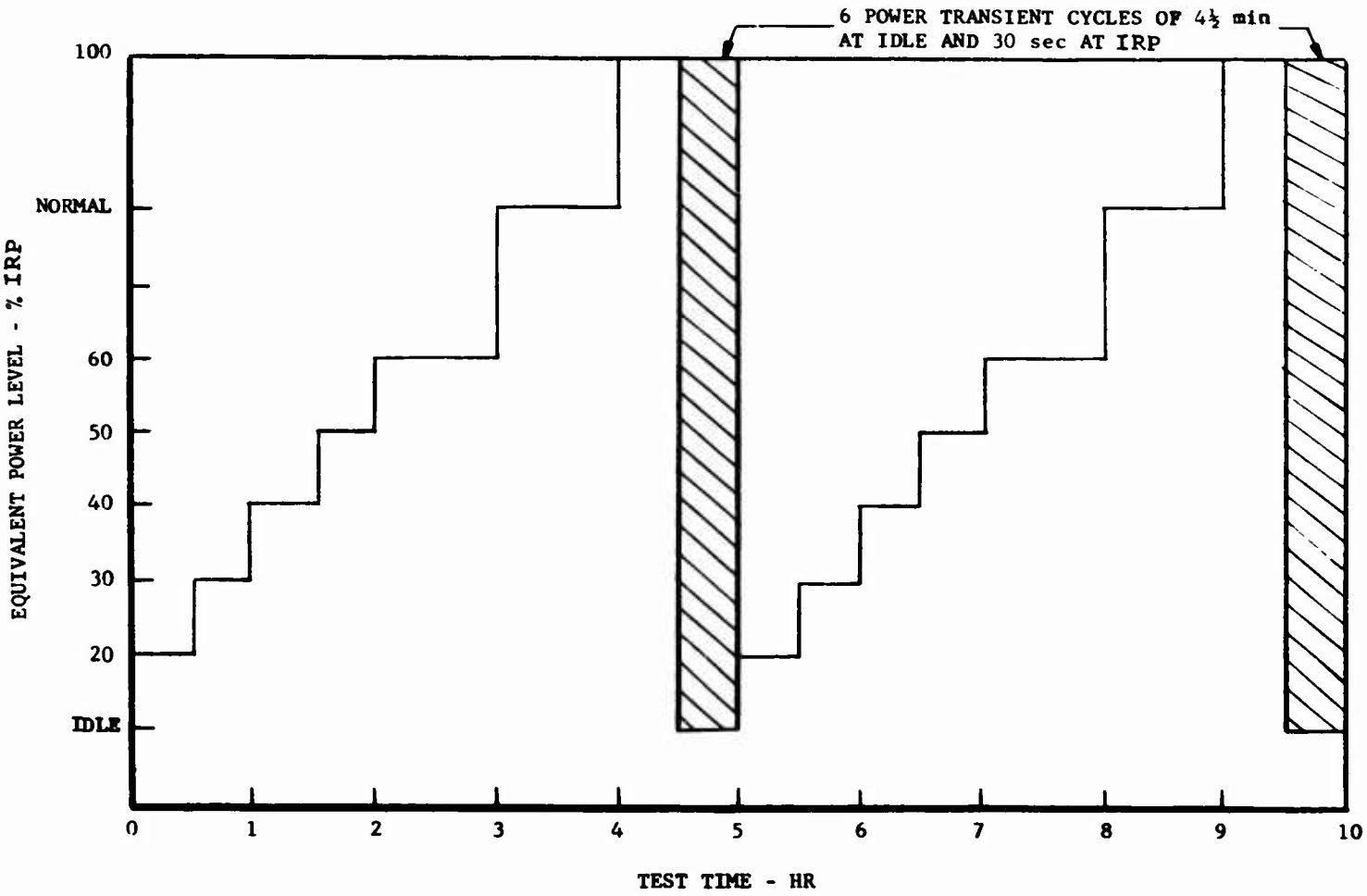

Figure 33. STAGG 10-Hour Demonstration Cycle

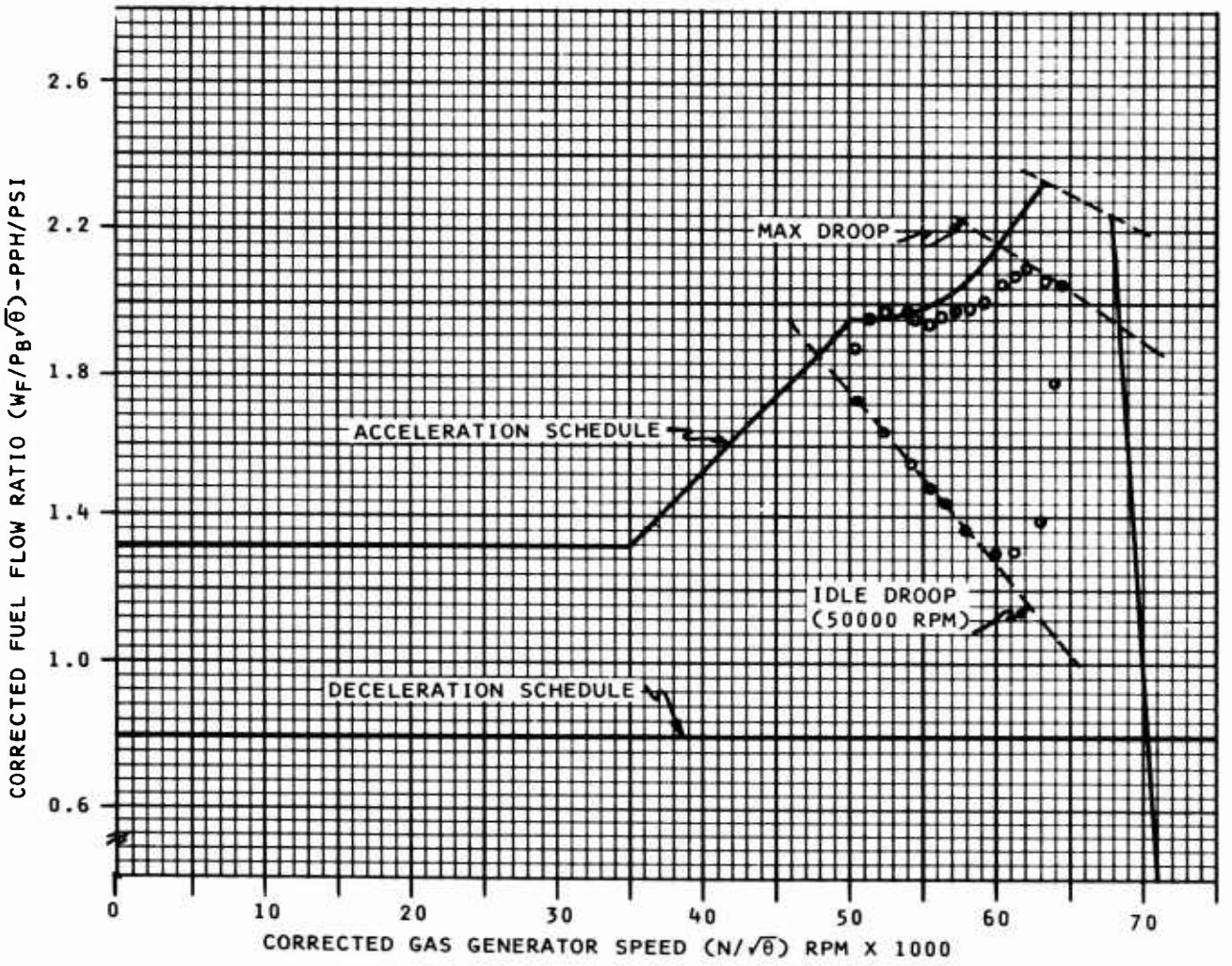

Figure 34. Engine Acceleration/Deceleration Transient - Active Mode

acceleration/deceleration transients. The underscheduling of ratio units indicated was attributed to sticking in the metering head regulator valve because the observed output signal from the electronic control to the hydromechanical unit coincided with the desired schedule. The metering regulator valve problem was identified and corrected in post-engine run bench calibrations.

Inlet Guide Vane Control

During the seven acceleration/deceleration cycles, the IGV control performance was excellent. Since the transient requirements were faster during decelerations, 3 to 4 seconds versus 13 to 14 seconds for the acceleration, only the deceleration transient is shown plotted in Figure 35. The close agreement with the commanded position (dashed line) typified all the IGV transients. The incremental changes in the actual position are the result of step change rotational increments of the actuator stepper motor. The capability of the control to schedule guide vane prewhirl automatically, reduced the elapsed time required for acceleration and deceleration. Acceleration from idle to design turbine conditions required 13.8 seconds as compared to 22 seconds with the STAGG breadboard control system and its manually actuated vanes.

Speed Governor

The only problem in the governor control was the small hysteresis attributed to the metering head regulator's sticking. Transient governor droop curves as shown in Figure 34 are right on design.

Fault Isolation

During the engine test program, no faults were indicated for the electronics. This fault status was verified by the recorded test data, which showed that the electronics performed correctly. On the final engine run, a fault was indicated during a snap deceleration. Since only the ΔP fault test is on-line after engine ignition, it was concluded that the metering valve pressure regulator

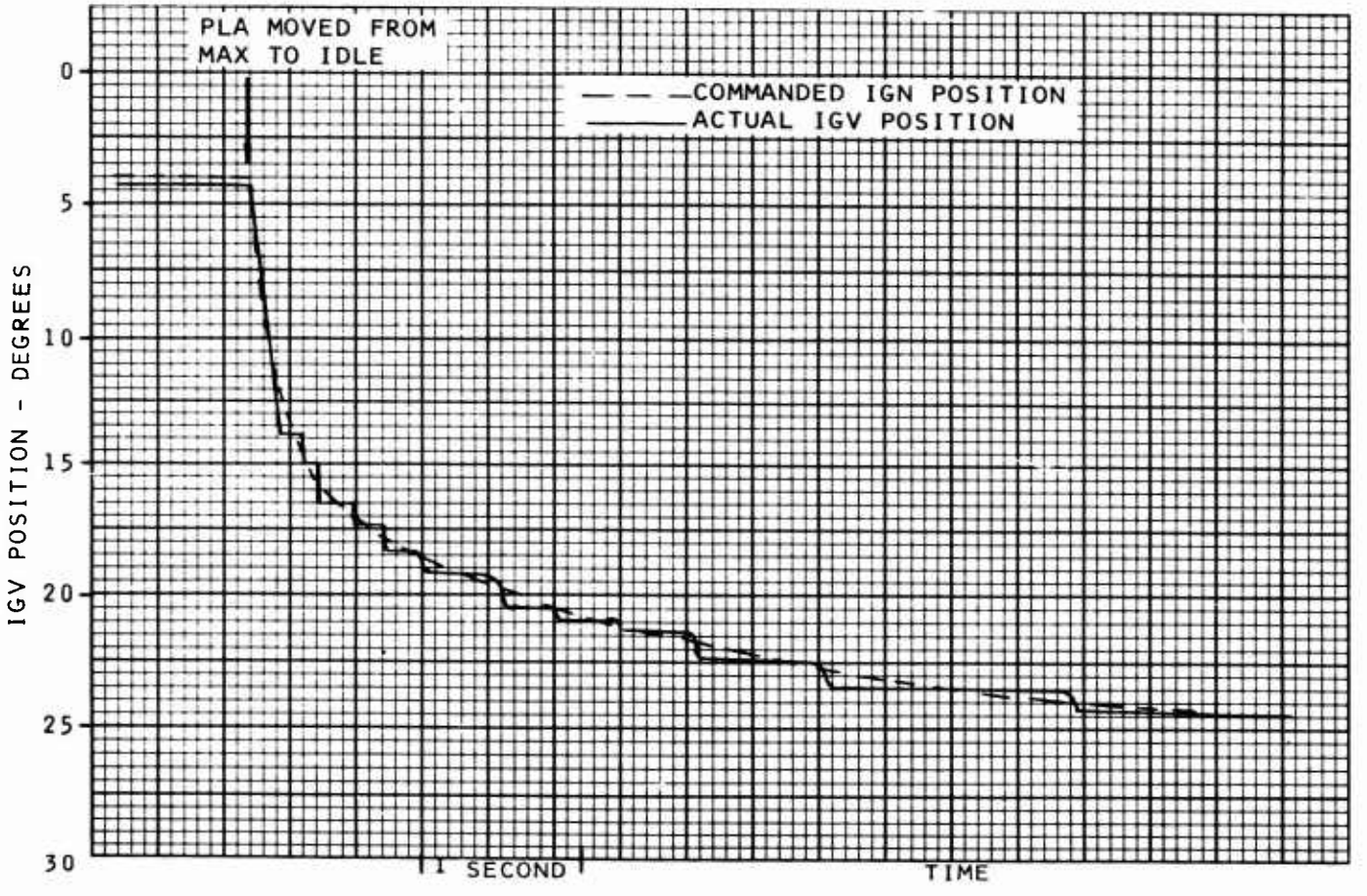

Figure 35. IGV During Deceleration from Max to Idle Speed - Active Mode

exceeded its test limits. This was in agreement with the performance data, which indicated that the valve was sticking during most of this engine run. However, in general, the amount of sticking did not cause ΔP to exceed the limits for indicating a fault.

Summary of Engine-Mounted Tests

During all of the engine testing, there were no failures or faults with the electronic computer, the alternator, or any of the sensors. The few problems encountered were related to the hydromechanical components. Failure of the fuel pump face seal was caused by cavitation of the pump inlet due to a short circuit caused by the IGV actuator servo valve's moving too far out of the valve sleeve. Connecting the valve to the ball screw with a wire corrected this problem. The overall performance of the control system successfully demonstrated the feasibility of full authority electronic control, high-speed dynamic pumping, and electrohydromechanical fuel metering and IGV activation. The goals of demonstrating control system operation at 180°F ambient and closed-loop blade temperature limiting were not accomplished because we fell short of being able to get all of the testing done within the STAGG test schedule and available engine running time. Apparently, it was too ambitious an undertaking to tie the engine demonstration of advanced control technology with a 50-hour advanced gas generator development test program.

COMPONENT DESIGN AND PERFORMANCE

FUEL METERING SYSTEM

The fuel metering section interfaces with the electronic computer to control fuel flow to the engine. It also provides fuel shutoff and a fault signal to indicate a failure or fault in the pump or fuel metering modules.

Design Requirements

Fuel Flow	0 to 400 pph
Fuel Temperature	-65 to 300°F
Fuel Inlet Pressure	15 to 880 psig
Resolution	0.5 pph per 7.5° step
Maximum Slew Rate	598 pph per second
Metering Head ($P_m - P_n$)	9 psid nominal
Indicate Failure If	$7.7 \geq P_m - P_n \geq 10.7$ psid
Servo Supply Filter Rating	3μ absolute
Fuel Shutoff	Seepage 1 cc/min

Description of Operation

A schematic of the fuel metering system is shown in Figure 36. The fuel metering section comprises the following components:

Rotating plate fuel metering valve
Throttling type metering head regulator
Stepping motor and gear reduction drive for positioning the fuel metering valve
Metering valve position feedback resolver
Metering valve ΔP indicator
3u absolute barrier filter for servo flow

High-pressure fuel (P_f) is delivered to the fuel metering section by a centrifugal pump. The fuel flow to the engine is metered by a rotating plate fuel metering valve and shutoff valve. The pressure drop across the metering valve ($P_m - P_n$) is held essentially constant by a throttling head regulator. The

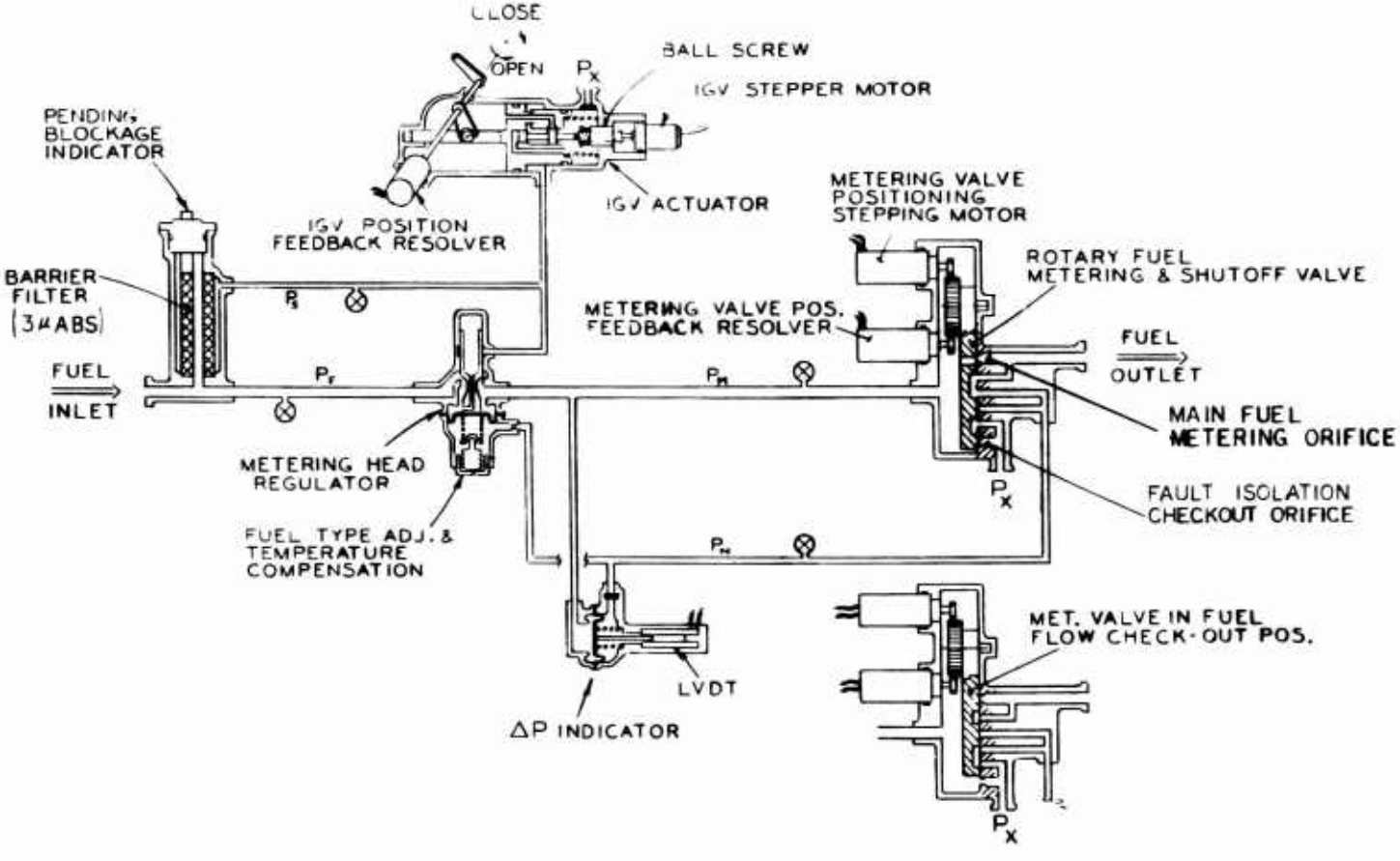

Figure 36. Fluid Controller Schematic

regulator has automatic compensation for fuel temperature variation and is manually adjustable to fuel type. The main fuel metering components accept unfiltered fuel and are capable, as presently demonstrated, of operating on fuel contaminated to the level of Army specification AV-E-8593B.

A metering head signal is provided by the fuel metering section for fault isolation of the pump and fuel metering modules.

Component Design Description

Fuel Metering and Shutoff Valve

A photograph and section drawing the fuel metering and shutoff valve is shown in Figure 37.

The drive to the metering valve is from a variable reluctance stepping motor through a gearhead directly mounted to the stepping motor. The ratio

$$\frac{\text{stepping motor rotation}}{\text{metering valve rotation}} = 113$$

is provided by antibacklash gears. The estimated metering valve torque is 4.9 oz-in. The torque provided by the stepping motor at the metering valve is 13.8 oz-in. at the maximum slew rate of 610 steps/sec including allowance for 48% mechanical efficiency for the antibacklash gear train. Hence, the safety factor for torque during slewing is 2.8. The relationship between angle of the metering valve and fuel flow is linear and is shown on Figure 38.

Feedback of metering valve position is by a resolver. The stepping motor, gears and resolver are all immersed in fuel, and the stepping motor and resolver have glass headers to seal between the fuel and ambient. The metering valve plate and metering orifice are aluminum; the sliding surfaces are hard-coated and lapped. To keep the metering valve plate and orifice in contact, the plate is pressure-loaded against the orifice using the metering head and is spring-loaded with a 0.5-lb spring.

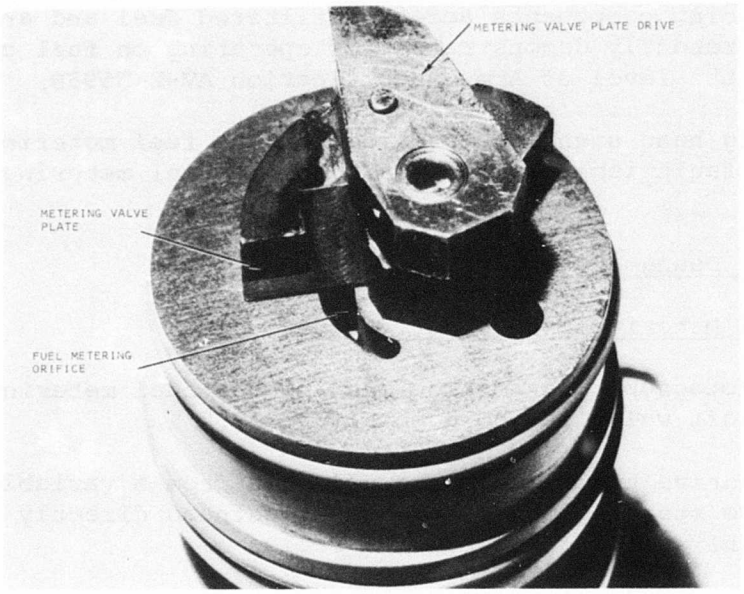

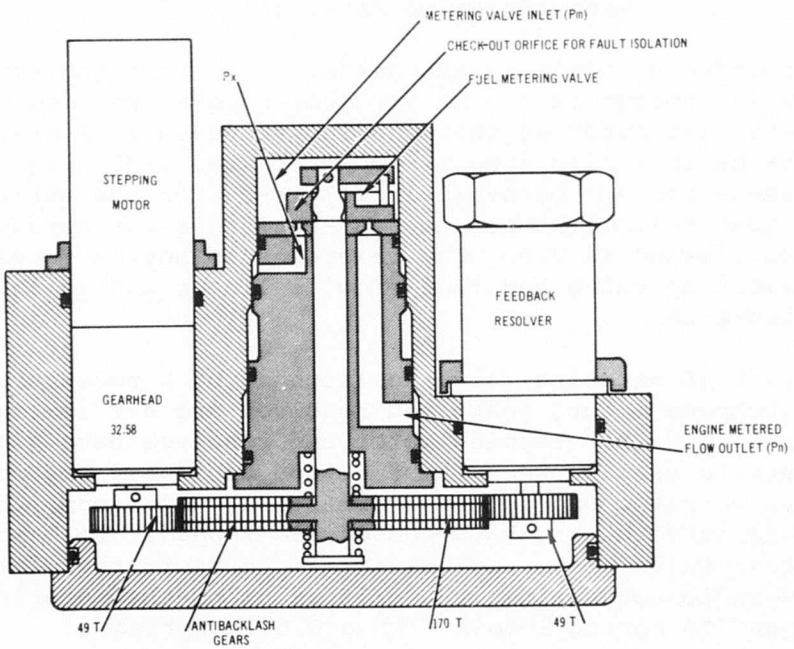

Figure 37. Fuel Metering and Shutoff Valve

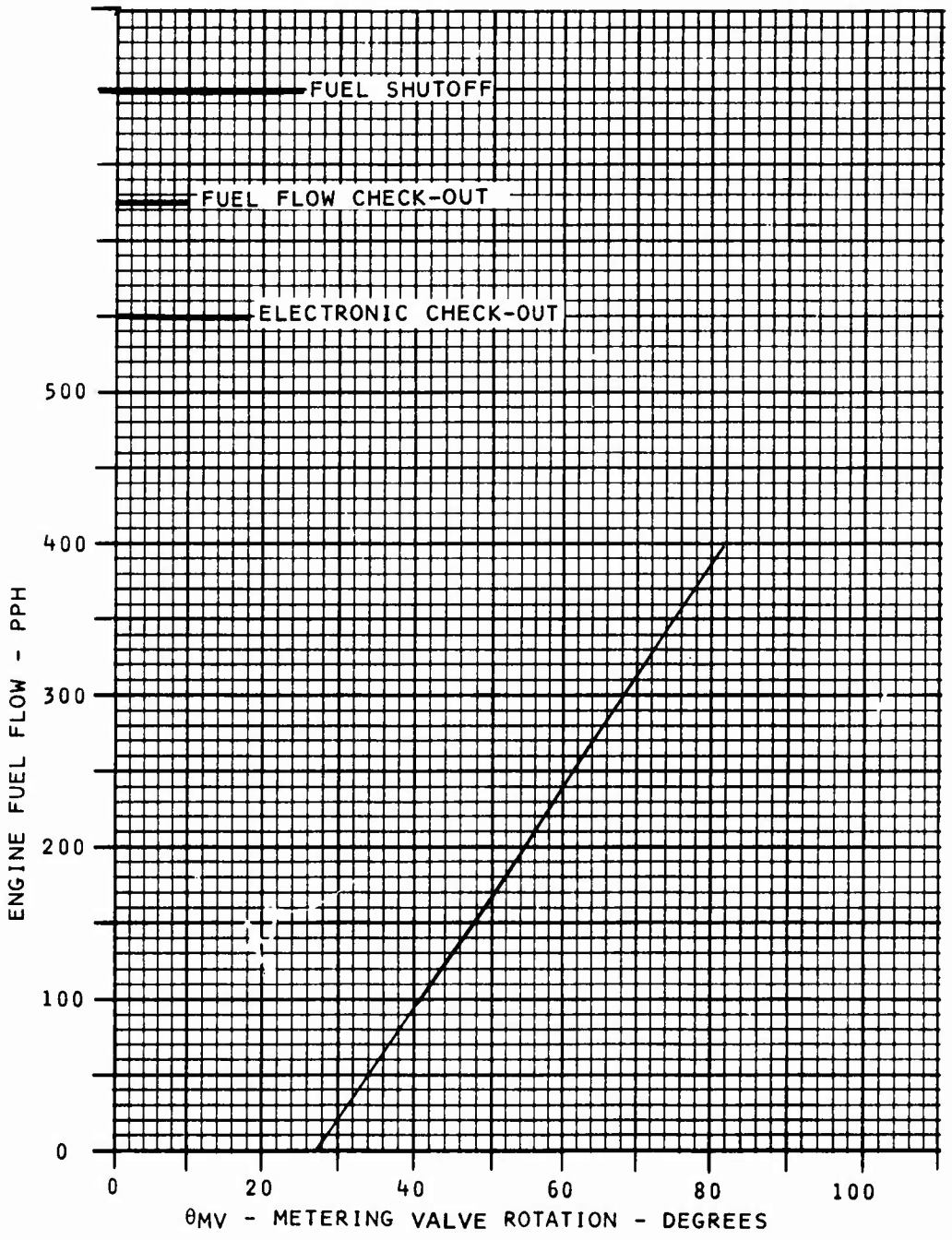

Figure 38. Metering Valve Characteristic

The fuel metering valve is capable of shutting off fuel flow completely. For this reason. it is also used as the shutoff valve. An adjustable minimum fuel flow limit is provided electronically, and the maximum flow stop is mechanical.

Metering Head Regulator

A section through the metering head regulator and a photograph of the valve is shown in Figure 39.

The metering head regulator is a throttling valve and has a fuel type adjustment and automatic compensation for fuel temperature over the range -65° to 300°F. The valve is flow force compensated; the inlet and outlet angles are 69° and 20° (half angles). The basic valve size is 3/8 inch diameter. The metering head is sensed by a fluorosilicone diaphragm with an effective area of 0.2875 $in.^2$.

The transient response of the regulator in conjunction with the fuel metering valve is controlled by the valve flow gain and damping orifice size (0.025 inch diameter) and, based on a previous test, has a 25-ms time constant from a step change in metering valve position to fuel flow. The valve and sleeve are aluminum and hard-coated at the sliding and controlling surfaces.

The metering head is nominally 9 psid, which represents the near lowest pressure drop practical to maximize the metering valve area. As the fuel flow to the engine increases, the head regulator valve has to stroke, and the spring load reduces due to the spring rate; this generates a head regulator characteristic which varies from about 9.5 psid at low fuel flows to 8.5 psid at high fuel flows. This variation in head is compensated for by increasing the metering valve area with increase in fuel flow. The head regulator characteristic is shown in Figure 40.

Fault Isolation

During built-in self-test, the ability of the electronic computer to position the metering valve is checked within the first 18° rotation (Figure 38) of the metering valve,

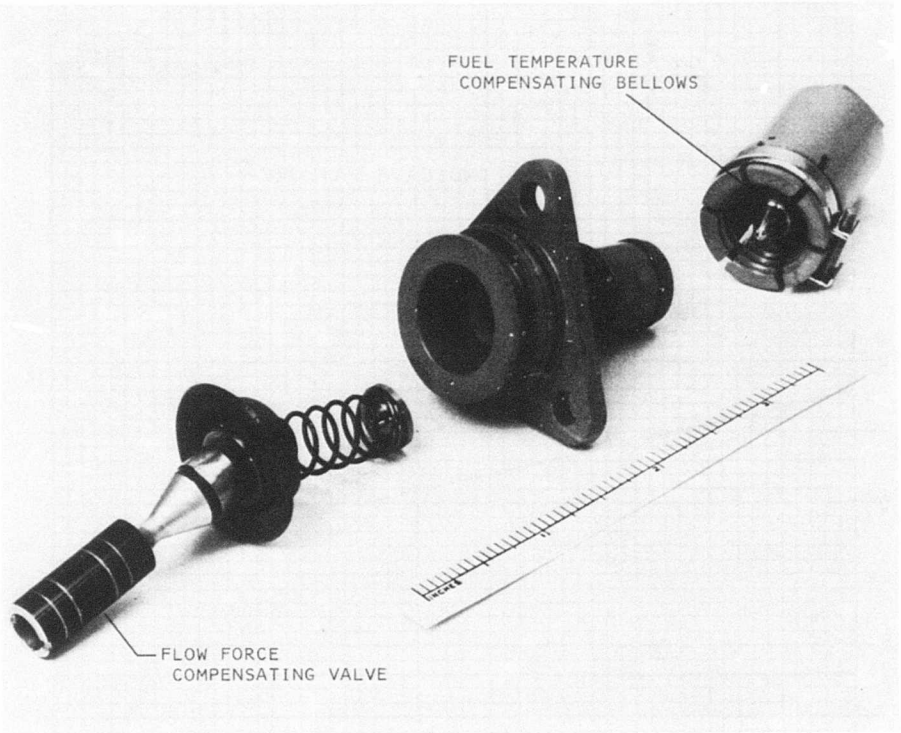

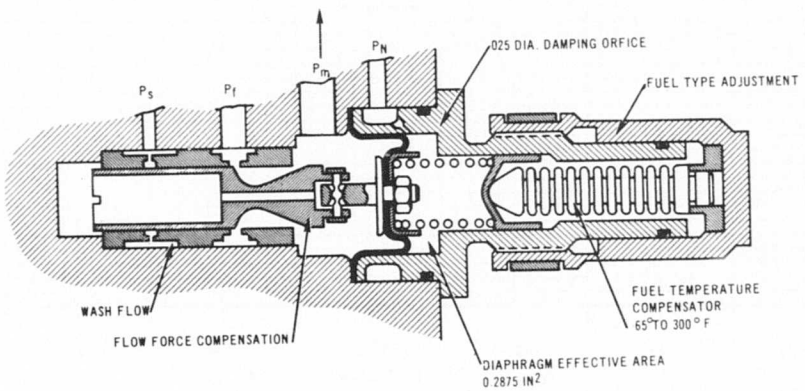

Figure 39. Metering Head Regulator

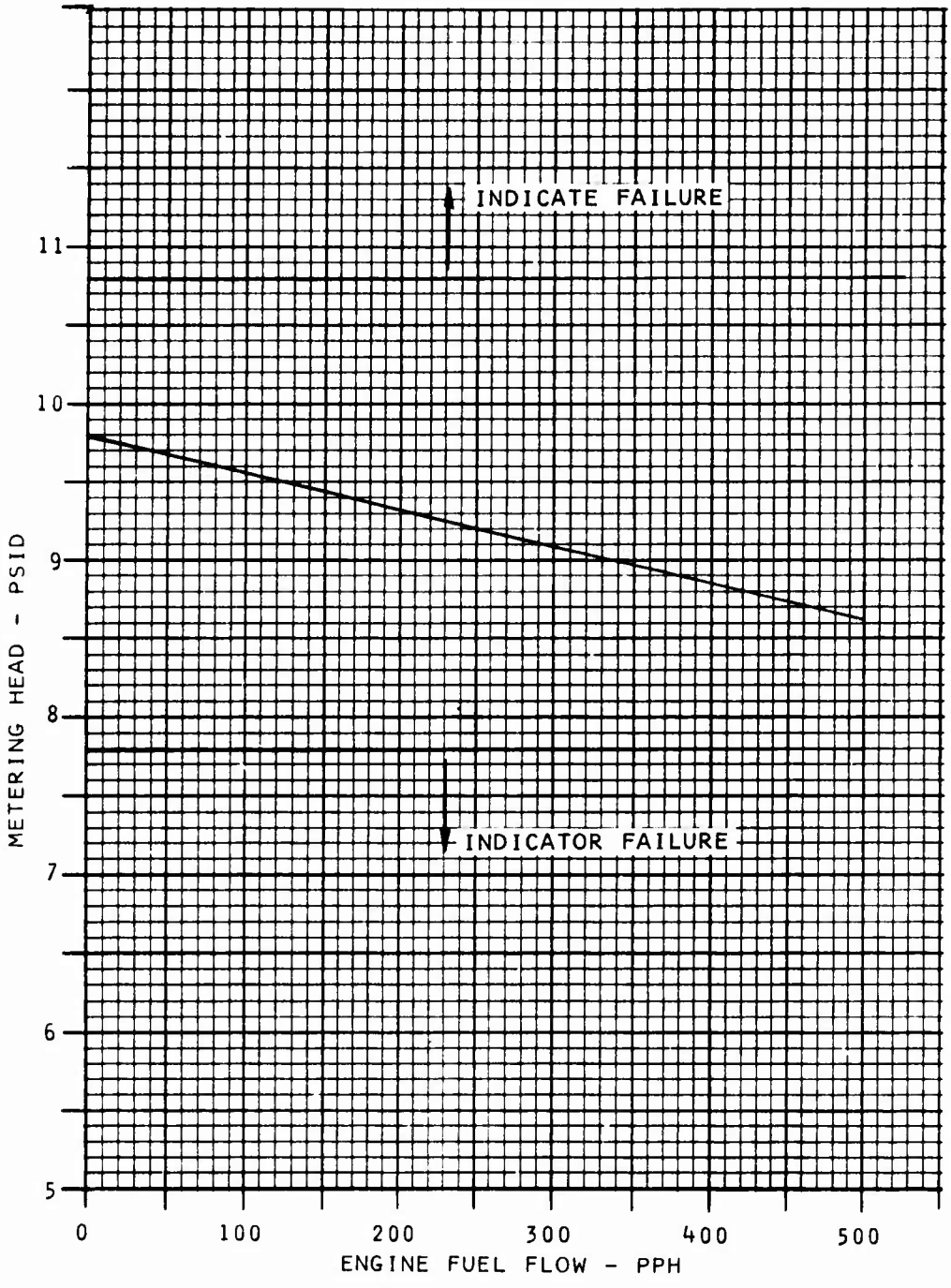

Figure 40. Metering Head Regulator Characteristic

with the fuel to the engine shut off. A fuel flow check-out orifice is provided in parallel with the fuel metering orifice. With the metering valve in fuel flow check position, fuel passes through the check-out orifice and back to the pump inlet. The check-out orifice is sized for 50 pph. The pressure drop across the orifice is ported to the head regulator through slots in the fuel metering valve plate. The functioning of the head regulator and pump is thereby checked by sensing metering head across a diaphragm and spring assembly before the engine is started and during normal operation. As the metering head is varied about a nominal value, the diaphragm is displaced, the displacement is measured with an LVDT, and the signal is then passed to the electronic computer and compared to maximum and minimum limits. These limits are set at 10.7 and 7.7 psid respectively, as shown in Figure 40.

When the fuel metering valve is being used in the normal mode and controlling fuel to the engine, the fuel check-out orifice and associated drillings and slots are shut off, and the pressure drop across the engine fuel metering orifice is rerouted to the metering head regulator via slots in the metering valve. This is shown on the schematic in Figure 36.

Barrier Filter

A barrier filter is provided to supply clean wash flow to the metering head regulator and servo flow to the geometry actuator. The supply to the metering head regulator is to provide weep flow between the valve and sleeve to reduce valve friction. The total steady-state filtered flow will not exceed 50 pph. The filter is sized for 150 hours using fuel contaminated to the level given in specification AV-E-8593. In normal use, the pressure drop across the filter will be less than 1 psi. To provide on-condition maintenance, the filter has a pop-out indicator set for 6 psid. The orifice between the fuel inlet and metering head regulator is introduced to ensure wash flow to the metering head regulator by making $P_f - P_f' > P_f - P_s$.

The filter is a 3u absolute glass fiber disposable element. The choice of 3μ absolute as compared to the more conventional 25μ absolute is based on experience gained on aircraft and commercial hydraulic systems. In these applications, component life has been extended by a factor of at least 2 by using ultrafine filtration.

Bench Test Results

The fuel metering valve, metering head regulator and ΔP indicator were developed and bench tested prior to and in conjunction with system testing. To allow testing of these components in conjunction with the use of electronic equipment in the same area, a low-volatility test fluid was used (Low Order Paraffinic Solvent). This fluid has a viscosity and specific gravity very close to those of JP-5.

Fuel Metering Valve and Stepping Motor Drive

The fuel metering valve and stepping motor drive were tested by using a test stepping motor drive to pulse the stepping motor with single 15° steps. A typical calibration of the fuel metering valve is shown in Figure 41. As indicated, there is a very good correlation with design characteristics close enough for system testing. The metering valve was tested in the shutoff position, no drops were produced in 6 minutes before and after engine testing.

Metering Head Regulator

Calibration data on the metering head regulator is shown in Figure 42. The regulator was tested to determine the effect of variation in pump supply pressure (P_f) from 100 to 700 psig. The performance was generally satisfactory; however, during engine testing, hysteresis in the regulator was seen to increase. After completion of engine testing, the metering head regulator was bench tested, and it was verified that at conditions where the pressure drop across the regulator sleeve ($P_f'-P_m$) exceeded 350 psid, the valve developed 1 psi hysteresis. The sticking was caused by the pressure's causing local distortion of

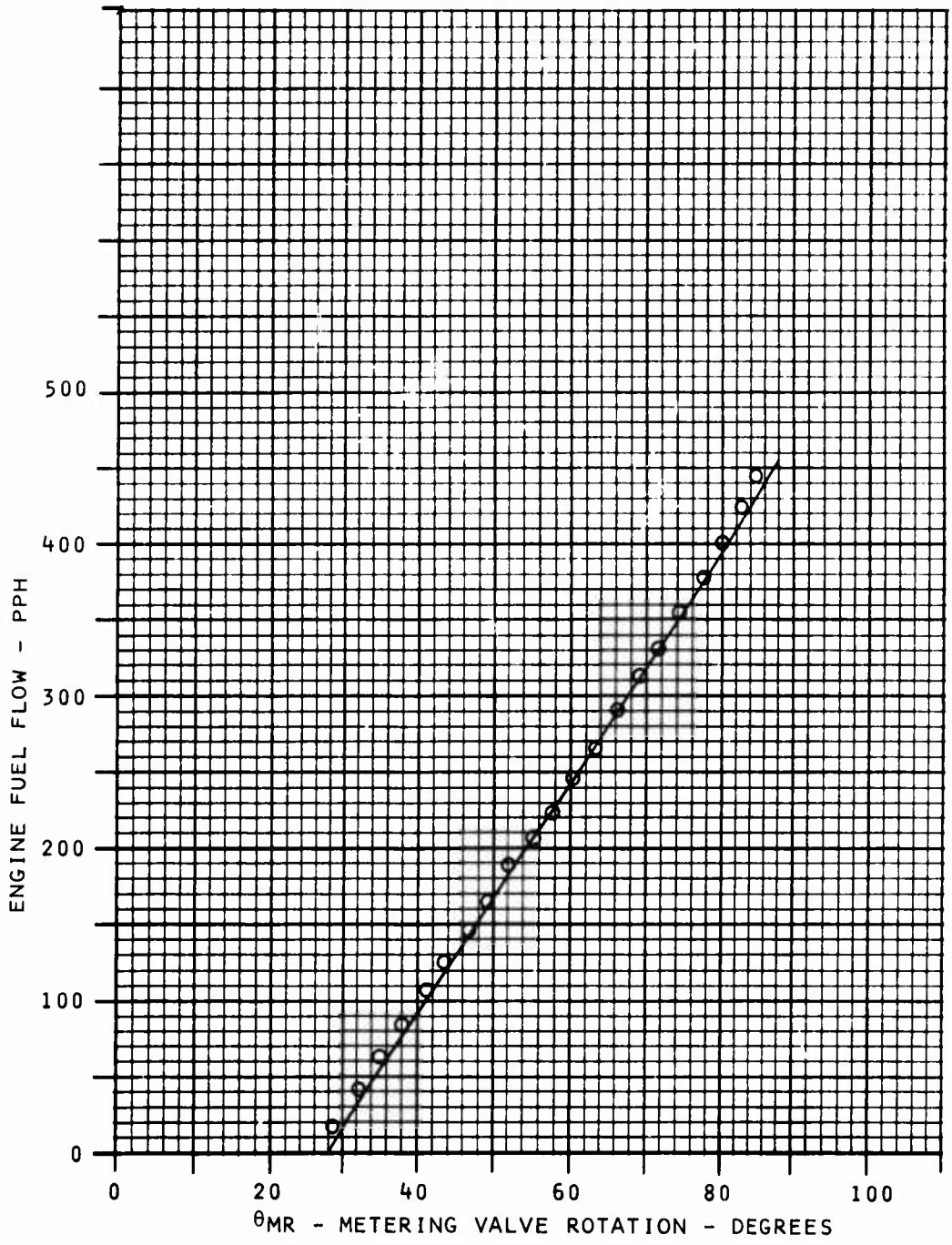

Figure 41. Metering Valve Fuel Flow - Bench Test

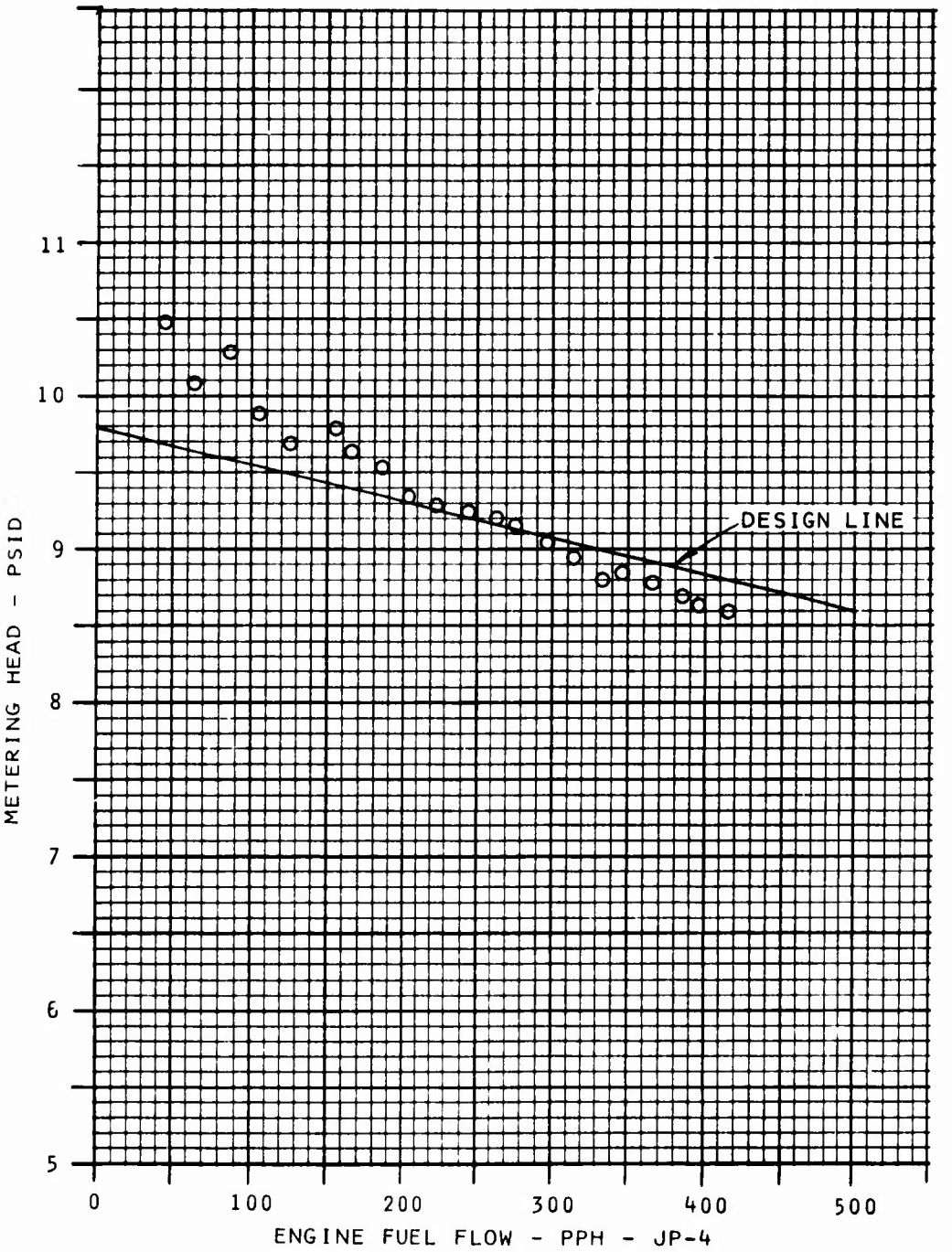

Figure 42. Metering Head Regulator Characteristic - Bench Test

the thin metering port in the valve sleeve. This was corrected by removing 0.0002 inch from the outside diameter of the valve in the region where the sleeve was distorting.

ΔP Fault Sensor

Typical test data on the ΔP fault sensor is shown in Figure 43. As indicated, a reasonably good linear signal is provided.

GEOMETRY ACTUATOR

The geometry actuator is required to position the compressor inlet guide vanes as a function of corrected gas generator speed. In the event of an electrical power failure, the actuator can also provide a backup control using a pressure speed signal from the pump.

Design Requirements

Rotation	30° with the provision for extending the range to 45°
Accuracy	±1/2° during steady state ±1° during a transient
Torque	24 in.-lb (14 in.-lb friction and 10 in.-lb aerodynamic, Figure 44)
Failure Mode	In the event of an electrical power failure, the actuator will continue to operate over its full speed range.

Description of Operation

A schematic of the geometry actuator is shown in Figure 36, and a cross-section drawing of the actuator is shown in Figure 45. The input command from the computer drives the variable reluctance stepping motor. Rotation of the stepping motor is

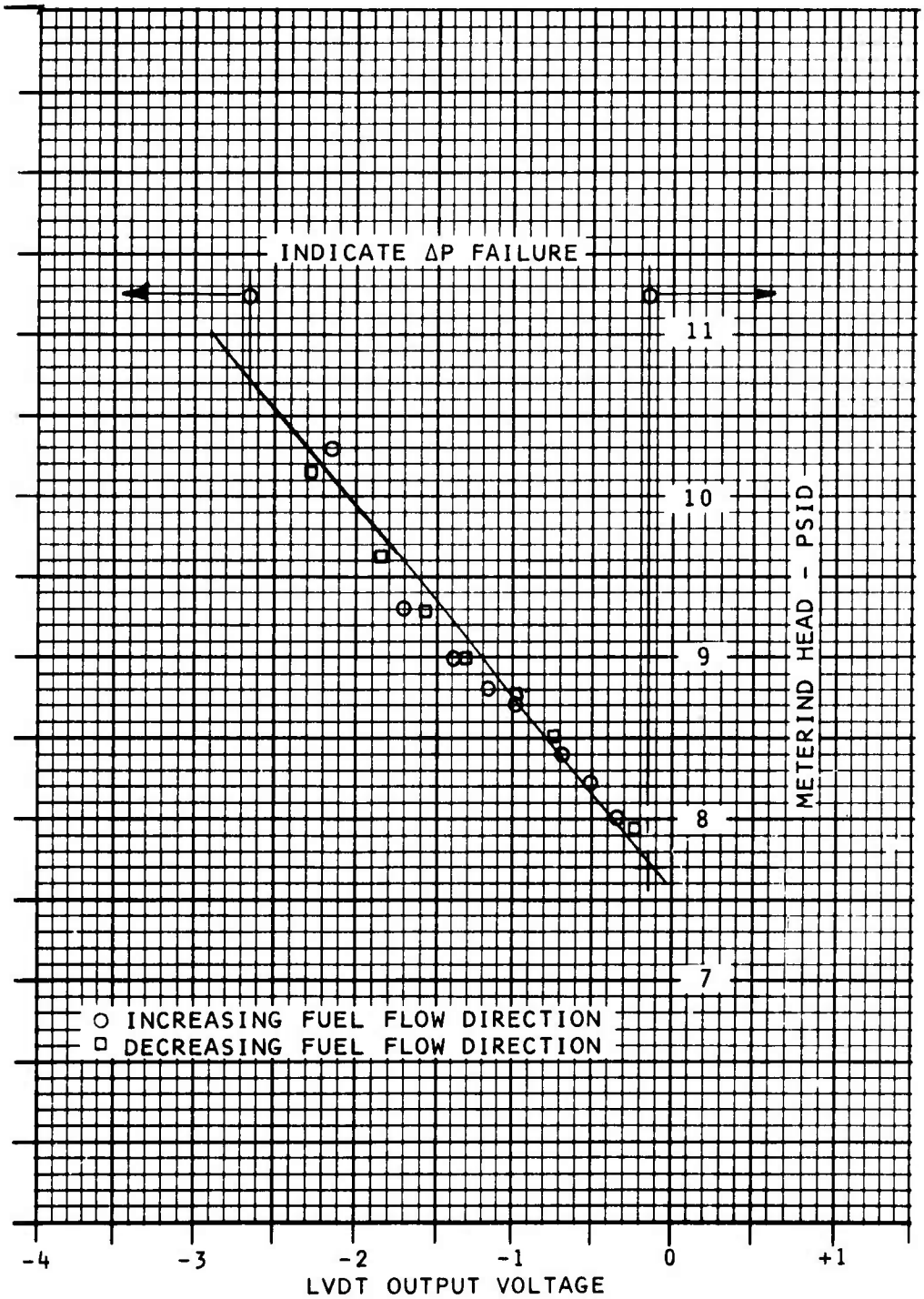

Figure 43. ΔP Fault Sensor - Bench Test

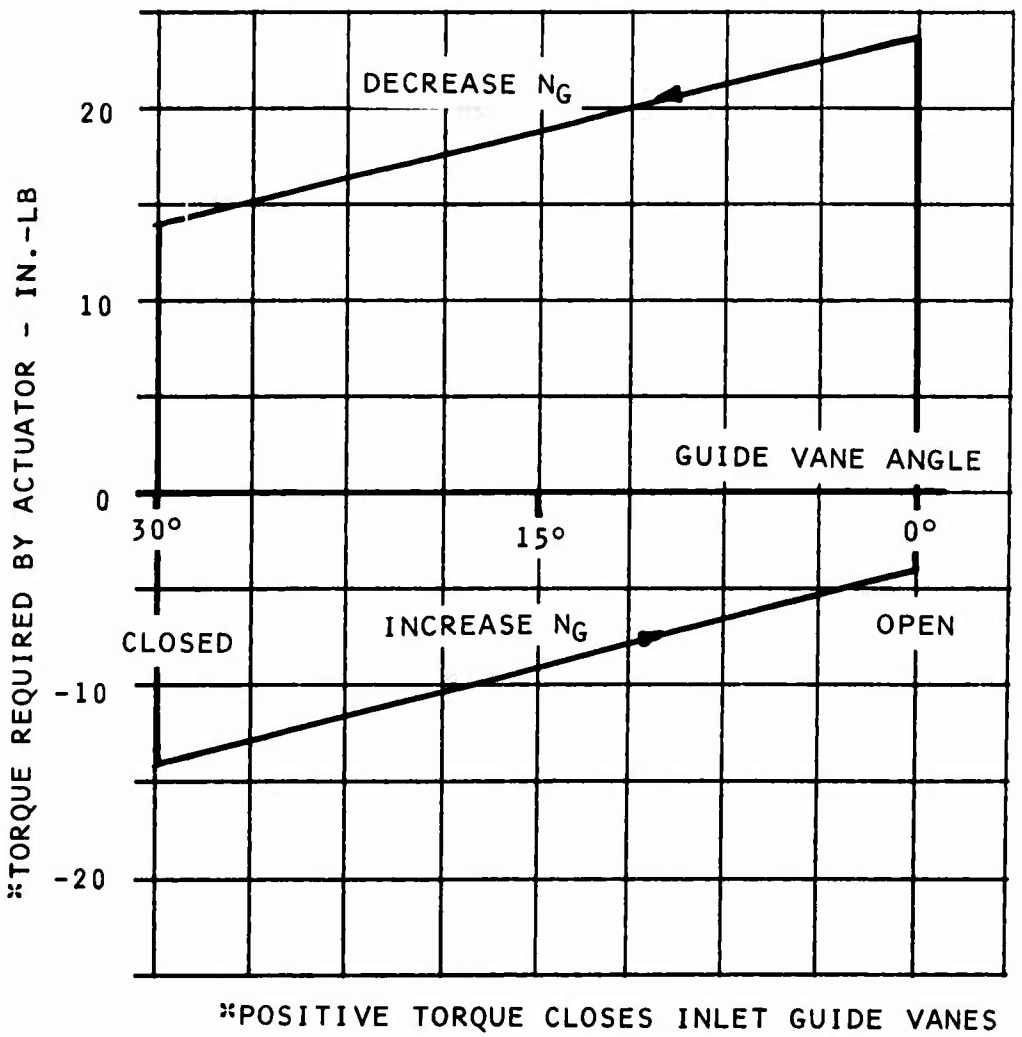

Figure 44. IGV Actuator Torque Requirement

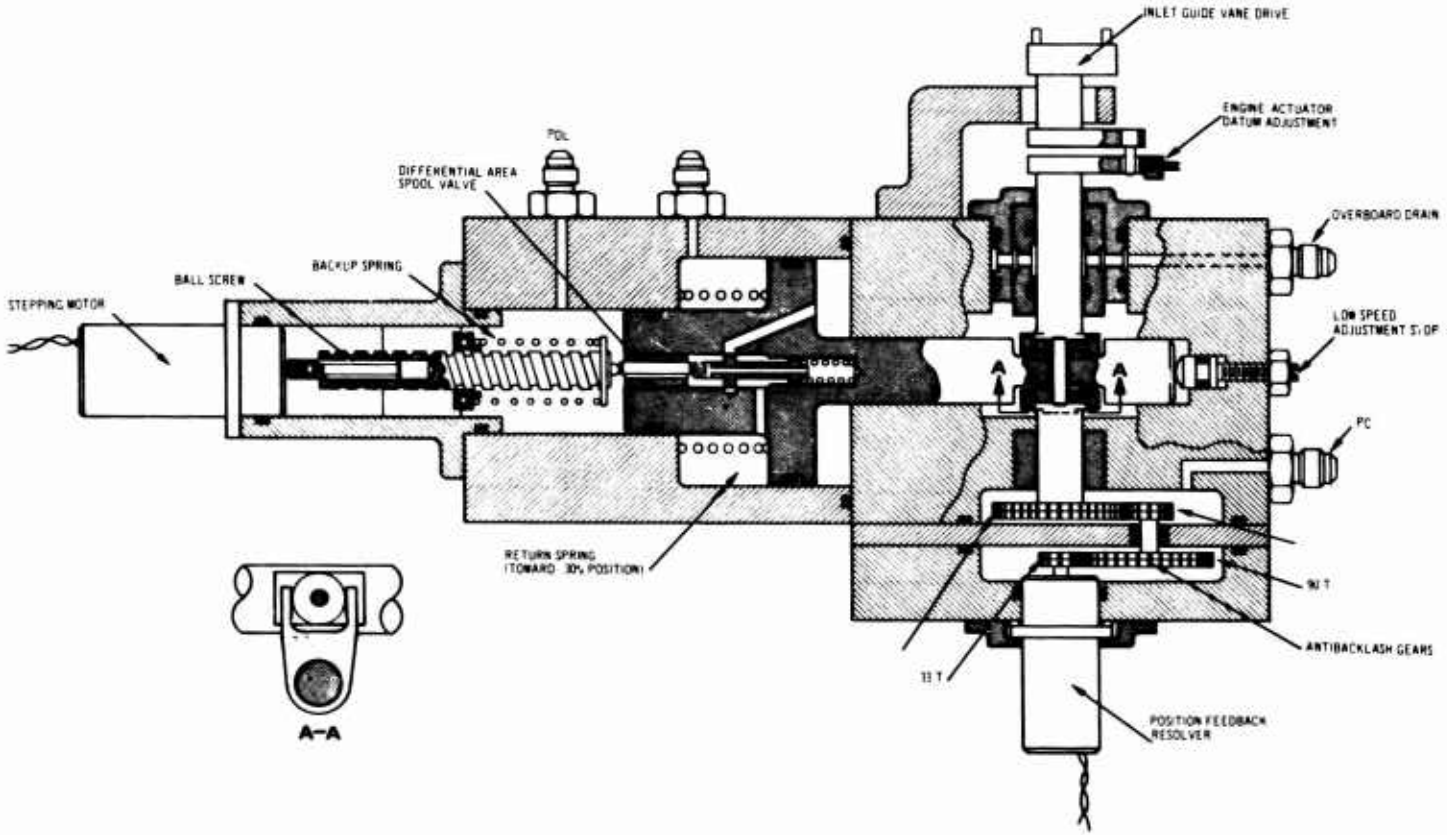

Figure 45. IGV Actuator

converted to axial displacement by a ball screw; the pitch of the ball screw is 0.1 inch. The axial movement of the ball screw translates a three-way servo valve in the center of the actuator piston. Filtered high-pressure fuel (P_a) is ported to one side of the actuator piston. The spool valve and actuator piston form a position follow-up servo. Axial movement of the piston is converted to rotation by a fork mechanism on the output shaft. The output shaft is supported in bronze journal bearings. A preload spring is provided to position the inlet guide vanes in the closed position (30°) at start-up when no electrical or fluid power is available. The spring is sized to provide a minimum force of 35 pounds, which is sufficient to overcome the seal friction and 14 in.-lb of inlet guide vane friction.

A resolver provides the feedback of inlet guide vane position to the electronic computer. The inlet guide vane rotation is amplified with antibacklash gears to provide 335° rotation of the resolver for 45° rotation of the inlet guide vanes.

In the event of an electrical power failure, a backup control is provided using a pressure speed signal from the pump. The three-way spool valve has a differential area. Pump pressure rise acting on the differential area provides a force acting toward the ball screw. The pressure force is compared to a spring force, and the difference causes the spool valve and actuator piston to move. The fuel supplied to the spool valve is from the centrifugal pump and, therefore, is a function of gas generator speed. $P_s - P_x = 0.088\% N_g^2$. Hence, the backup control positions the inlet guide vanes as a function of gas generator speed with no engine inlet temperature correction. The theoretical schedule is shown in Figure 46 for standard day conditions.

The inlet guide vane torque requirements are shown in Figure 44. The actuator piston size is determined by the ball screw size plus space required by the return spring. This results in a piston which is larger than that required to drive the actuator load. For example, the force available to open the inlet guide vanes at a minimum gas generator speed is 120 pounds

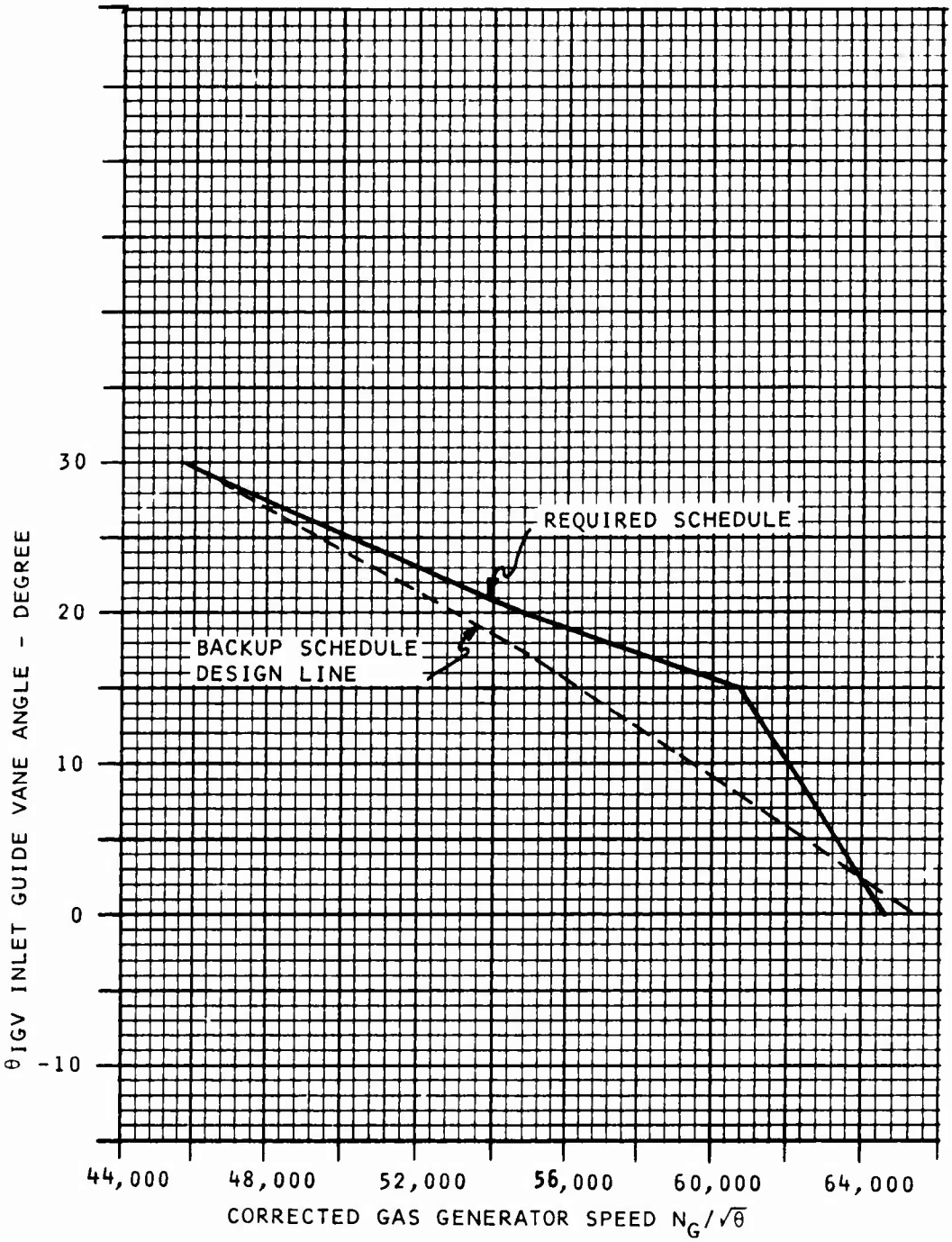

Figure 46. Inlet Guide Vane Backup Schedule

compared to the load requirements of 31 pounds. In the inlet guide vane closing direction, the force available is 393 pounds compared to a load requirement of 49 pounds.

The resolution of the actuator is 0.44° inlet guide vane movement for one 15° step of the stepping motor. Deflections due to loads are sufficient to keep the accuracy to within $\pm 1/2°$. The transient response of the actuator was demonstrated to be within 1° during previous programs. The actuator for this program theoretically has to move twice as fast because the engine speed scheduling range is half of the previous requirement. However, this design has less than half the piston area; therefore, there will be no problem meeting transient requirements.

During initial engine testing, the geometry actuator performed erratically, giving evidence that the servo valve and ball screw were not maintaining contact. Although this fault could not be repeated on the control test stand, the problem was eliminated by directly coupling the spool valve and ball screw with a wire. The redesign is shown in Figure 47.

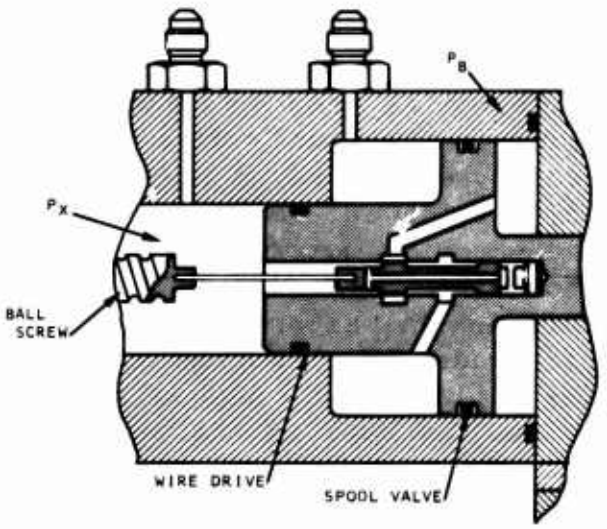

Figure 47. Servo Valve/Ball Screw Wire Coupling

After the spool valve drive was modified, the geometry actuator satisfactorily completed 21 hours of testing mounted on the engine including 8.6 hours mounted on the engine and driving the guide vanes. The test results of inlet guide vane against corrected gas generator speed were shown in Figure 26.

Bench Tests

Bench testing of the geometry actuator consisted of calibrating the spool valve, mechanically moving the spool valve and checking the actuator output position, pulsing and slewing the stepping motor with a power supply separate from the alternator, and testing the backup system. All closed-loop system testing was done in conjunction with the electronic computer and alternator.

The lands of the spool valve were ground to give optimum pressure gain about the null position. The gain achieved was 143 psi/.001 inch with a servo supply pressure of 520 psig, which is typical for a three-way servo valve.

Backup Control Mode

The axial pressure force on the three-way spool valve is a function of the supply pressure (P_s), which acts on the spool valve differential area as shown in Figure 45. The pressure supplied to the spool valve was set by hand, and it was found that the balance of pressure against spring force was so critical that the design value of current supplied to the stepping motor (0.6 amp) produced insufficient torque to drive the ball screw. It was found that 1 amp was required. The alternator was not designed to provide 1 amp; because of this, the differential area spool valve was replaced with a spool valve of constant diameter to reduce the load on the stepping motor.

The spool valve design change eliminated the capability of demonstrating the backup system on the engine; however, the backup system concept was demonstrated during bench testing. The test data of inlet guide vane angle against servo supply pressure is shown in Figure 48. This schedule was produced by trying different backup spring rates

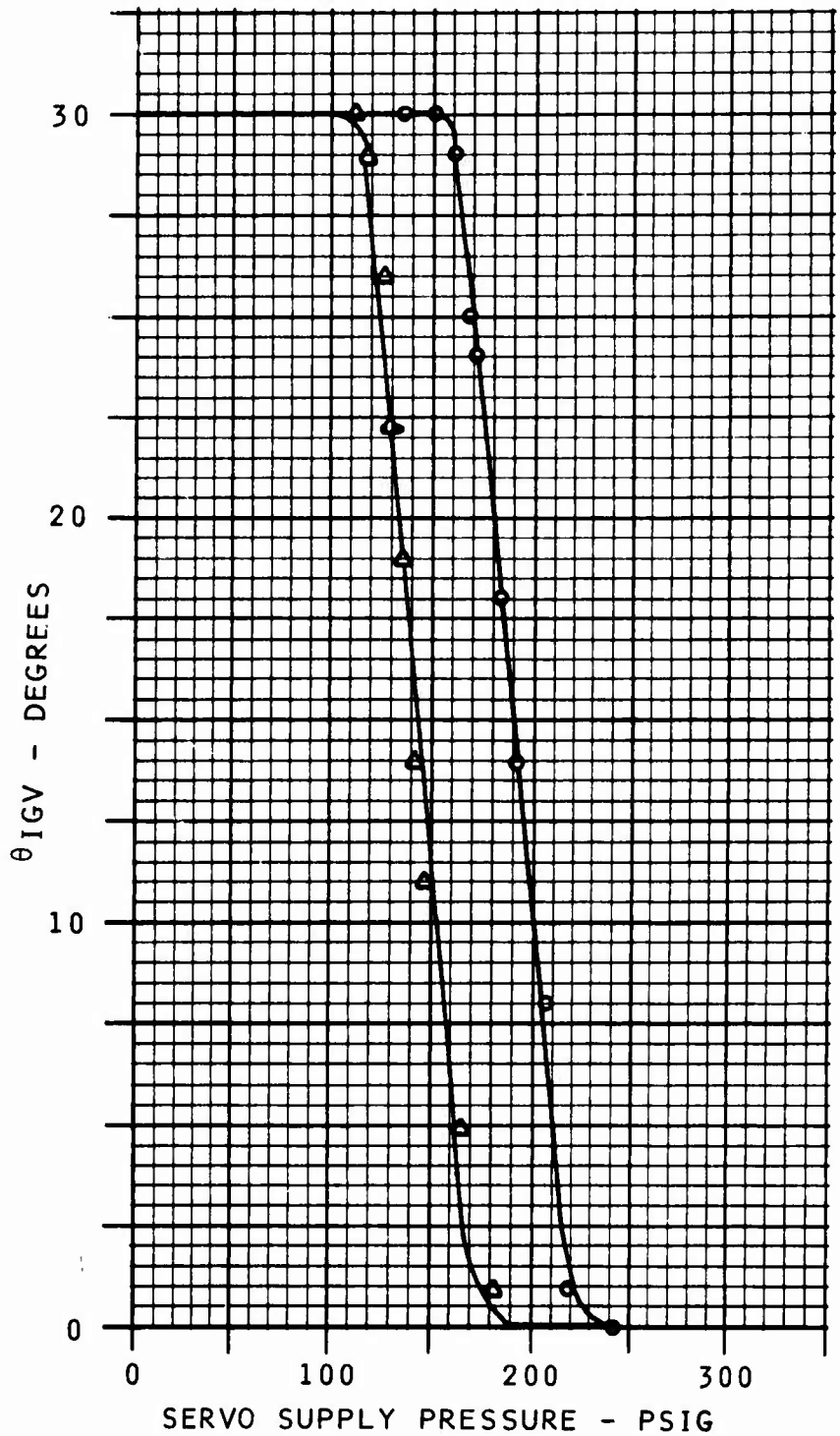

Figure 48. IGV Backup Control Mode Test Data - Bench Test

to produce a smooth movement of the geometry actuator as a function of servo supply pressure. This method optimizes the force balance on the servo valve.

The constant-diameter spool valve design was assembled into the actuator, and then the geometry actuator was tested closed-loop in conjunction with the electronic computer, alternator and pumps. No further problems were experienced.

PUMP/ALTERNATOR

The pump and alternator module is mounted in the nose cone of the engine and operates at engine shaft speed. The pumping system consists of a centrifugal main stage and a centrifugal boost stage operating on a common shaft direct-driven through the alternator rotor shaft from the engine main shaft. The permanent magnet (samarium cobalt) alternator provides six separate windings: two each for control power, stepper motor drives, and engine ignitors. The orientation of the pump/alternator components provides:

1. An unobstructed inlet to the boost impeller to ensure .45 V/L capability.

2. Isolation of pump shaft from alternator shaft to eliminate alignment problems.

3. Separation of fuel and engine oil by the alternator cavity which is vented to drain.

4. Insulation of the boost area from the higher temperature main discharge.

5. Axial location of the alternator shaft by the engine shaft.

Design Requirements

Fuel flow requirements for the engine are as follows:

At rated condition - ΔP 500 psi min
Fuel Flow 380 pph
RPM 65,000

At starting - ΔP 21 psi
Flow 23 pph
RPM 11,000

where ΔP is the pump pressure rise, (P_{dis}-P_{inlet})

The pumping system is sized to meet the starting requirements and produces 730 psi at rated conditions. Oversizing the pump is required to ensure adequate starting performance. The advantage of this design is the elimination of a separate positive displacement starting element.

The pumping elements must also be sized to provide an additional 100 pph of fuel for IGV actuation.

Boost Stage Requirements

RPM 65,000
ΔP 80 psi
Flow 500 pph
Inlet 50 psi max to 5 psi above TVP min
V/L = .45
ΔP at .45 V/L = 40 psi min

Main Stage Requirements

RPM 65,000
ΔP 700 psi
Flow 500 pph

Design Description

Impeller design parameters for the boost and main stages are summarized below.

Boost Stage

RPM	65,000
ΔP	80 psi
Flow	500 pph
N_s	1100
Head Coefficient	.3
No. of Blades	3
O.D.	.583 in.
Inlet Diameter	.234 in.
Inlet Angle (Tip)	14.8°
Type	Constant lead conical
Material	AMS 5643
Collector	Constant area with conical diffuser

Main Stage

RPM	65,000
ΔP	700 psi
Flow	500 pph
N_s	241
Head Coefficient	.65
No. of Blades	14
O.D.	1.129 in.
Inlet Diameter	.325 in.
Type	Radial open blades
Material	AMS 5643
Collector	Constant area with conical diffuser

Mechanical Design

The two pump impellers are mounted overhung on each end of a common shaft. A common journal bearing supports the impeller shaft. Thrust surfaces at each end of the bearing prevent axial movement. A cross section of the pump is shown in Figure 49, and a photograph of the boost and main impellers is shown in Figure 50.

The impeller bearing design is summarized below.

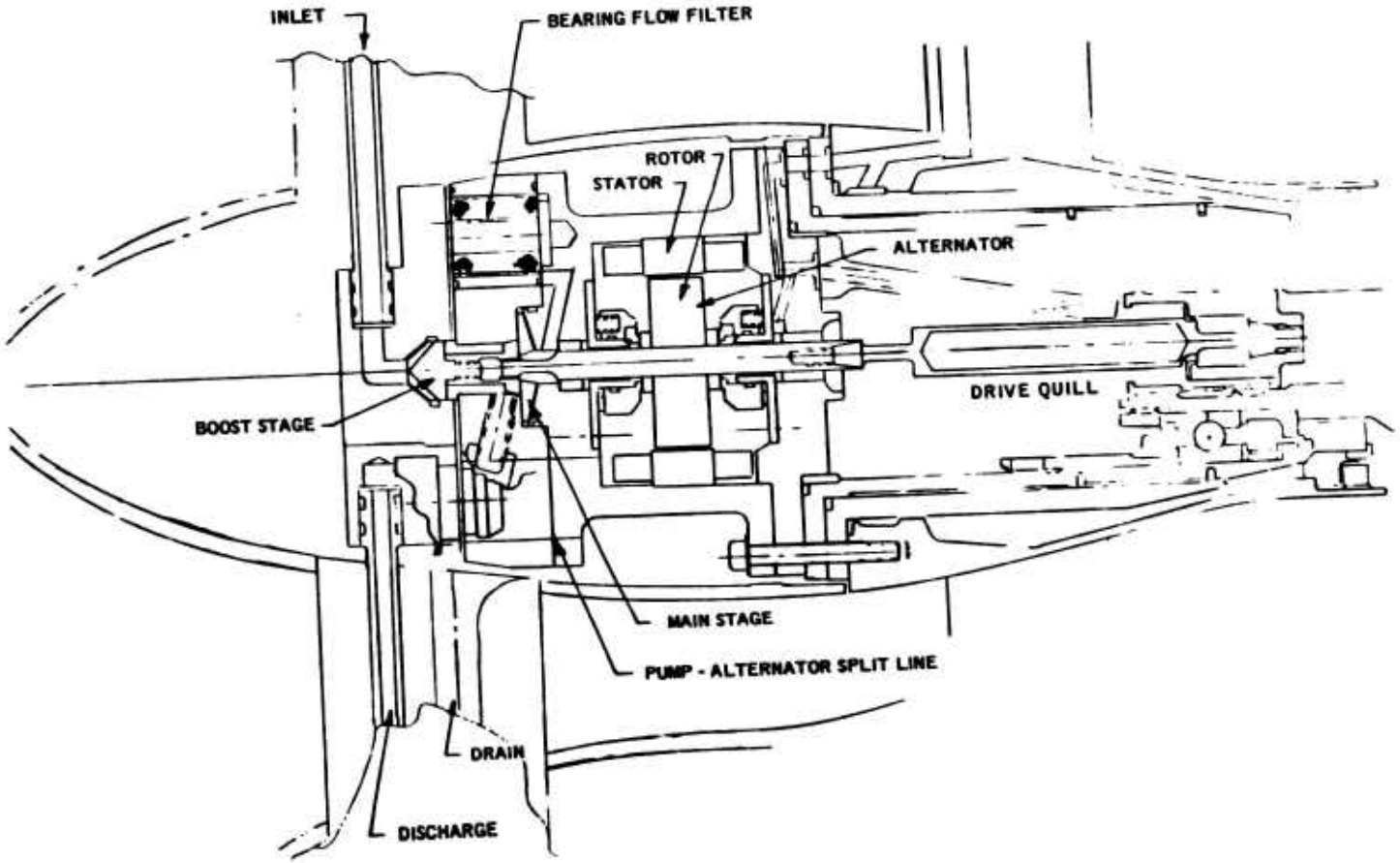

Figure 49. Pump/Alternator Cross Section

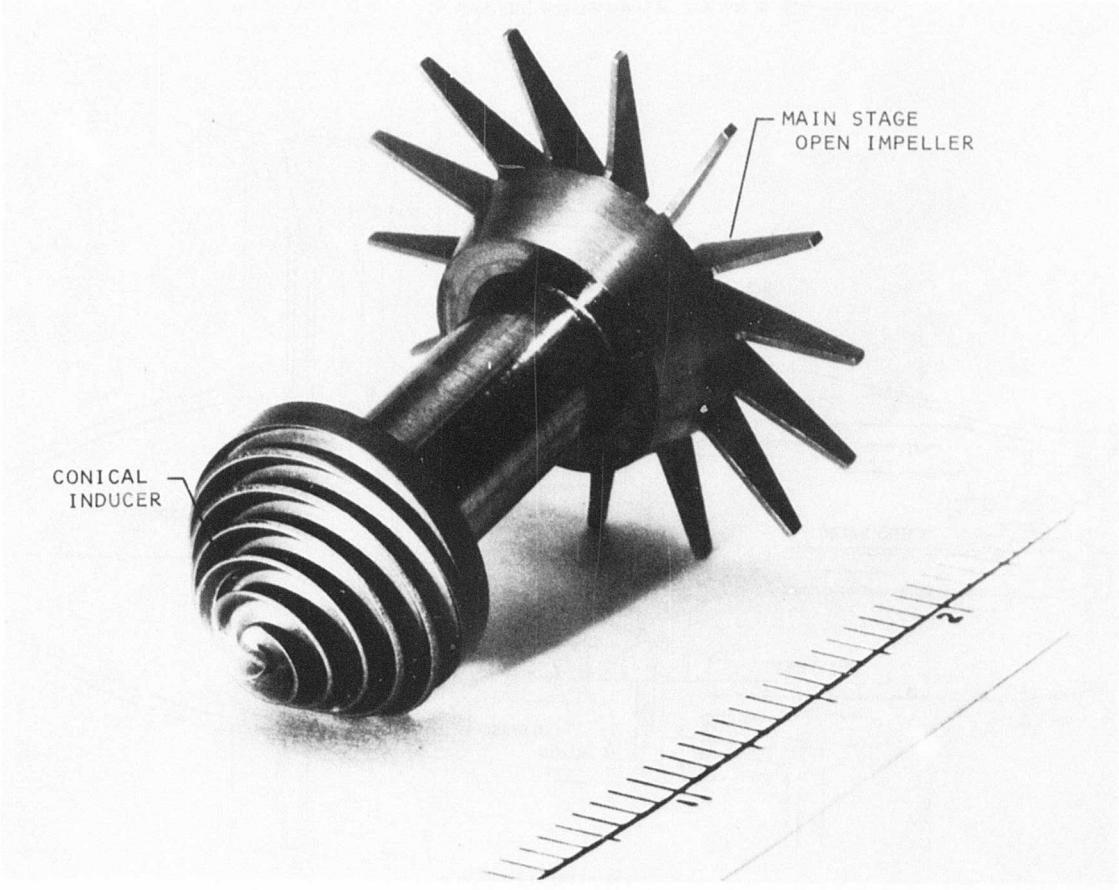

Figure 50. Boost and Main Impeller

Radial Loads -	Main Impeller	7.74 lb
	Boost Impeller	1.25 lb
Resulting UBL		54.6 psi
Journal Velocity		4779 ft/min
PV		261,163 psi ft/min
Shaft Area x ΔP		4.9 lb
Thrust face area		.202 $in.^2$
UBL		24 psi
Velocity (O.D.)		9864 ft/min
PV		236,755 psi ft/min

The bearing material is Pure Carbon Company P5AG. Journal material is AMS 5643. Journal-bearing diametral clearance is .0005-.0009 in.

1. Shaft Seals

Two shaft seals are used to prevent fuel and oil from the bearings from leaking overboard. The fuel seal must seal against pump inlet plus boost pressure rise. A balanced seal design was selected with an 8-pound spring preload. Calculated PV for this seal is 1,059,045 psi ft/min. Seal data are summarized below:

Seal face material - silver-impregnated carbon
Seal runner material - AMS 5616 with Linde LC-11 60% chrome carbide coating

RPM 65,000
ΔP 135 psi
Load 8 lb
Area .0643 $in.^2$
O.D. .50 in.
Velocity 8515 ft/sec

$$UBL = \frac{8 \text{ lb}}{.0643 \text{ in}^2} = 124.37 \text{ lb/in.}^2$$

Calculated power loss .020 hp

The oil seal seals against engine oil pressure. The seal is identical to the fuel seal except for the preload springs. Oil seal data are summarized below.

RPM 65,000
ΔP 40 psi
Load 4 lb
PV = 529,522
Calculated power loss .01 hp

The impellers are driven through the alternator shaft with the three in-line bearings line bored to ensure proper alignment.

The impeller shaft bearing and the alternator fuel side bearing are lubricated by fuel from the main stage discharge. Flow rate is regulated through an orifice for each bearing. The AMS 5643 shaft runs in a Pure Carbon Company bearing material P5AG.

The oil side alternator bearing is lubricated by oil from the engine. An orifice regulates the flow to 7 pph. Materials and clearances are identical to those of the impeller side bearing.

2. Shaft Stress Calculations

The torque required to turn the pump is 5 in./lb. The maximum stresses in the impeller drive shaft are located between the drive spline and the thrust face undercut. The material used is AMS 5643.

Stress values calculated are:

Combined shear	1439.4 psi
Tension	1440.0 psi

A safety factor of 3.32 has been calculated for the alternator shaft pump drive quill.

Calculations for tooth shear capacity and compressive wear torque capacity show a safety factor of 23.1 for tooth shear and 1.34 for compressive wear.

The above calculated values plus test experience demonstrated adequate strength in the drive train shafting and splines.

3. Vibration Analysis

An analysis of the drive system as composed of two masses connected by a torsional spring, one mass being the two impellers and connecting shaft and the other mass the alternator rotor calculated the natural frequency of the system as 1718 Hz.

Rotation of the impeller's 14 blades at 65,000 rpm impresses a frequency of 15,166 Hz.

An analysis of the impeller and alternator assembly as one mass on the end of a torsional spring calculated the natural frequency at 654 Hz.

From the above calculations, it is concluded that torsional vibration should not be a problem in the normal range of pump operation (758.3 x 1083.3 Hz).

4. Critical Speed

Critical speed calculations for the alternator shaft and alternator rotor assembly show an expected critical speed of 94,000 rpm. This value is sufficiently high to ensure that the unit will not operate at or near the first critical speed.

Bench Test Results

Testing of the pump included head-flow calibrations of boost and main elements and temperature rise evaluation of the combined elements. In addition, V/L testing of the boost element was accomplished in a test fixture. Testing of the complete pump/alternator was accomplished using the engine quill shaft in a special test fixture to simulate the engine installation.

Development testing of the unit disclosed that a nitrided steel seal runner was not adequate to meet the fuel seal requirements. A chrome carbide surface on an AMS 5616 steel ring provided a satisfactory seal runner material.

The test program demonstrated satisfactory seal performance for 50 hours of operation prior to termination of testing.

Figure 51 shows a complete pump calibration from 70% to 100% rpm. At a starting speed of 11,000 rpm, the pump produced 23 psi at 23 pph fuel flow. Temperature rise data is plotted in Figure 52.

A head-flow calibration of the boost stage is plotted in Figure 53. V/L performance of the boost impeller running in a test fixture is shown in Figures 54, 55 and 56. The impeller was capable of .45 V/L with a maximum flow of 225 pph.

Final calibration of the pump after bench and engine testing is shown in Figure 57. No degradation in performance was evident throughout the test program.

The pump accumulated approximately 100 hours of bench testing and 40 hours on the engine. The pumping system met the requirements for starting and operation through the STAGG engine speed and power range, including both environmental control mode tests and active control mode tests.

Further development effort is required to increase flow capacity of the boost impeller at .45 V/L. Also, it is recommended that further endurance testing be conducted to determine the life expectancy of the face seals and journal bearings.

Inspection of the pump after engine tests and final bench calibration showed that the fuel-lubricated journal bearing had worn about .0005 in. However, the drive spline, face seals and oil-lubricated journal bearing were in very good condition.

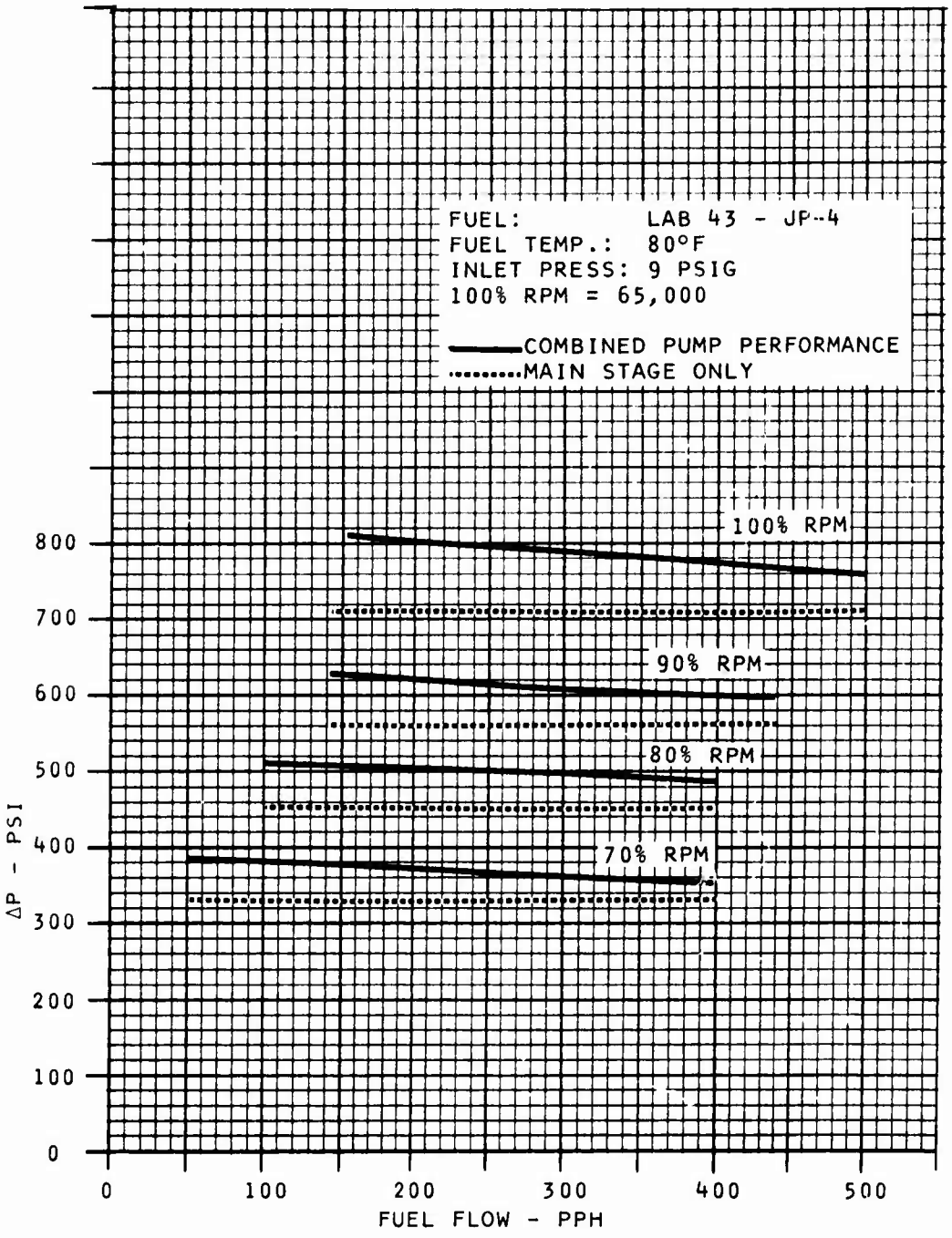

Figure 51. Pump Calibration - Bench Test

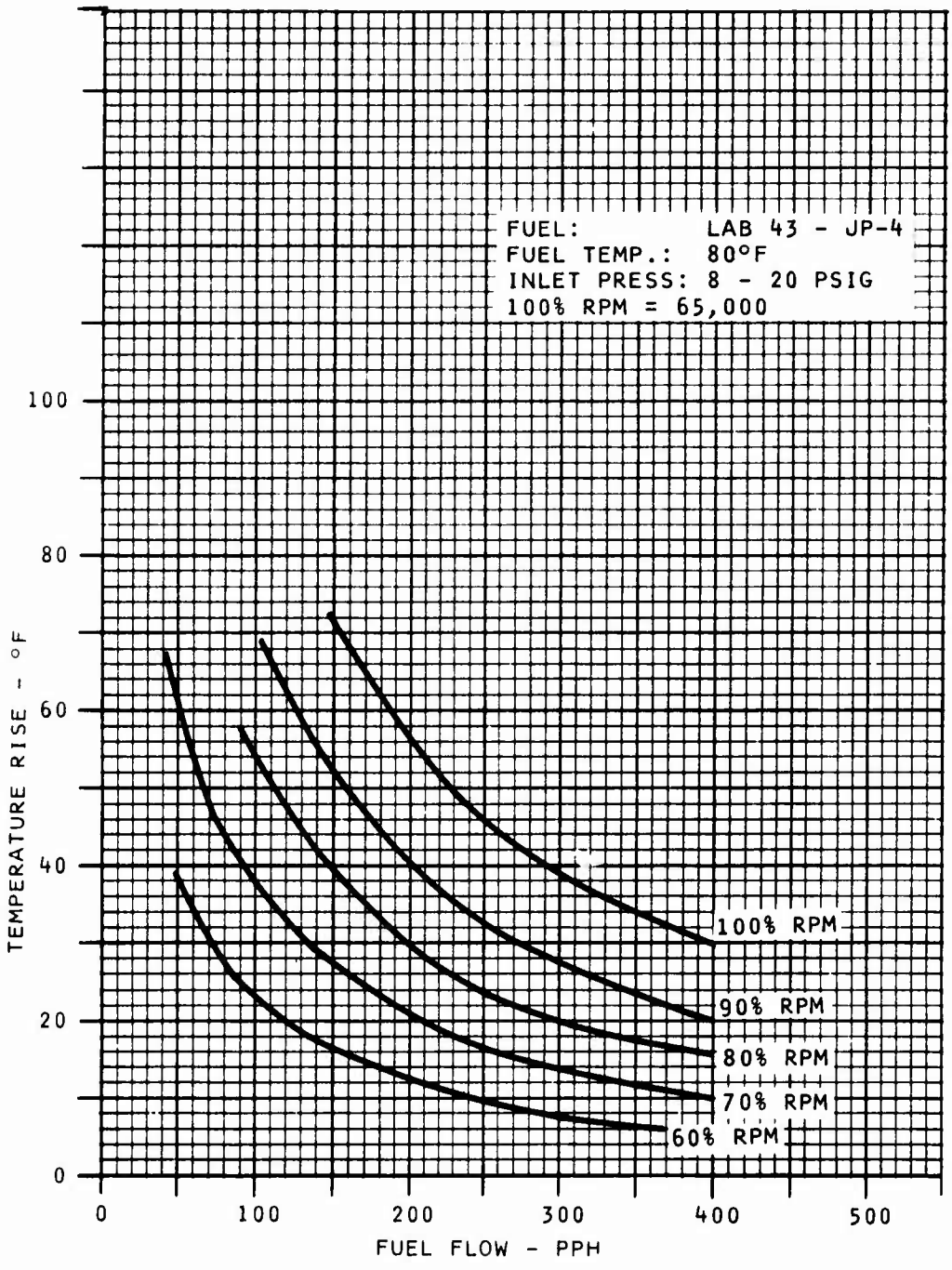

Figure 52. Pump Temperature Rise - Bench Test

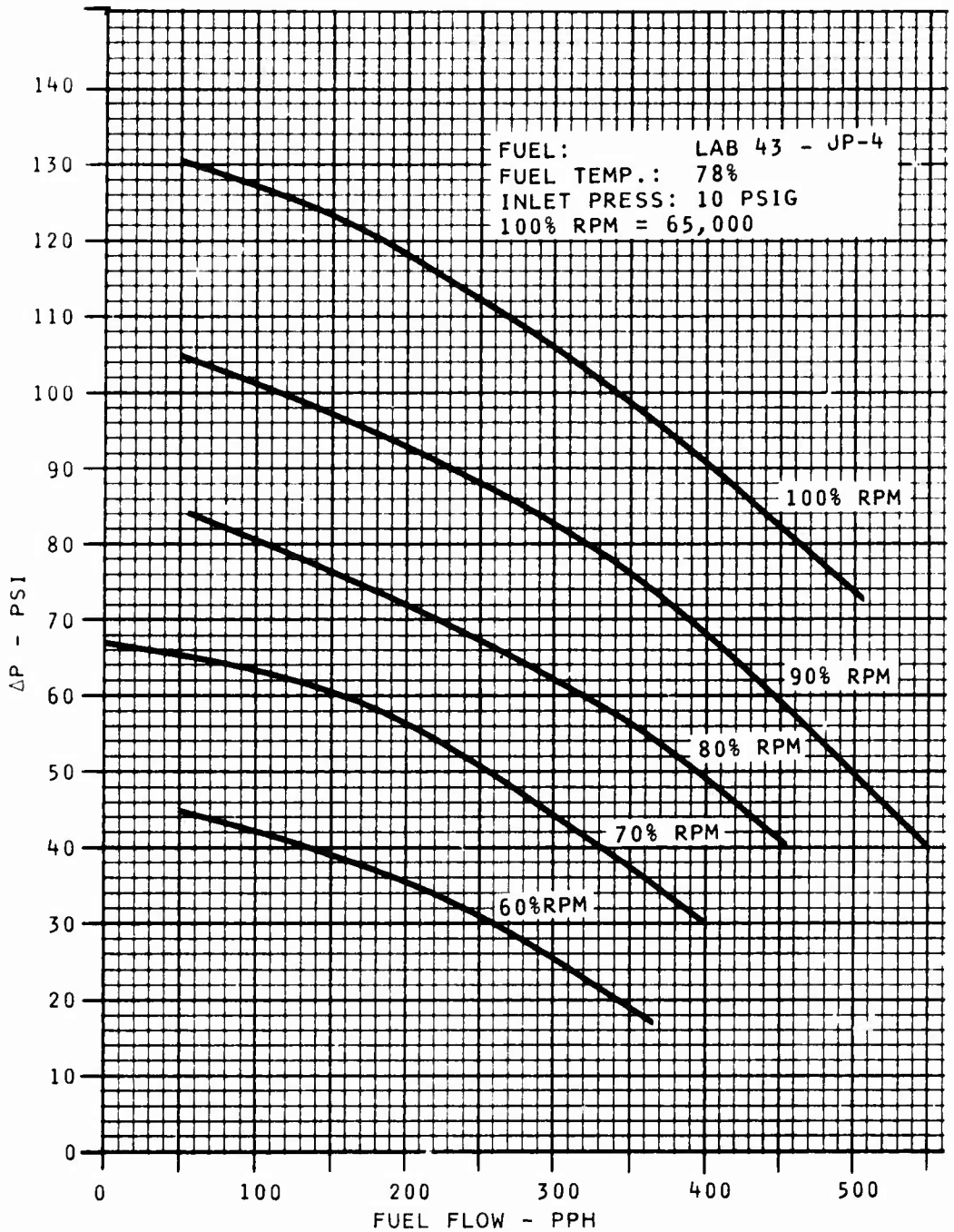

Figure 53. Boost Stage Calibration - Bench Test

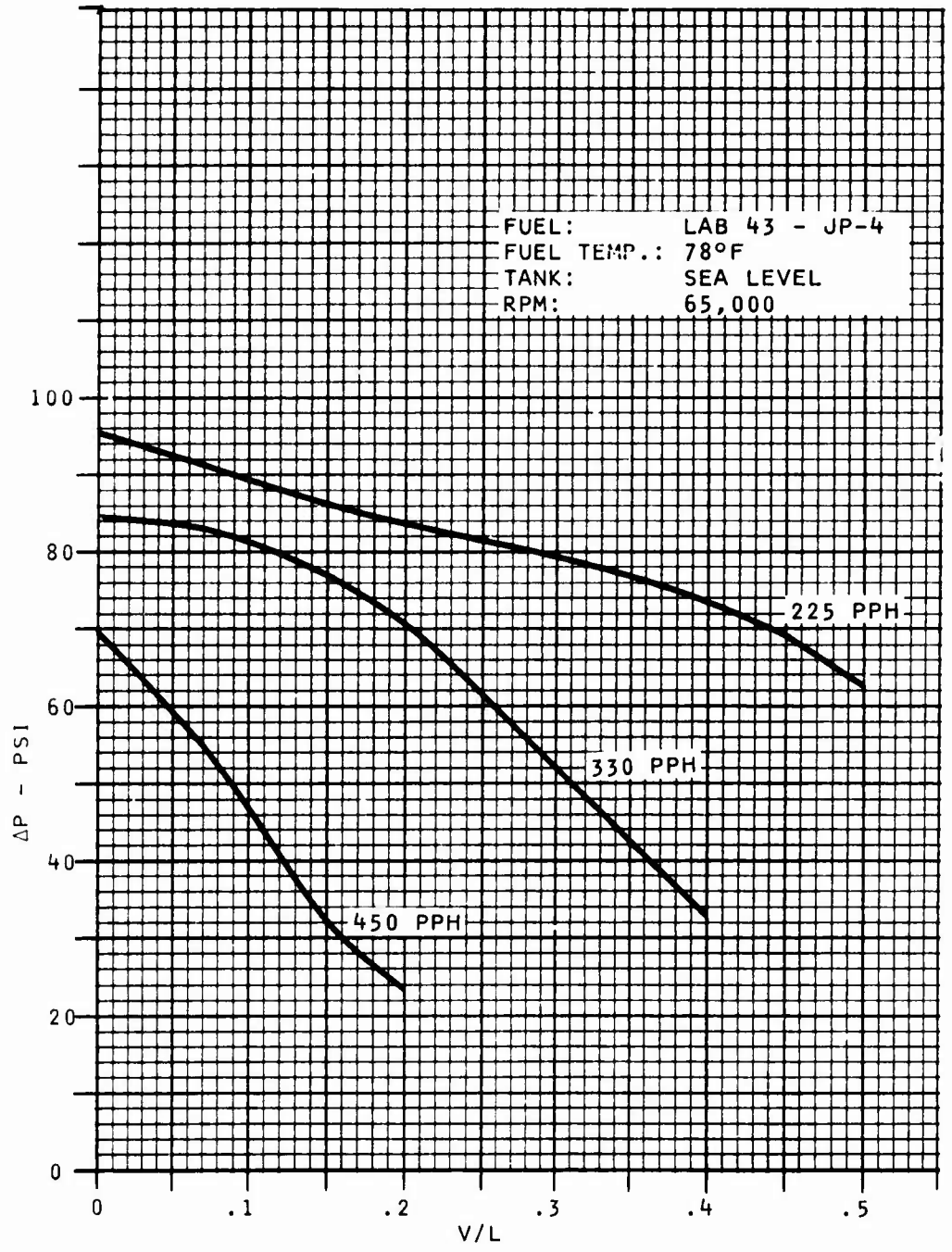

Figure 54. Boost Pump V/L - Sea Level Bench Test

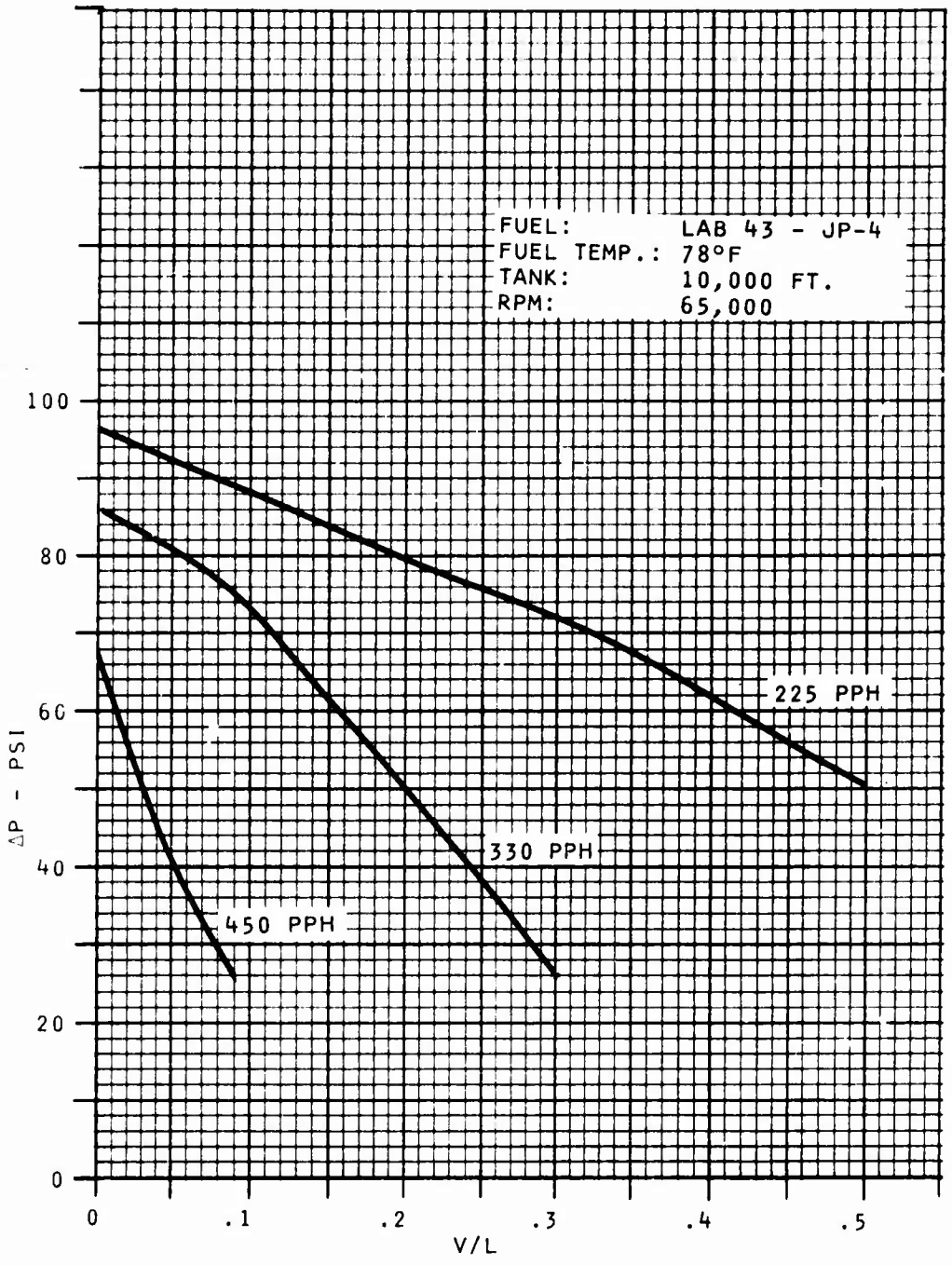

Figure 55. Boost Pump V/L - Bench Test for 10,000 Feet Altitude

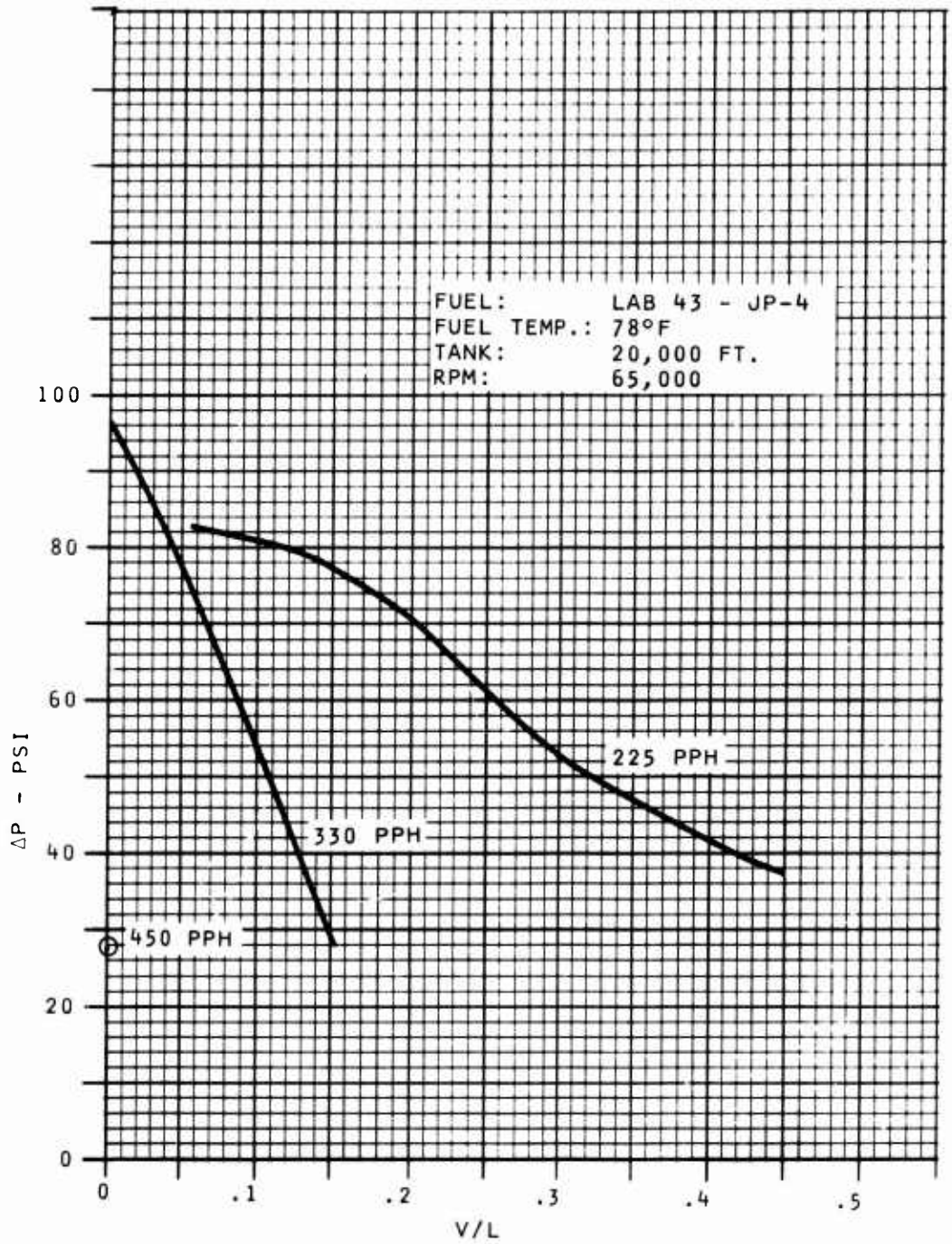

Figure 56. Boost Pump V/L - Bench Test for 20,000 Feet Altitude

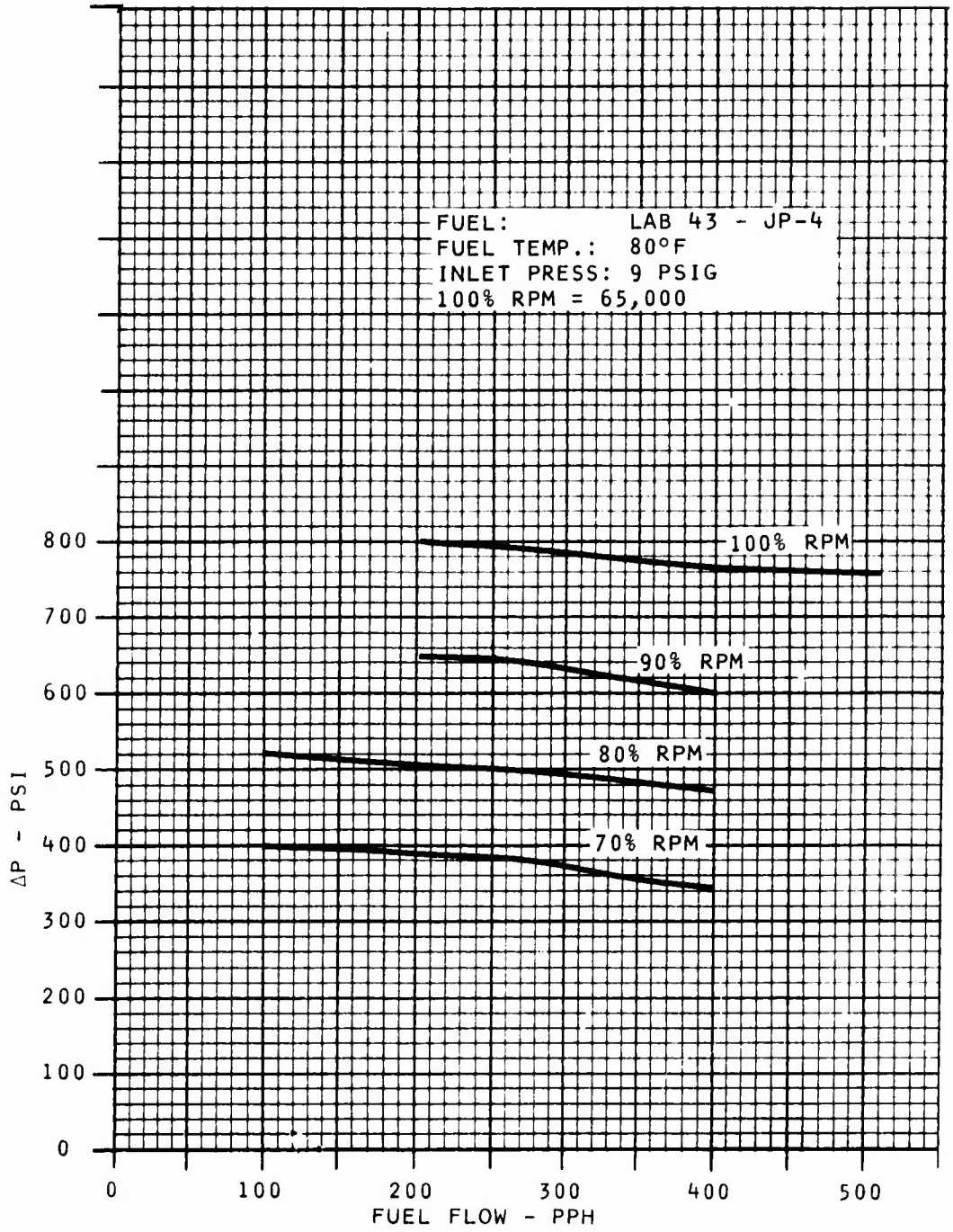

Figure 57. Final Pump Calibration - Post Engine Bench Test

ELECTRONIC COMPUTER

The electronic computer was designed specifically for testing on the FRDC Small Turbine Advanced Gas Generator. However, the design incorporates provisions for all functions necessary in a complete helicopter gas turbine engine control. As such, the designed package includes space for the power turbine governor, rotor shaft torque limiting, twin-engine load sharing, and collective pitch load anticipation. Basically, the computer is a special-purpose hybrid incorporating low-power CMOS electronic components. However, flexibility is included by the incorporation of programmable read-only memories (PROM's) for the acceleration and IGV bivarient functions and the fault isolation test data. The PLA schedule also has the flexibility of changing the idle and maximum power flats with an adjustable dual slope intersection between the two flats. A detailed description of the computer design is included in the following sections.

Design Requirement

The electronics were designed to be mounted on the engine bellmouth. The environmental limits set were:

Vibration

0.0001" double amplitude from 20 Hz to 1050 Hz axially
0.001" double amplitude from 20 Hz to 1050 Hz axially

Ambient Temperature

-65°F to 180°F

Ambient Pressure

5.5 to 20 psia

The operational goals were as follows:

Power Dissipation - less than 10 watts
Component Temperature - 200°F maximum
Computational Accuracy as follows:

Acceleration schedule	±2.1% of rated ratio units
Deceleration schedule	±3.5% of rated ratio units
IGV schedule	±1.5% of range
PLA schedule	±1.5% of rated ratio units
Speed governor	±0.5% of rated ratio units
Temperature limiting	±2.5% of rated ratio units
P_b multiplication	±0.5% of point

Packaging

Figure 58 presents the layout of the electronic computer package. The majority of the components are mounted on three multilayer printed circuit boards (designated A, B and C for discussion) with a packaging density of between 70 and 78%. The remaining electronic components are mounted on a fourth, much smaller, double-layer PCB, designated D.

The functions contained on each board are as follows:

Board A

1. Alternator interface and voltage regulation for the electronic computer.

2. MMV position loop including the stepper motor drive and resolver interface.

3. IGV position loop including the stepper motor drive and resolver interface.

4. MMV minimum flow stop function.

5. Fuel shut off control functions.

6. Buffered test points for the applicable elements on this board.

Board B

1. Space allocation for the power turbine section for a turboshaft engine control that includes load sharing,

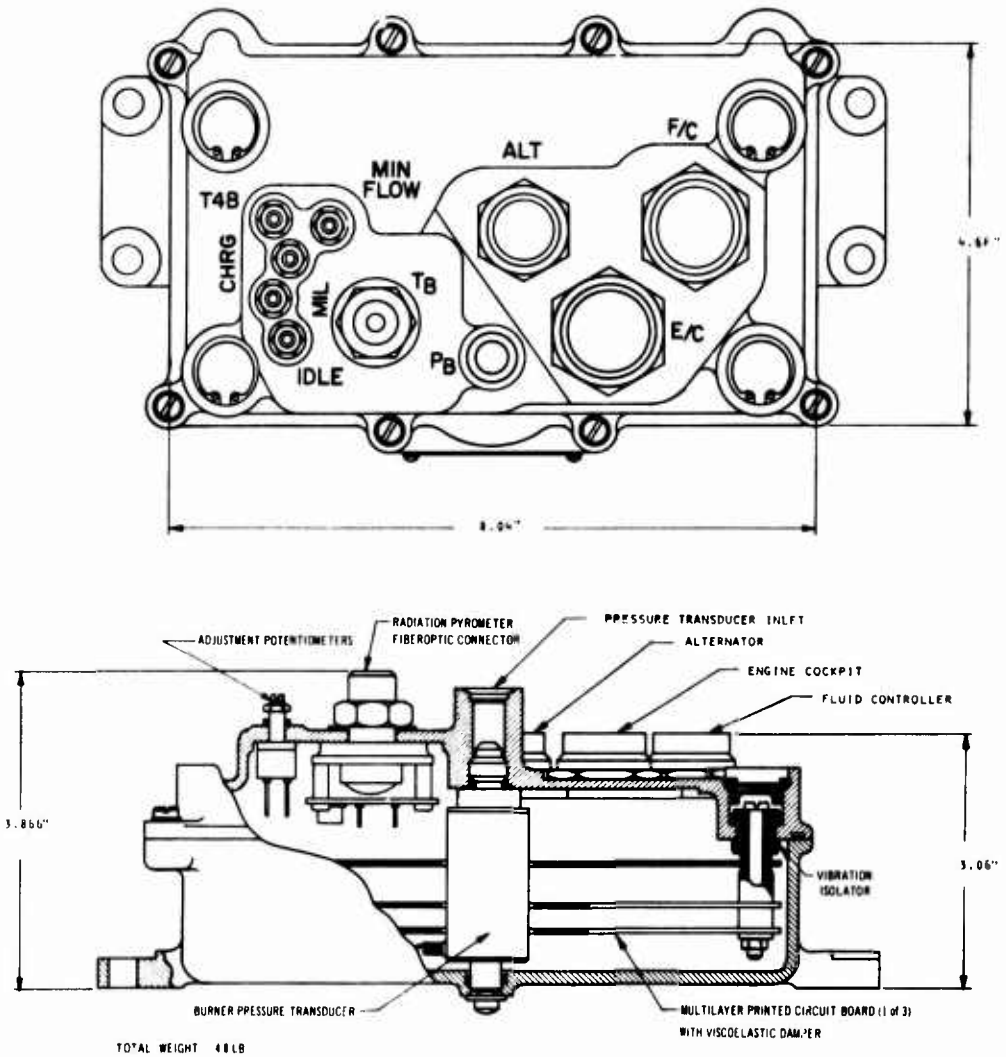

Figure 58. Electronic Computer Layout

overtorque protection, collective pitch load anticipation and power turbine governor integrator reset.

2. Select low and high circuits.

3. PLA to corrected set speed schedule.

4. $\sqrt{\theta}$ conversion.

5. Computer oscillator and timing circuit.

6. N_g speed signal processing.

7. Buffered test points for the most significant signals on this board.

Board C

1. Fault isolation functions.

2. Acceleration schedule $W_f/P_b = f(N_g, T_{t2})$

3. IGV schedule $\theta_{IGV} = f(N_g, T_{t2})$

4. P_b transducer signal processing, together with W_f/P_b multiplier.

5. Radiation pyrometer failure detector.

Board D

1. Radiation pyrometer signal processing.

Three hermetically sealed connectors are provided: one each for interfacing with the alternator, fluid controller and test interface box.

Five single-turn externally adjustable potentiometers are provided: one each for setting idle speed, maximum speed, minimum flow stop, fuel line charging time adjustment, and turbine blade temperature limit.

The P_b pressure transducer is mounted within the computer package. For rigid support, the transducer screws into the pressure port in the cover and is screw fastened to the base of the housing.

Also included within the package is the photovoltaic detector used in the radiation pyrometer function. This element is mounted on the rear of Board D, thereby minimizing the interconnection length between the detector and the first stage of signal processing in the pyrometer function. All elements within the package are interconnected via two flexible printed circuit cables. This concept is considered to be superior to that of discrete interconnection wiring because it costs less and is more reliable.

The computer housing is constructed of cast aluminum, and an O-ring seat is provided between the cover and base of the housing. Mounting to the engine is achieved by two flanges that bolt directly to the engine test bellmouth.

Cabling was constructed to interface the electronic computer to the fluid controller, alternator and test interface box. These cables were constructed using individually shielded conductors to provide reliable operation and minimize the effect of external electrical noise.

Vibration Protection

The vibration protection concept used herein was developed during a previous Chandler Evans Army-sponsored program (DAAJ02-72-C-0084). This concept provides for mounting the three main PCBs on four studs using aluminum spacers and bolting the complete assembly to vibration isolators inside the computer cover. Additionally, the backside of each PCB board is bonded to a viscoelastic coated material to form a sandwich construction which provides damping. Testing during previous programs demonstrated that PCB resonance could be limited to 30 g's with a maximum specified input of 20 g's in the plane perpendicular to the surface of the PCB's. Resonance in the plane normal to the surface of the PCBs was negligible.

The vibration specification defined for the FRDC STAGG engine was:

.0001"	d.a.	20 Hz to 1050 Hz axial
.001"	d.a.	20 Hz to HR radial

As a consequence of this specification (50 g's radial), all components within the electronic computer package have been mounted such that their most sensitive vibration axis is in alignment with the engine shaft, thereby taking advantage of the low vibration level in this plane (5 g's minimum). This results in the P_b transducer, connectors, potentiometers, photovoltaic detector, and all active electronic components being mounted in axial alignment with the engine shaft and all the printed circuit boards being mounted normal to the engine shaft.

With this arrangement and with all components conformal-coated, the possible axial vibration levels specified should present no problem to any element within the computer.

With regard to radial vibration, protection for the three main boards is based on the concepts developed during the aforementioned prior program.

The radiation pyrometer photovoltaic detector assembly and associated signal processing on Board D are hard-mounted to the computer housing. This was necessary because of the optical interface. Although this installation exposes the board to the full input vibration, it does not present any problems because all components, including the photovoltaic detector, are suitable for operation at 50 g's. Further, Board D is very small and has a resonant frequency outside of the vibration frequency range of interest.

The P_b transducer is mounted axially in line with the engine shaft, thereby exposing its most sensitive axis to the lowest plane of vibration. The mounting of the transducer, by virtue of the pressure fitting at the front of the transducer and the mounting boss at the rear, provides rigid mechanical support against the radial vibration. The transducer itself is rated for the specified 50 g's radial vibration.

Vibration Bench Testing

A spare electronic housing and printed circuit boards were assembled as a unit for vibration testing. Only one of the three PCB's included components. The results of this testing verified earlier studies, in that the vibration isolator, together with the viscoelastic damping, was necessary for satisfactory vibration isolation at the center of the PCB's. One inherent problem manifested by these tests was a resonance of the housing at about 900 Hz excitation frequency. Further test showed that the resonance was centered at the heavier stock left for mounting the identification plate. Figure 59 shows the original housing vibration characteristics, and Figure 60 shows the results following the remachining of the housing to remove the excess stock. The peak resonance of 76 g's was reduced to 26 g's. The axial vibration of the PCB for a 5 g radial input is shown in Figure 61; as indicated, the housing resonance of 26 g's at 850 Hz has been damped to less than 5 g's.

Cooling

As a result of development work during earlier programs, the electronic cooling concept used in this design consists of:

1. Hard-mounting the computer housing to the engine inlet, thereby allowing the housing to conductively interface with the inlet air to the engine. Also, this area of the engine will provide the lowest ambient temperature.

2. Providing a good conductive thermal path between the computer housing and all components within the package.

3. Minimizing hot spots within the package and keeping total power dissipation and power dissipation/component to a minimum.

By the incorporation of the above features, bench test from previous work showed that component case temperature less than 220°F are possible with an ambient of 180°F. This arrangement

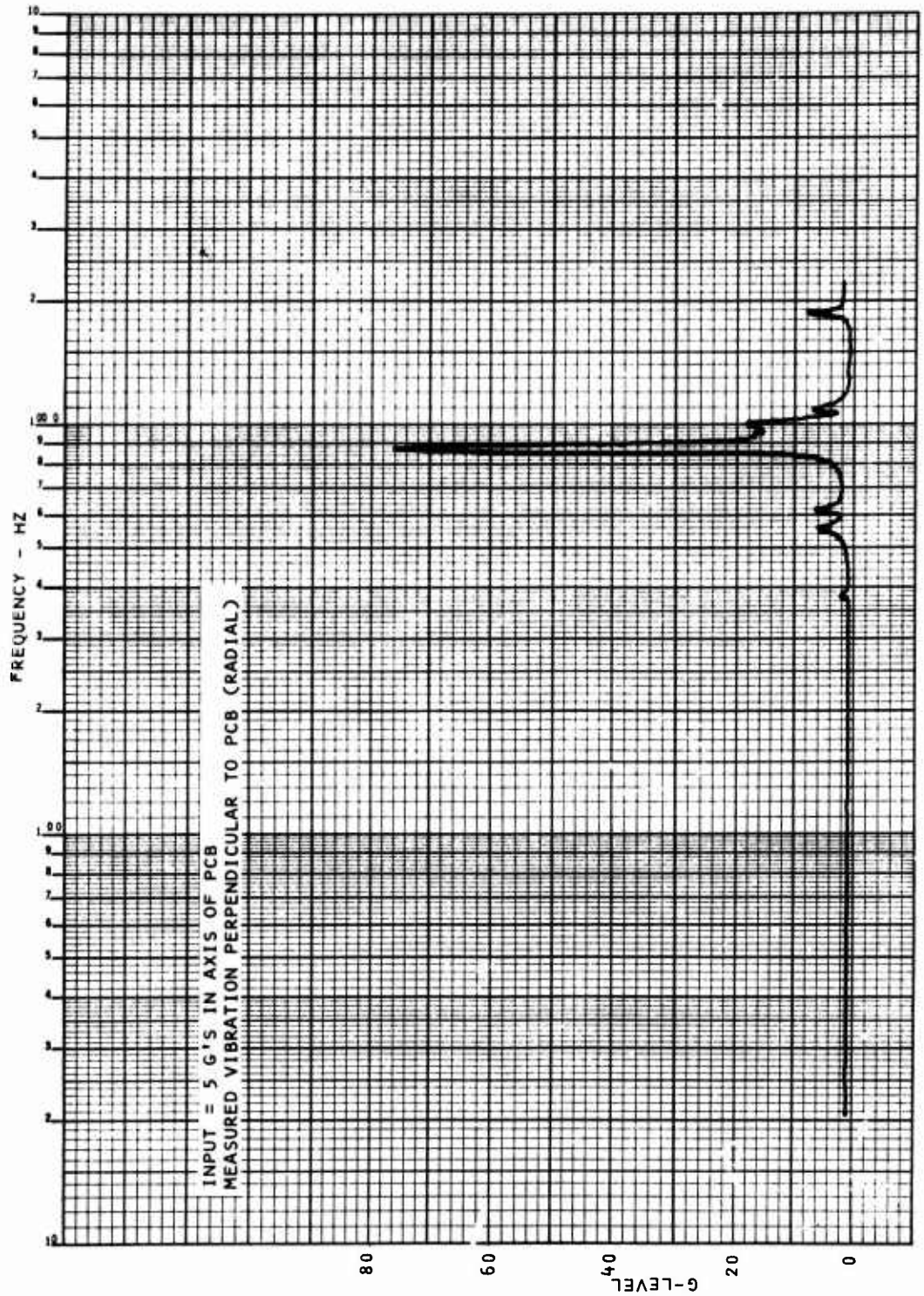

Figure 59. Original Computer Housing Vibration

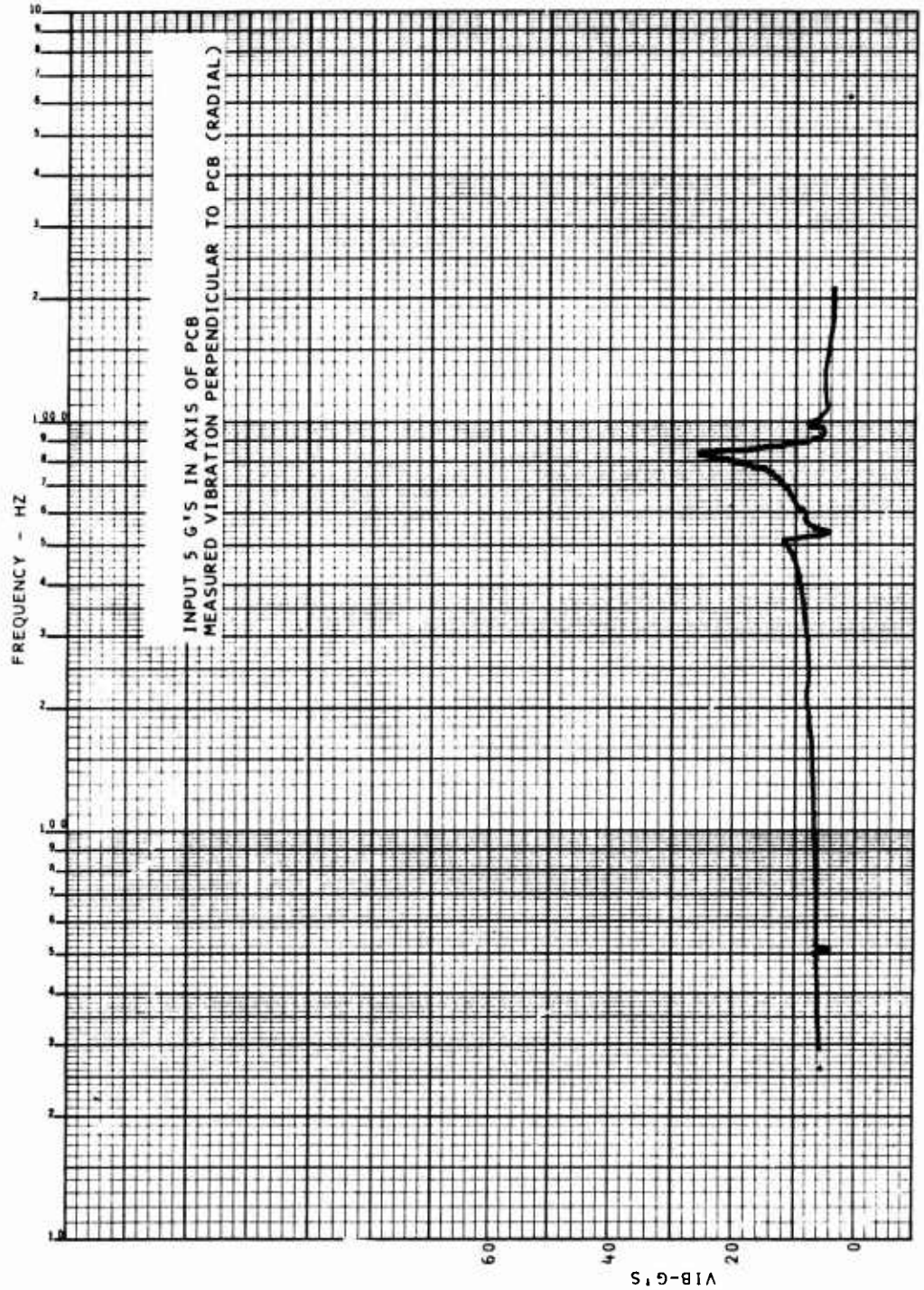

Figure 60. Computer Housing Vibration After Machining

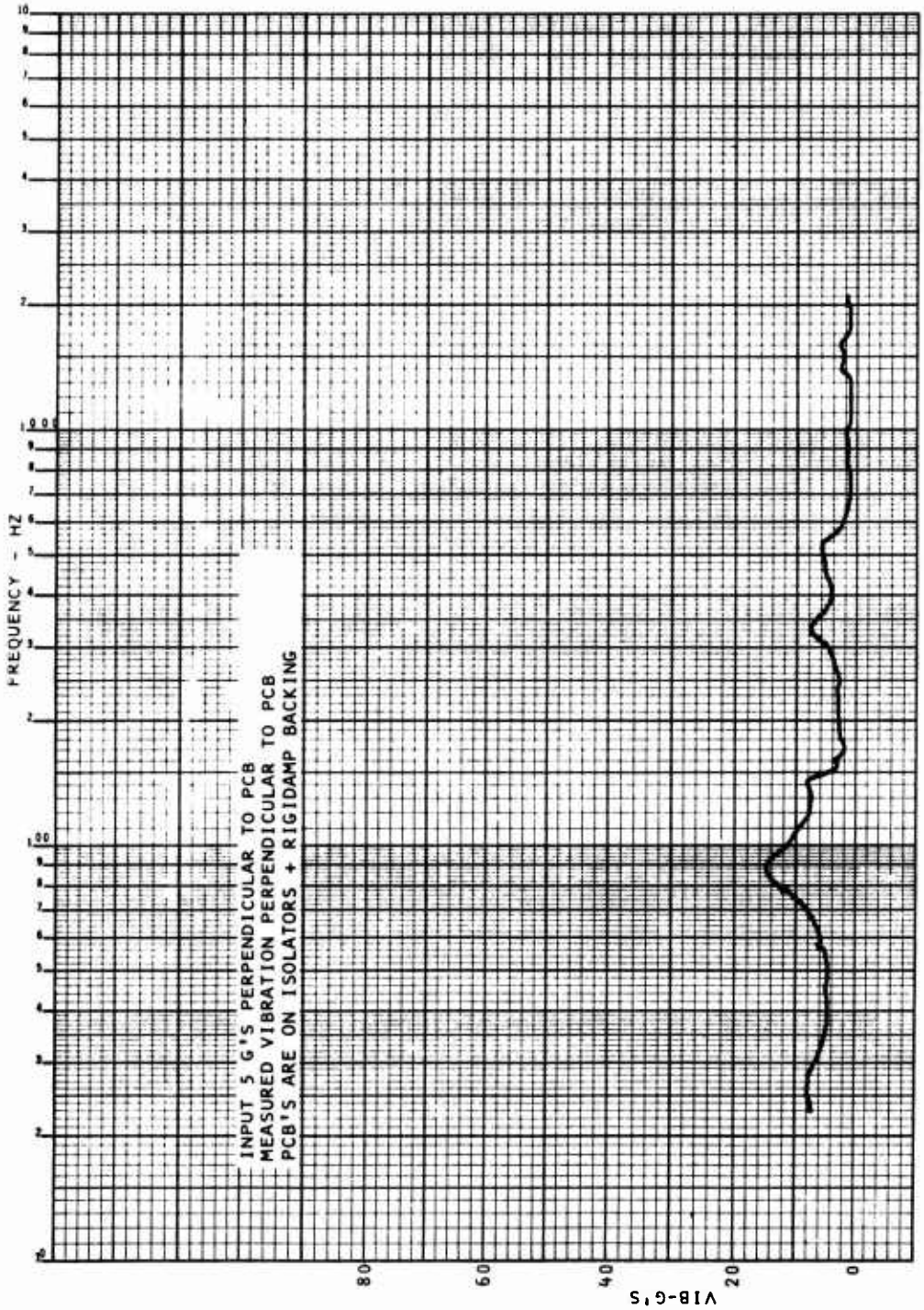

Figure 61. PCB Vibration

provides a healthy safety margin between the maximum allowable component case temperature of 250°F and will thereby improve reliability. For the demonstrator program, 180°F was specified (AV-E-8593A) as the maximum ambient temperature.

For conducting heat and minimizing hot spot temperatures, one layer of each multilayer board is a "thermal plane" comprised of a layer of copper, broken only to provide minimal spacing for component leads. This isolated surface is connected to the housing cover by a flexible braided copper strap.

Functional Design

Figure 62 illustrates the functional block diagram of the electronic computer. In addition to the functions depicted, the computer has been designed to provide space for the functions necessary to implement the power management elements of a full turboshaft engine for twin-engined helicopter application.

The acceleration, IGV and fault isolation functions have been made general purpose in nature. This has been achieved by the use of a Programmable Read-Only Memory (PROM) for each function. Three PROMs are mounted on Board C in plug-in receptacles. With this arrangement, should any function require changing, it is only a matter of removing the computer housing cover, followed by the removal of the subject PROM for reprogramming or replacement by a new unit. The PROMs are held in their receptacles by metal straps and screws.

PLA Interface Schedules

The PLA schedule implemented in the computer includes a multiplication by $\sqrt{\theta}$, thereby providing an output signal proportional to N_g*. Further, the function provides:

1. Independent adjustment of idle and maximum power flats.

2. A dual slope intersection between the two flats even through the present function is a constant gain. Basically, the function is mechanized by defining the

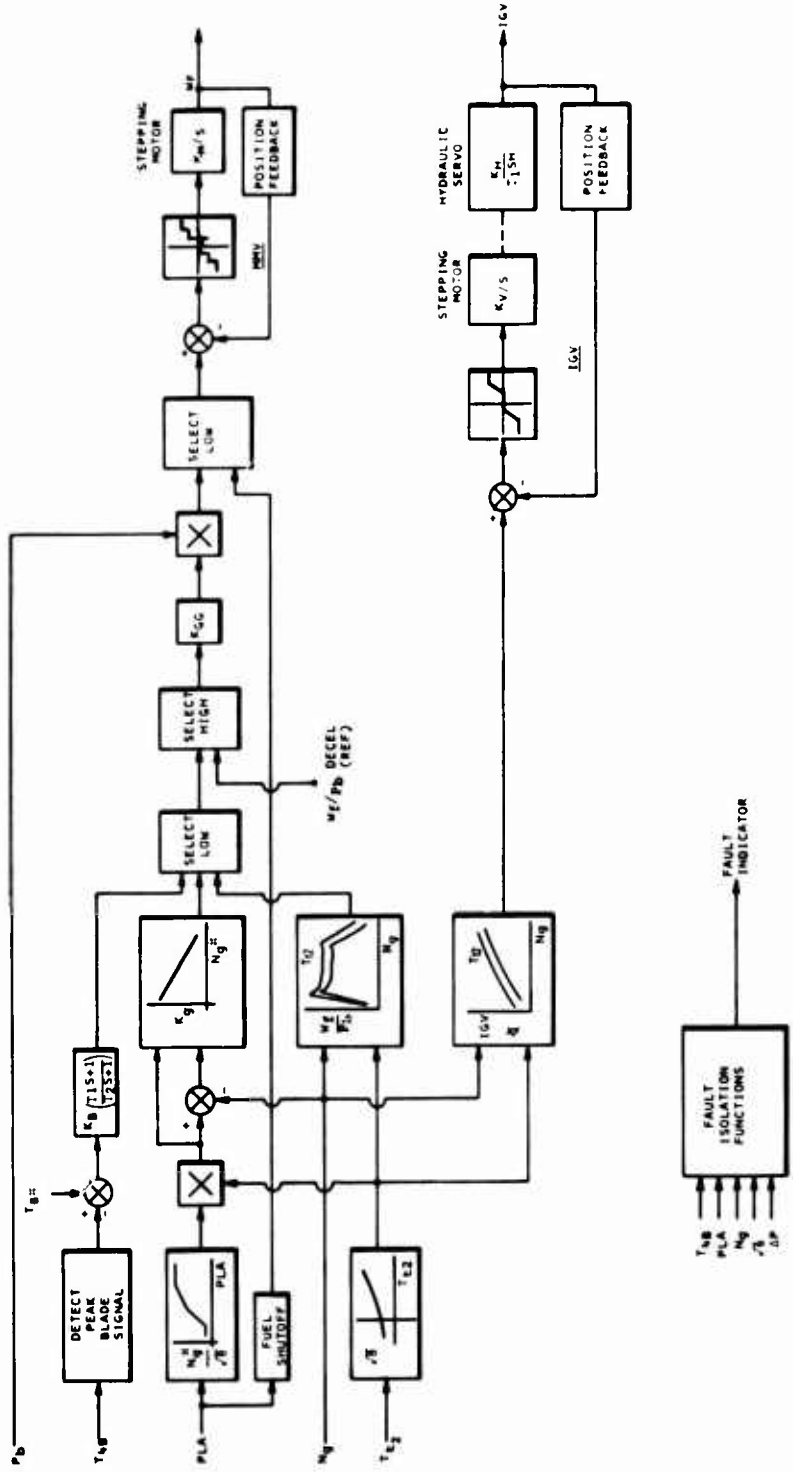

Figure 62. Control System Functional Block Diagram

idle and maximum settings with trim pot adjustments on the outside cover of the electronic control module. The potentiometer's excitation is a voltage proportional to $\sqrt{\theta}$, so the wiper voltages include the multiplication by $\sqrt{\theta}$ necessary for giving a corrected speed schedule. The dual slope function is performed through slope generating operational amplifiers, with the selection of the slope or maximum and idle flats by means of highest and lowest wins logic networks. An analog multiplier is used for computing the commanded speed setting from the power lever potentiometer input and the selected slope or flat.

Data plotted from a PLA output voltage trace is shown in Figure 63. This shows excellent agreement with the desired schedule.

Bivariant Function Generators

Figure 64 illustrates the functional implementation of the bivariant function generators required for acceleration and inlet guide vane schedules. Each analog voltage representing speed and temperature is converted into a digital form. The digitized signals from the A/D converters (representing N_g and $\sqrt{\theta}$) select an address location in the programmable PROM. A pre-programmed output is provided in accordance with the magnitude at the input functions. This output, which is a binary form, is converted to an analog signal by a D/A converter.

Since the size of the memory would have to be very large in order to accurately represent the required function, the magnitude of the memory is effectively expanded by use of interpolation. The interpolation signals (90° phase shifted sine waves) have an amplitude equivalent to $\pm 1/2$ the least significant bit and are injected into the summing amplifiers of the speed and temperature A/D converters. Therefore, if the analog voltage signal corresponds to the value between significant bits, the 1/2 bit sine wave will cause the output digital word to oscillate one bit such that the average value is proportional to the

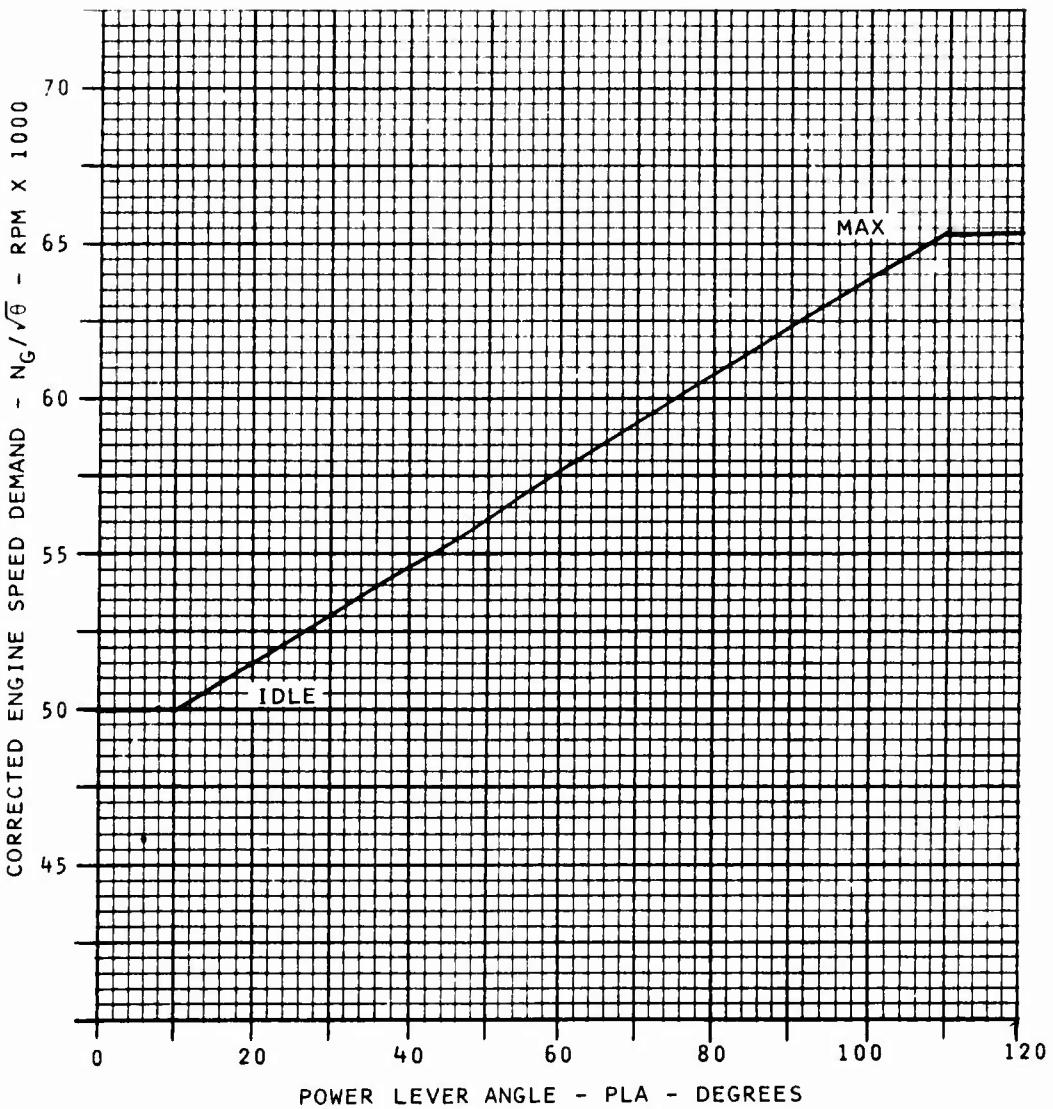

Figure 63. PLA Schedule - Bench Test

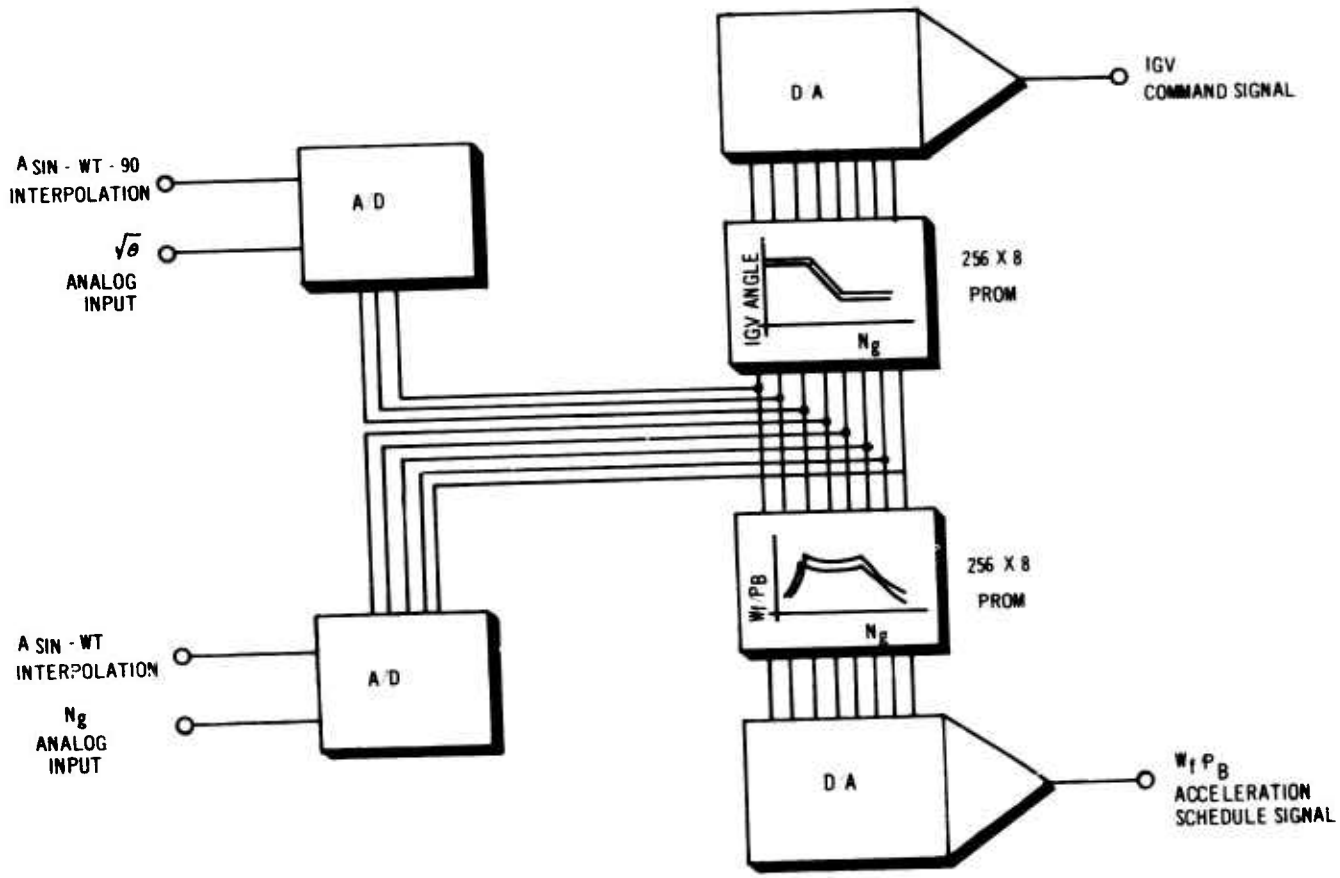

Figure 64. Bivariant Function Generator Block Diagram

input analog voltage. This provides sufficient accuracy to satisfy acceleration and inlet guide vane schedule requirements.

1. Test Results

The electronically computed schedules were recorded while varying signals, simulating the engine speed N_g and the compressor inlet temperature T_{t2}. Figures 65 and 66 show the recorded data against the specified acceleration and IGV schedules respectively. The only significant errors are those shown at points on the schedule where there is a sharp slope change. These errors are inherent in the interpolation between data points stored in the PROM. If greater accuracy is required at these points of discontinuity, it would be necessary to increase the effective memory size. For the existing schedules which are constant up to 30,000 rpm speed, the 32 data points for speed could be used to define the schedule between 30,000 and 70,000 rpm rather than the present 0 to 70,000 rpm. This would increase the resolution considerably (almost 2 to 1). However, there is some sacrifice in flexibility if schedule changes are required in the region below 30,000 rpm. For the STAGG engine, this flexibility was considered to be more important than the existing discontinuity errors.

Gas Generator Speed Governor

The desired gas generator speed governor includes a fanned droop defined by the variable gain depicted in Figure 67. Since the droop gain is proportional to the scheduled set speed N_g^*, then

$$K_g = C_1 N_g^* + C_2$$

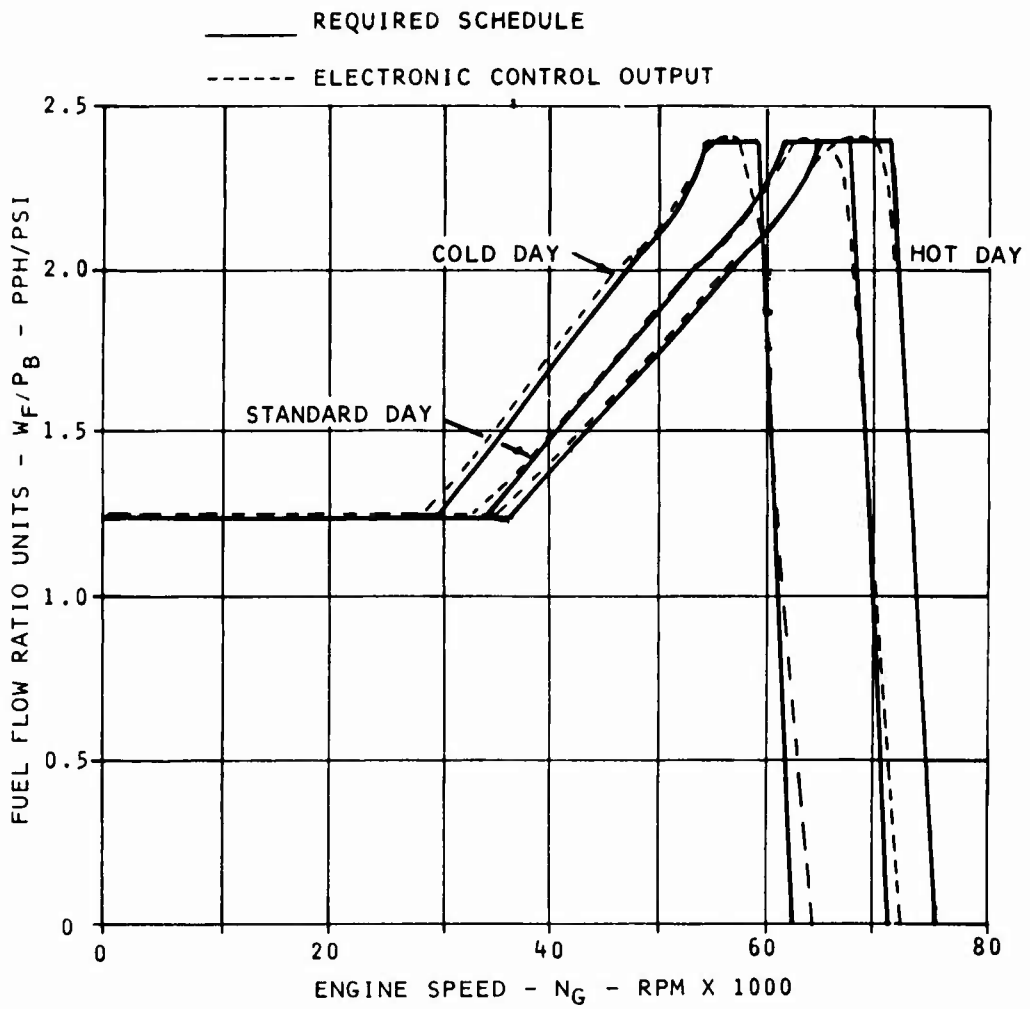

Figure 65. Electronic Acceleration Schedule - Bench Test

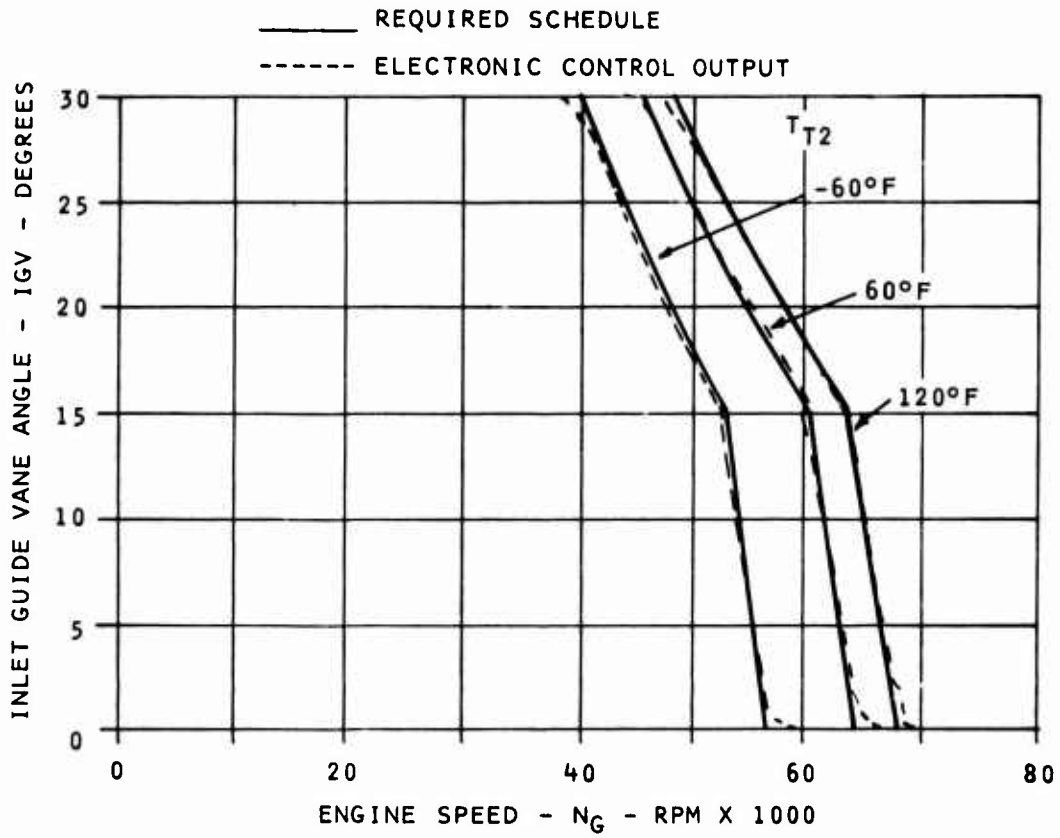

Figure 66. Electronic IGV Schedule - Bench Test

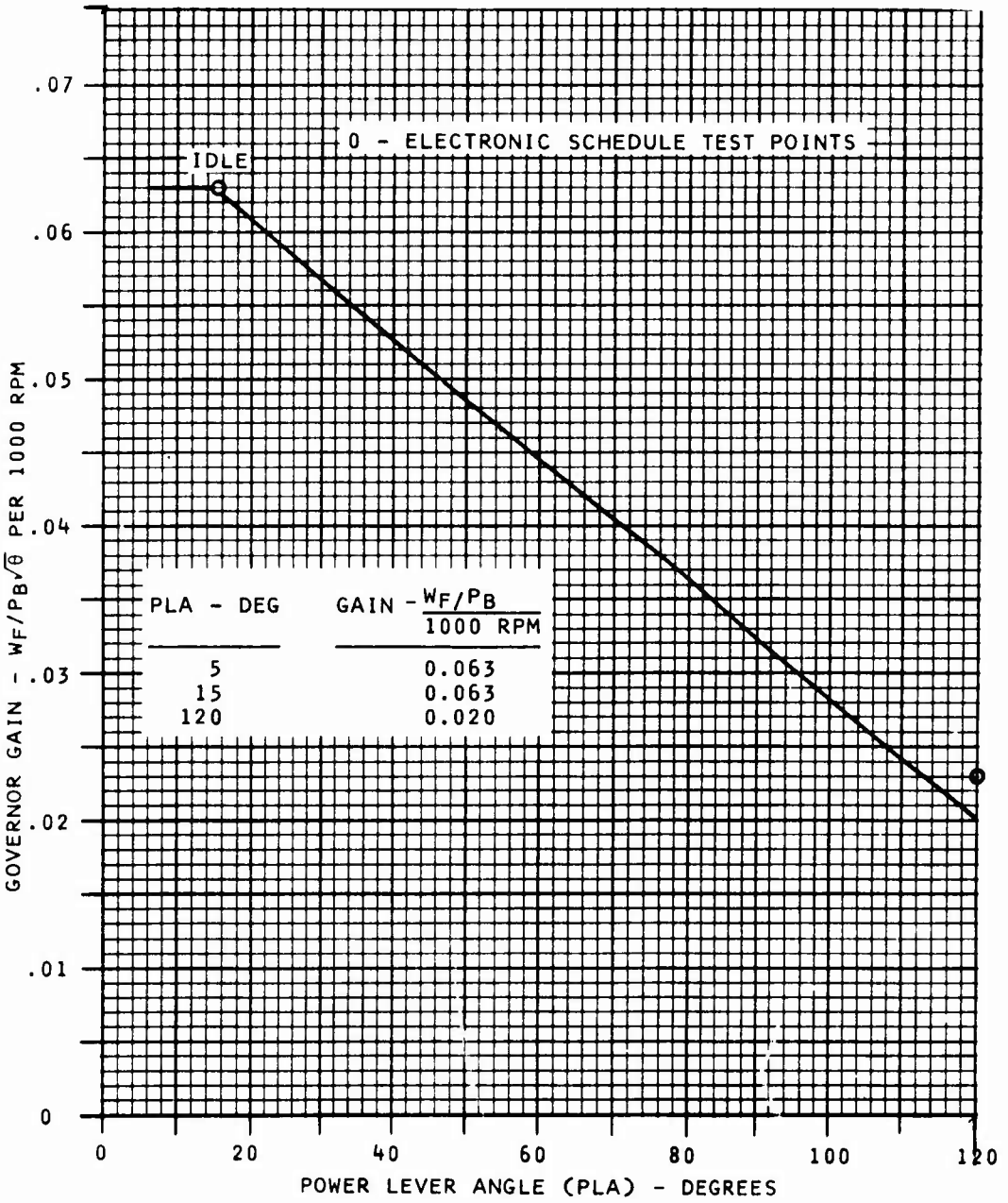

Figure 67. Governor Droop Gain Schedule

where C_1, C_2 are constants and K_g is the droop gain.

The desired proportional governor output is

$$W_f/P_b = (N_g^*-N_g)\ K_g = (N_g^*-N_g)\ (N_g^* + C_2/C_1)\ 1/C_1$$

The multiplier used in the electronics forms the function (X_1-X_2) x (Y_1-Y_2) so that with the multiplier inputs X_1 and Y_1 connected to N_g^*, X_2 connected to N_g, and Y_2 connected to a constant, the output of the multiplier can be made to satisfy the governor requirements. The electronic schedule test points are shown in Figure 67. A thermistor/resistor network is included to compensate for multiplier inaccuracies due to temperature.

Turbine Blade Temperature Limiting

The radiation pyrometer, together with its interface circuit, produces a voltage as a function of the peak turbine blade temperature. The electronics compares this voltage with the limiting temperature voltage (set by the potentiometer on the outside cover) with a differential amplifier. The gain of the amplifier is set so that its output represents the desired fuel flow ratio unit change with temperature error. These ratio units are compared with those computed for acceleration and deceleration and the lowest value selected for engine control. If the temperature limiting control loop should require dynamic compensation either for stability or for increased response, the design includes the facility for adding passive components in the amplifier feedback. Typically, a first-order lag or a lead/lag can be included.

Fault Isolation

The fault isolation section of the control was designed as a preignition self-checkout in which the normal engine control signals are disconnected from the control computation section and substituted by preprogrammed values defining a known output. The actual output (metering valve position, inlet guide vane position, or metering head ΔP pressure) is compared to limits set for the test,

and a fault is indicated if the limits are exceeded. Tests are sequenced so that each control loop (acceleration, deceleration, speed governor, temperature limiting and IGV) is exercised and functionally checked. A Programmable Read-Only Memory (PROM) is used to store up to a maximum of 32 tests or 256 data points and can be simply reprogrammed for any control changes affecting any of the tests. At the conclusion of the electronic self-check, the ΔP metering valve regulator pressure signal is switched to the fault comparator and remains on-line throughout the normal engine operation.

Figure 68 is a block diagram of the fault isolation sequence. The criterion for enabling the fault isolation sequence is that the power lever is in the shutoff position (0-5°) and that the engine speed exceeds 13%. Moving PLA to idle at any time will abort the fault sequence if it is not complete. Once the fault logic is enabled, the normal control inputs, PLA, N_g, $\sqrt{\theta}$, T_{4b} and P_b are switched out and substituted by test parameters set up on holding capacitors. A 300-Hz clock supplies the input to a counter, the output of which selects a memory location from the PROM and also multiplexes the PROM's data outputs to the holding networks (accurate low-drift capacitors). After 8 data points have been sequenced, logic freezes the counter until the stepper motor deadband signal indicates that the motor has settled at its new test position defined by the set parameters. The deadband signal enables the position resolver signal to be compared to high and low limits set for the test. If either of the limits is exceeded, the fault indicator lamp is turned on. If the signal is within limits, the logic unfreezes the counter and enables the next 8 data points to be sequenced to their holding networks for Test 2. When the counter reaches a predetermined count defining the total number of tests to be performed, logic will disable the fault isolation routine and switch the normal engine signals on line to the control computational section. The ΔP signal is then switched to the fault comparator to be compared to preset limits.

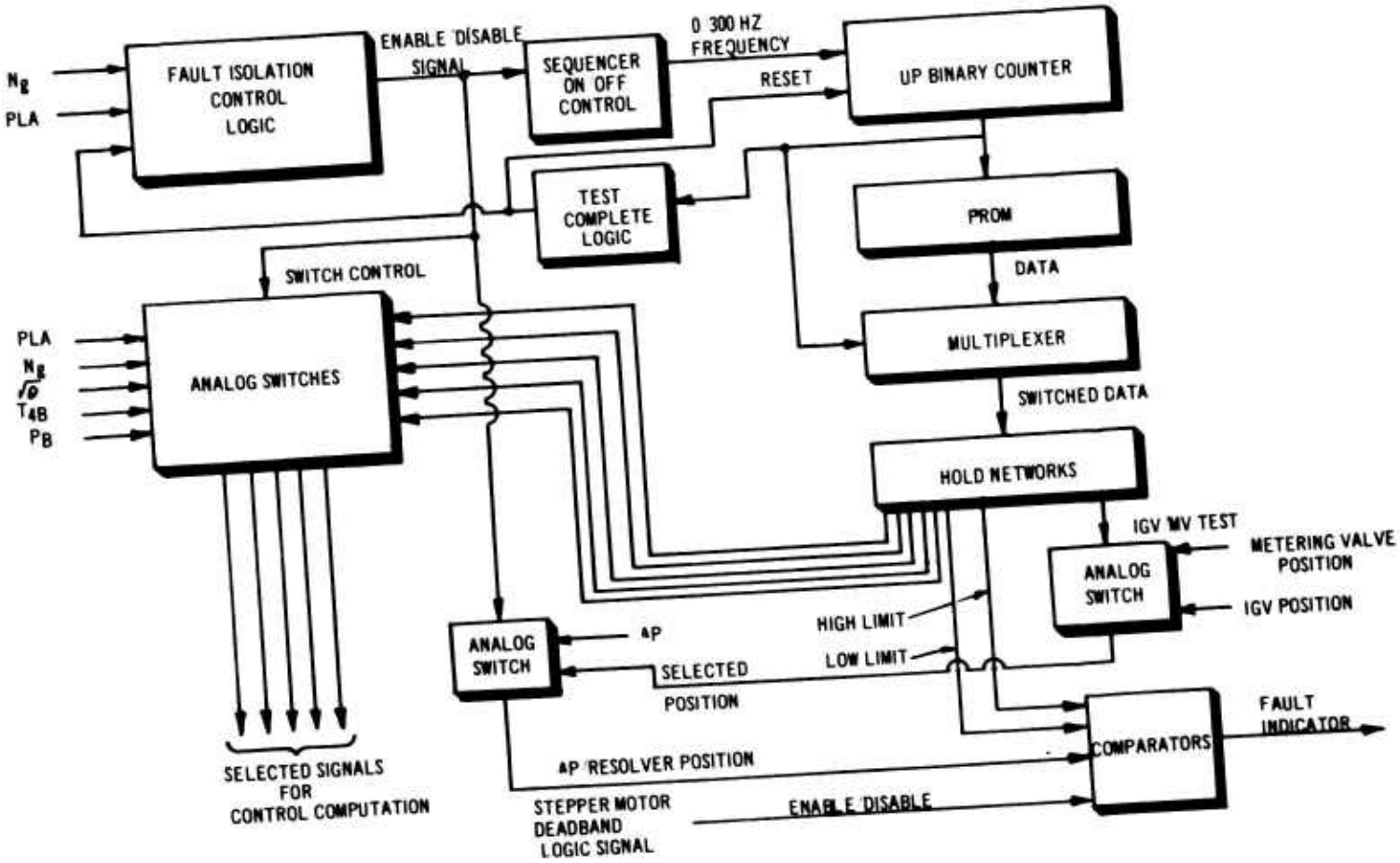

Figure 68. Fault Isolation Functional Block Diagram

Seven tests were programmed on the PROM for demonstrating the fault isolation routine. This was sufficient to check out all of the control loops at one operational point. A summary of the tests and the nominal test limits are presented in Table 3.

TABLE 3. FAULT ISOLATION TESTS

Test No.	Type	Limits	Set Point
1	Acceleration	$\pm$0.1 ratio unit	Start Schedule
2	IGV	$\pm$2.0 degrees	30° Position
3	N_g Governor	$\pm$0.125 ratio unit	Idle Droop
4	IGV	$\pm$2.0 degrees	30° Position
5	T_b Limit	$\pm$0.15 ratio unit	1850°F
6	Deceleration	$\pm$0.08 ratio unit	$W_f/P = 0.8$
7	ΔP	+7.7 psi minimum +10.7 psi maximum	On-Line Operation

The fault isolation action was tested by recording the fault indicator signal used to trigger the fault lamp against an internal fault sequencing signal. The sequencing signal switches state (logic 1 or 0) at the completion of each test, allowing the fault indicator to be associated with a particular test. (This signal is not available during normal operation.) Faults were intentionally induced, and the operation of the fault section was monitored on a two-channel recorder. In all cases, the fault indication signal correctly identified the simulated fault.

The time required for the system to complete the fault isolation test is approximately .45 second.

Speed Processing Circuit

Since the alternator is directly coupled to the engine shaft, the frequency of the voltage provided by the alternator is directly proportional to the engine speed. The basic AC waveform from the alternator, after

attenuation, drives a comparator to form a square wave with suitable magnitude to interface with a frequency to DC converter. The voltage provided by the frequency to DC converter is proportional to the alternator frequency and, therefore, to the engine speed. The accuracy of the converter is better than $\pm$.2% over the temperature range -65°F to 250°F.

Time Circuit

The timing signals to the entire electronic computer are provided by the crystal oscillator. These signals are used for sequencing the fault isolation circuitry, bivariant schedule generation, resolver frequency excitation and stepping motor rate frequencies. Since multiple frequencies are required for different functions, the basic 10 MHz oscillator frequency is broken down by means of a binary counter. The oscillator has a .05% frequency accuracy and .02% frequency stability over the military temperature range.

T_{t2} Sensor Interface

The relationship between $\sqrt{\theta}$ and T_{t2} is nonlinear over the operating range of inlet temperature, -65°F to +135°F. The required relationship is that the output voltage be proportional to $\sqrt{\theta}$. This relationship can be conveniently achieved by utilizing the natural characteristic of the thermistor in a resistor/thermistor network. This network is integral with the temperature probe and is designed such that the temperature versus resistance characteristic has a relationship

$$\sqrt{\theta} \propto 1/R_{TH}$$

where R_{TH} is the effective resistance of the network.

The interfacing circuitry consists basically of the DC amplifier shown in Figure 69 and the reference voltage.

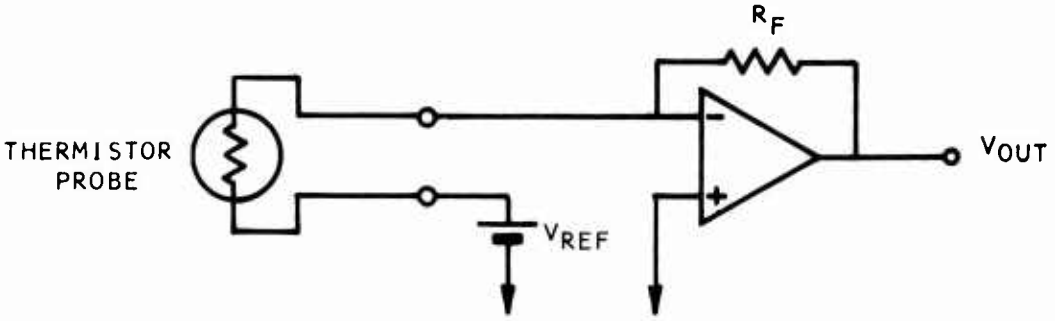

Figure 69. T_{t2} Sensor Circuit Schematic

The circuit equation is given by

$$V_{out} = \underbrace{(V_{RT}R_F)}_{K_1} \; 1/R_{TH}$$

$$\therefore V_{out} = K_1 \; 1/R_{TH}$$

but $$\sqrt{\theta} = \frac{K_2}{R_{TH}}$$

$$\therefore V_{out} = K_3 \sqrt{\theta} \quad \text{where } K_3 = \frac{K_1}{K_2}$$

There now exists a linear relationship between θ and the output voltage. The total accuracy of the electronic interface circuitry including the thermistor probe accuracy was 1.2%.

P_b Sensor Interface

The strain gage type pressure transducer is connected to a differential DC amplifier in the short-circuit current mode. In this circuit, the differential output of the bridge is maintained at zero, since the opposite sides are connected directly to the inputs of an operational amplifier with feedback. Thus, the amplifier is used to measure the current flowing into the bridge under short-circuit conditions. Since it was required to compute W_f by multiplying W_f/P_b by P_b, the W_f/P_b signal was used as an excitation for the strain gage bridge, allowing direct multiplication without any additional circuitry. The simplified circuit is shown in Figure 70.

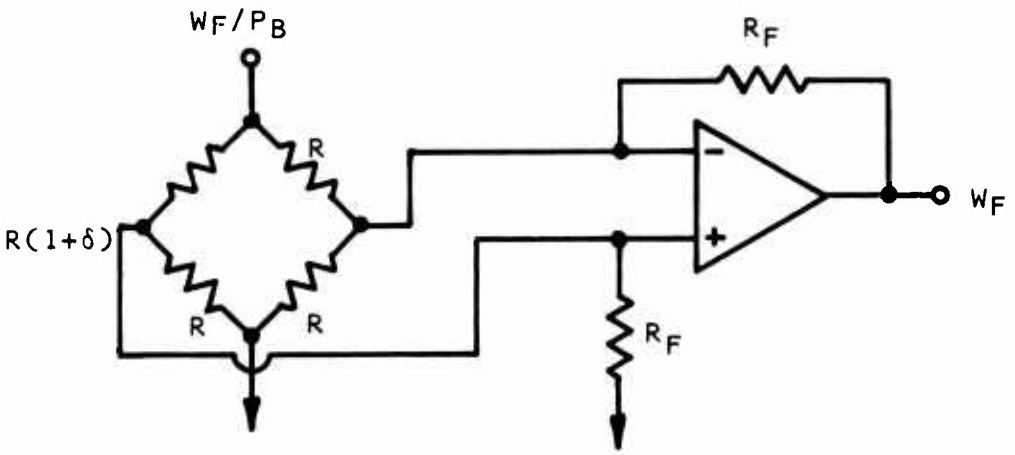

Figure 70. P_b Sensor Interface Circuit

Since $\delta << 1$ and $R_f >> R$, an approximate form of the equation for the output voltage is

$$V_o \approx W_f/P_b \; (\delta) \; \frac{R_f}{2R} \; \frac{}{K}$$

where $\delta \; \alpha \;$ to P_b.

$$\therefore \; W_f(\text{volts}) \cong W_f/P_b \; (P_b) \; K$$

The total accuracy of the interface circuit is .15% under worst-case conditions.

Electronic Computer Power Supply

Figure 71 shows a functional block diagram of the power supply system. The AC voltage provided by the alternator (one winding for positive and one for negative) is full wave rectified and filtered. This provides an unregulated ±20 VDC to the series pass voltage regulator, which in turn supplies a regulated ±15 VDC to the electronic computer. The +5 V +10 V and -9 VDC digital logic supplies are formed by using zener diode voltage regulators, where the raw supply voltage for these is tapped off from the unregulated ±20 VDC supply. The ±15 VDC supply variation due to temperature does not exceed 1%, and the load regulation over the temperature range (-55°C to +125°C) is .2%. The digital logic supply voltage variations due to temperature and load do not exceed 10% and 5% respectively.

MMV and IGV Stepping Motors Power Supplies

Power supplies for MMV and IGV stepping motors consist of full-wave bridge rectifiers and filtering capacitors. No voltage regulation is necessary since the stepping motors are basically current-actuated devices and require a constant current characteristic to provide a given torque/speed relationship over the full temperature range.

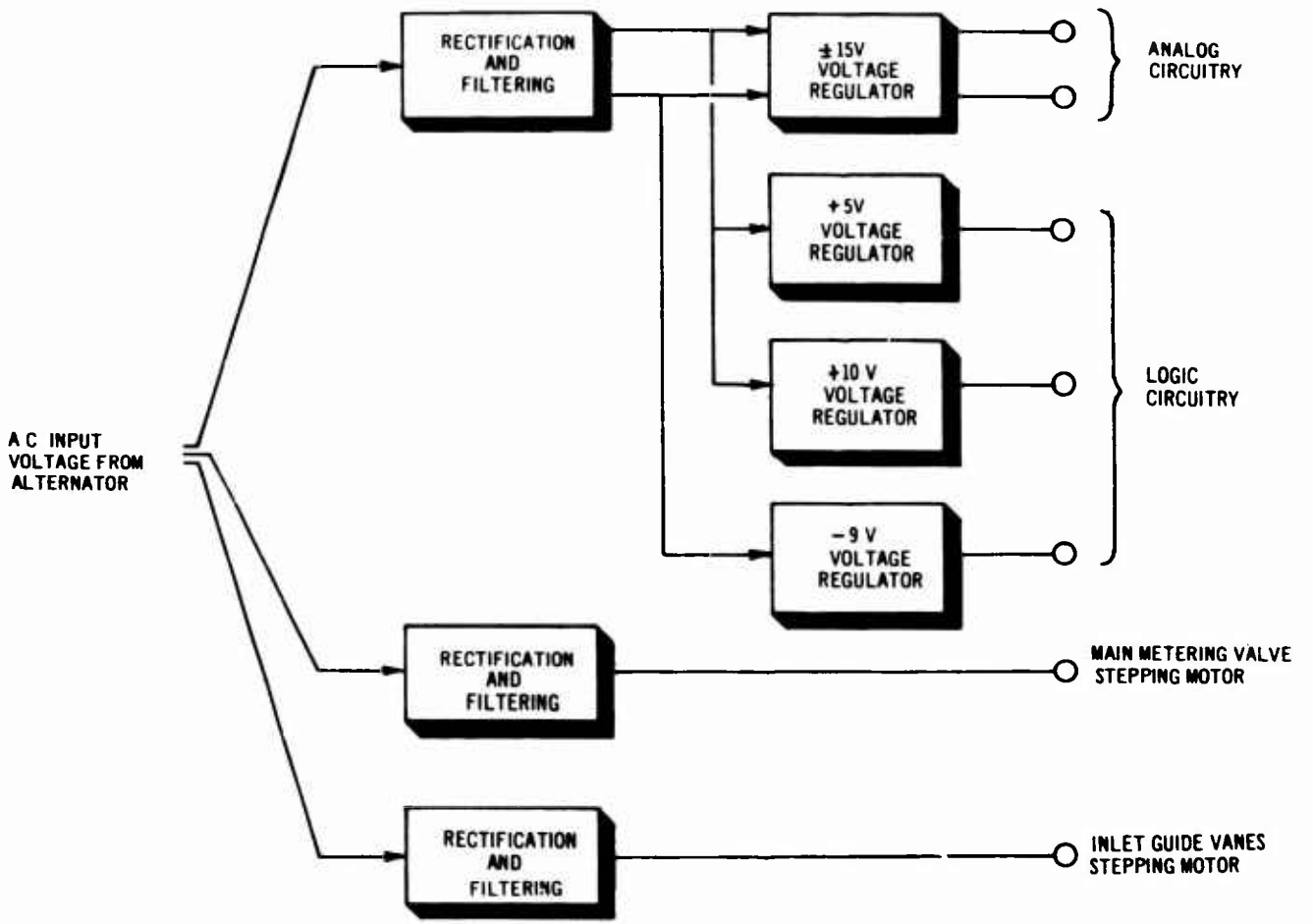

Figure 71. Power Supply Block Diagram

Stepping Motor Interfaces

To comply with system requirements of minimum size and power dissipation, maximum torque, stepping rate and stability, identical size eight, four-phase variable reluctance stepping motors are used to position MMV and IGV valves. The translator for the MMV stepping motor is basically a four-phase clock with provisions for incrementing the stepping motor at a constant rate or by individual steps in either forward or reverse direction.

In the MMV translator, one of two step sizes can be selected on command: 15° or 7.5° of rotation. The step size is controlled by the magnitude of the error signal. For large errors, the stepping motor slews in 15° steps, and when the error reaches a certain predetermined low value, the stepping motor moves in increments of 7.5°. This provides increased accuracy for metering fuel in the low range of operation.

The IGV translator operates in a similar manner to the MMV, the main difference being that it uses a variable frequency rate for incrementing the stepping motor instead of a fixed rate. The error voltage drives a voltage controlled oscillator so that the rate at which the stepping motor approaches its commanded position is proportional to the position error. The variable stepping rate is required for stability because of the hydraulic servo lag in the IGV control loop.

Resolver Interface

The resolvers are used to measure the mechanical position of the main metering valve and inlet guide vane actuator. The temperature compensating windings ensure an accuracy of .1% over the temperature range of -55°C to 125°C.

The MMV and IGV resolver interface circuits are identical except for the implementation of the pulse width to DC converter.

The sine wave excitation signal for the resolvers is derived by filtering the 1.22 kHz square wave signal from the timing circuit. The cosine wave is obtained by phase shifting the reference sine wave by 90°, and both signals drive the resolver excitation windings. The resolver sinusoidal output signal, together with the sine wave reference signal, is passed through a zero crossing detector, which generates a phase to pulse-width conversion. The pulse-width modulated signal is proportional to resolver position.

Since the MMV function required faster response and greater accuracy, the implementation of pulse-width to DC conversion differs from the simpler mechanism used for the IGV. As shown in Figure 72, it consists of gating the pulse-width signal with a high-frequency clock to drive the binary counter, which feeds the storage register. The function of the storage register is to retain the information during the reset cycle of the counter. The output of the register which is in a binary form is converted to an analog signal by a D/A converter. The analog output voltage is proportional to the resolver position.

The IGV pulse-width modulated signal is converted to a DC voltage by a simple low-pass filter. Since the amplitude of the pulse-width signal is not always sufficiently accurate, a duplicate pulse-width signal is generated using a precise reference voltage. Therefore, the amplitude of the filter pulse-width signal is constant. Although simple, this approach provides sufficient response and accuracy over the full military temperature range.

Minimum Fuel Flow and Shutoff

The electronic control incorporates logic to limit flow to a nominal value of 60 pph. An adjustment of approximately ±20 pph is incorporated with a trim potentiometer on the housing front cover. If the metering valve position voltage is smaller than the voltage set by the trim pot, the normal stepper motor direction logic is overridden and forced to a state that will cause the valve to open.

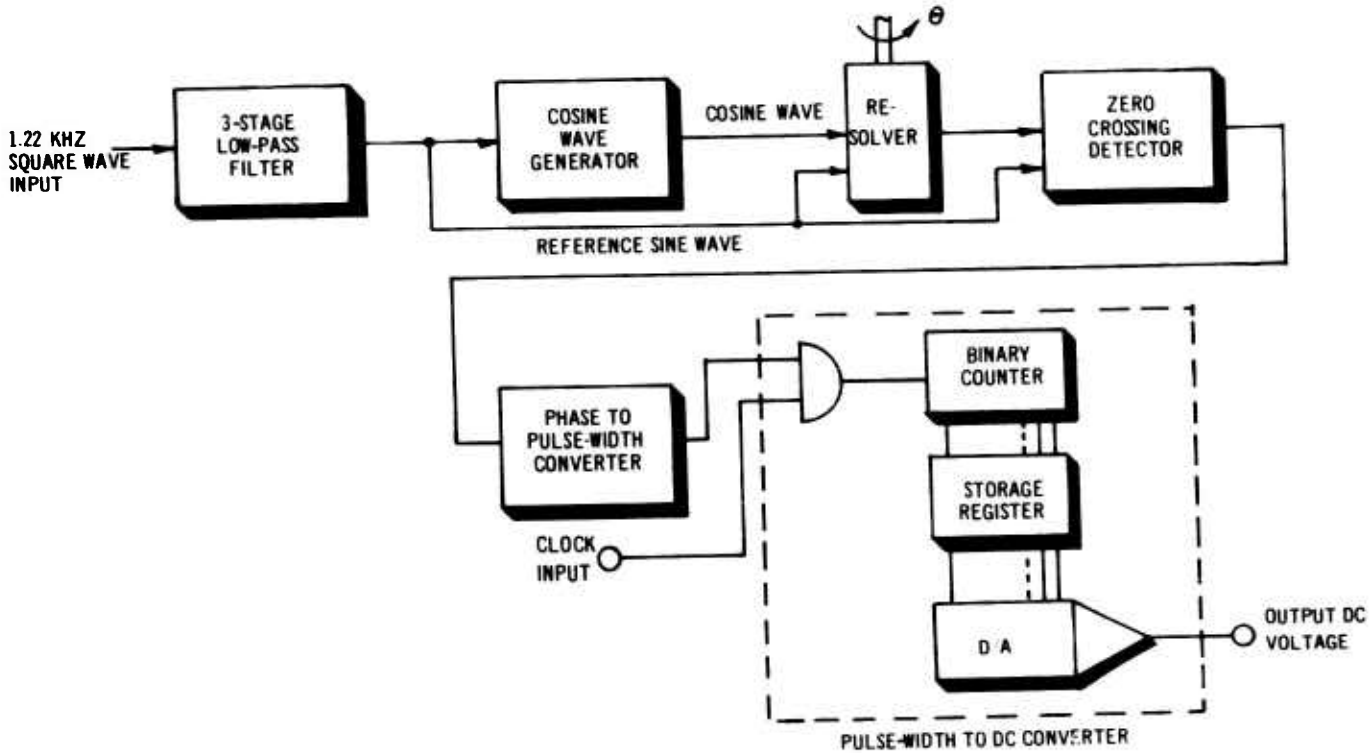

Figure 72. MMV Resolver Interface Circuit Block Diagram

When the valve position voltage is equal to or greater than the minimum position, the normal direction logic controls. The minimum flow logic is inhibited during the fault isolation routine or when the control is switched to the shutoff position.

When the PLA input to the control is positioned between 0° and 5°, the electronics will sense a negative voltage from the PLA position potentiometer. This voltage forces the metering valve command signal to zero volts, causing the valve to slew to the shutoff position.

Electronic Computer Temperature Testing

Critical parameters were recorded at standard day, -65°F and 200°F temperatures, and the results are shown summarized in Table 4.

TABLE 4. ELECTRONIC CONTROL TEMPERATURE DATA

Parameter	Std. Day Volts DC	200°F Volts DC	-65°F Volts DC	Maximum Variation % of Point
N_g	8.005	8.002	8.009	0.05
θ	9.990	9.937	9.943	0.53
W/P_n	4.996	5.056	4.920	1.52
W/P_{tb}	10.02	10.14	9.870	1.30
W/P_a	8.750	8.750	8.840	1.03
W/P	5.010	5.060	4.946	1.28
I_c	4.103	4.120	3.930	3.14
N_g*	7.510	7.546	7.556	0.61

The most significant error was in the speed governor (1.52), caused mainly through the inherent error in the multiplier used for the PLA schedule and the variable droop gain function. The 3.14% of point variation in the IGV position (I_c) computes to $\pm$.43% error in the guide vane angle, while the 1.3% error in

the temperature limiting parameter W/P_{tb} will result in an insignificant temperature error when using the high loop gain required for the limiting control mode. All errors are considered to be acceptable when compared to the required system accuracies.

Alternator

The alternator was designed with the following goals:

a) Provide power for the electronic computer.

b) Provide power for the IGV and MMV stepping motors.

c) Provide power for the engine ignition system.

The alternator consists of the rotor and stator shown in Figure 73. The rotor has 12 poles and utilizes samarium-cobalt magnets. For mechanical integrity, the magnetic structure of the rotor is completely enclosed in a steel hub and Inconel hoop. This design enables the alternator to be operated at speeds up to 75,000 rpm. The rotor has an outside diameter of 1.760 inches, is .576 inch wide, and weighs .3 pound.

The stator has 18 teeth on which are placed 6 separate windings. The windings are positioned so that any winding could be short circuited or fully loaded without causing interaction in adjacent windings. The stator has an outside diameter of 2.600 inches and an overall length of 1.175 inches, and it weighs .45 pound.

Since the electrical load for each winding is relatively constant over the operating speed range, the alternator magnet flux circuit was designed to saturate at about 13% speed, where power is first required. Therefore, with a relatively constant load, the alternator output voltage will inherently regulate to within 10% over the entire operating speed range (13% to 110%).

Ignition windings were designed to provide power to exciters requiring two joules/second of stored energy. The electronic computer dissipates approximately 10 watts, and the stepper motors about 6 watts each.

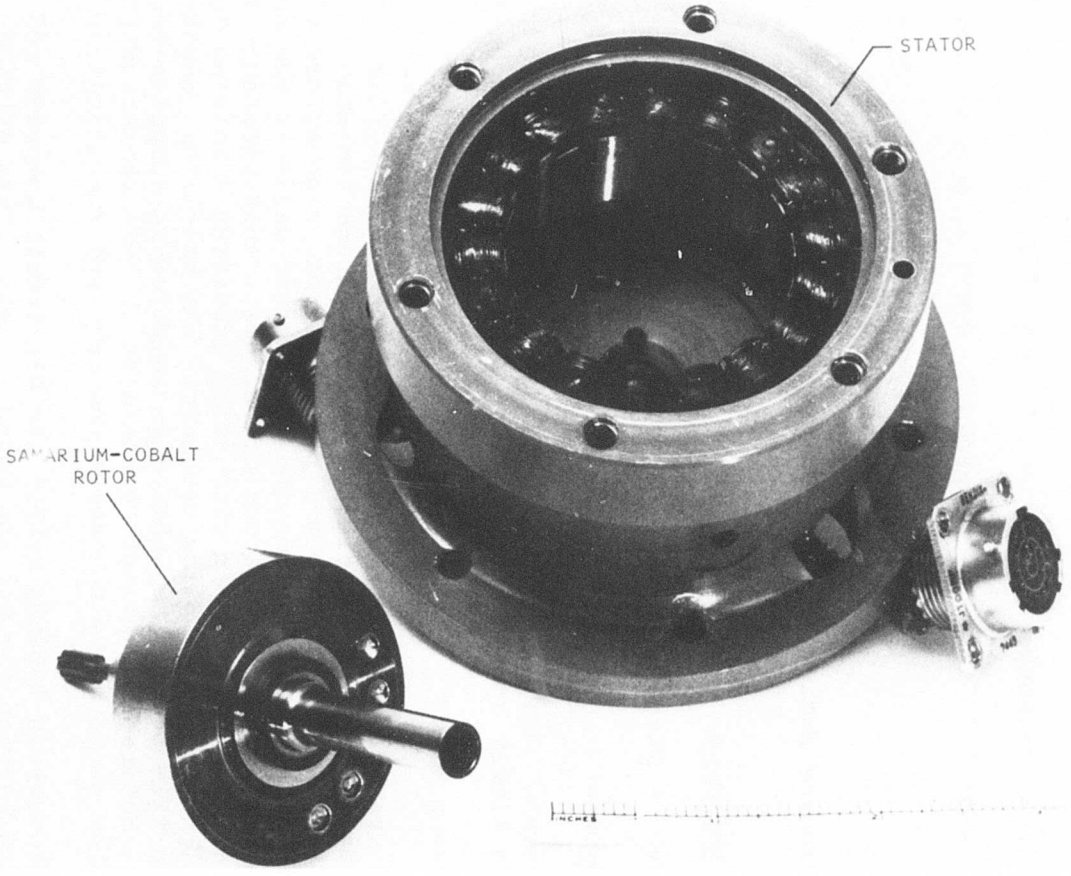

Figure 73. Alternator Components

P_b Transducer

The environmental and performance requirements for the pressure transducer are as follows:

Environmental

Temperature Range	-65°F to +200°F
Vibration	Radially 0.001 inch d.a. from 20 to 1050 Hz Axially 0.0001 inch d.a. from 20 to 1050 Hz
Operating Medium	Compressor discharge pressure

Performance

Pressure Range	8 to 220 psia
Response	.01 sec time constant
Accuracy with linear change to	±.2% (full scale) at 8 psia ±1.0% (full scale) at 220 psia
Warm-up Time	≤ 10 ms

The pressure transducer is a Statham Instrument thin-film strain-gage type. It comprises a beam diaphragm assembly mounted to a thin-film vacuum-deposited strain-gage bridge via a ceramic substrate. Application of pressure deflects the beam, thereby throwing the bridge out of balance. This unbalance is then detected by electronic circuitry, providing a voltage proportional to maximum applied pressure. The monolithic deposited thin-film bridge, together with temperature compensating elements, provides excellent common mode thermal characteristics which allow performance to exceed the required specification.

The transducer is located within the electronic computer and is mounted between the top and bottom covers. This arrangement keeps the mounting simple, yet allows for adequate support

against the engine vibrations. Figure 74 illustrates the envelope and mounting arrangement of the transducer.

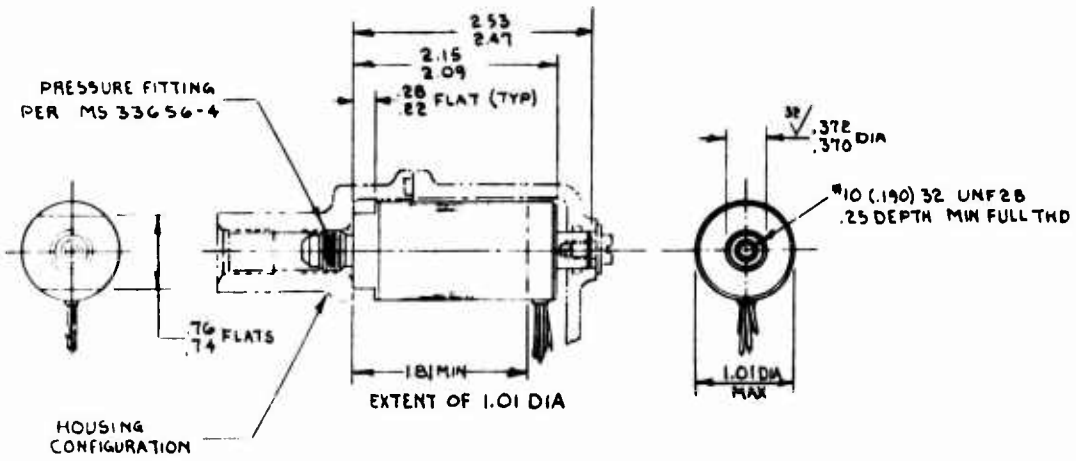

Figure 74. Pressure Transducer Envelope

Test Results

The pressure sensor, together with its electronic signal conditioning interface, was calibrated from 14.7 to 200 psia pressure over the temperature range -65°F to 200°F. The results of calibrations completed prior to and after engine running (Figures 75 and 76) show that the sensor accuracy meets the specified requirements. The high vibration levels experienced by the sensor early in the engine test program (up to 80 g's) did not result in any noticeable performance deterioration at the time. The final calibration indicates that no significant calibration shift had occurred as a result of the engine operation.

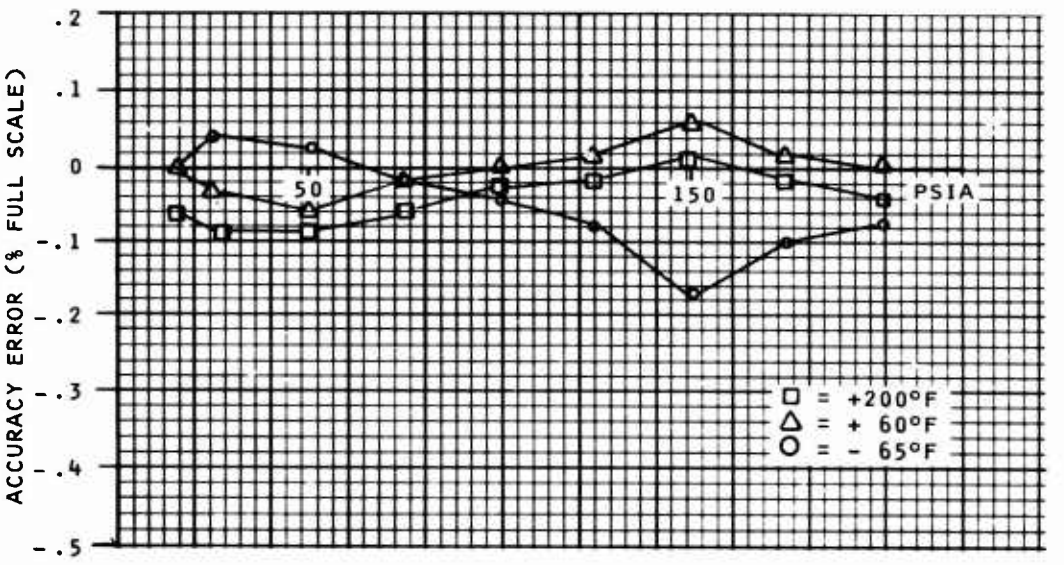

Figure 75. Pressure Transducer Test Data - Bench Test Before Engine Test

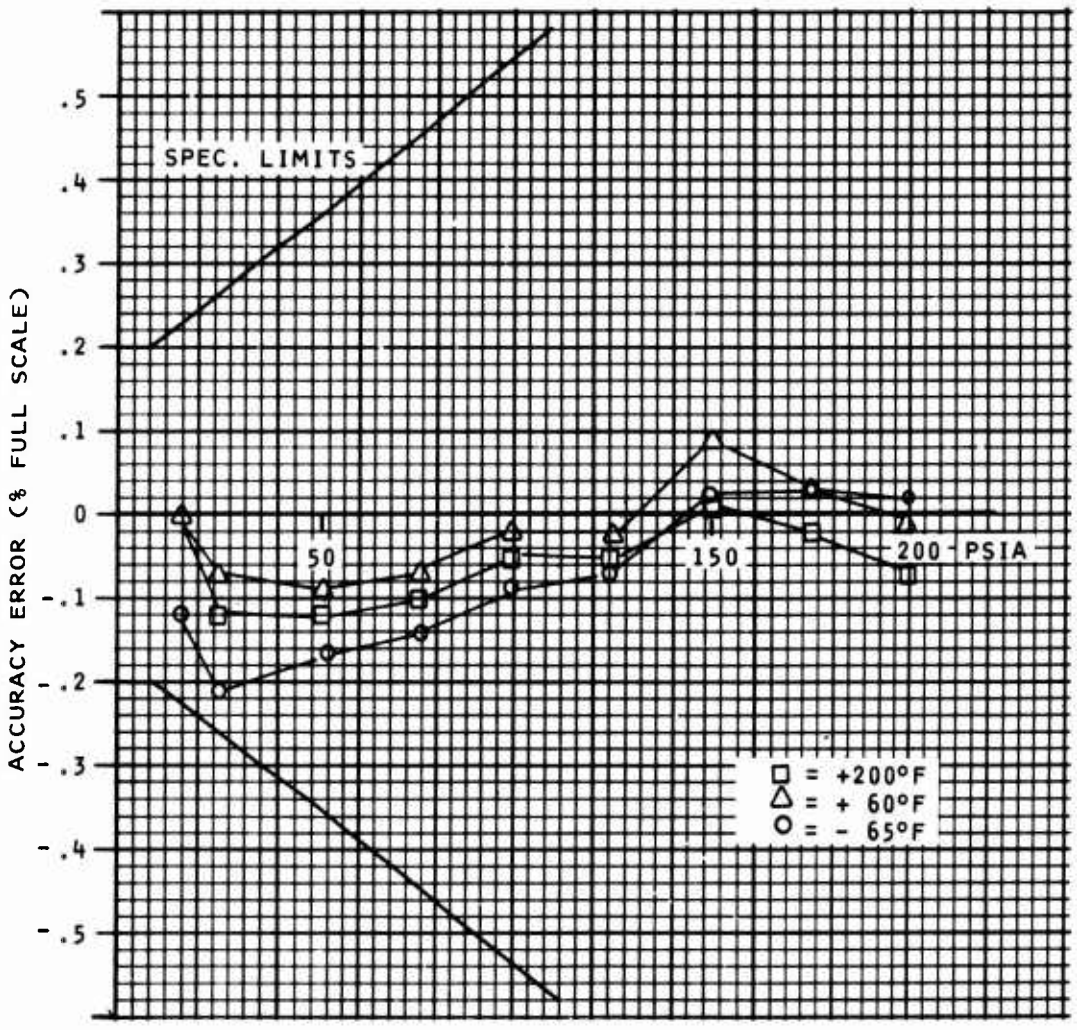

Figure 76. Pressure Transducer Test Data - Bench Test After Engine Test

Inlet Temperature Sensor

The inlet temperature sensor utilizes a thermistor/resistor network as a temperature sensing element. The network shown in Figure 77 is encapsulated in a stainless steel tube (.187 inch in diameter and about .875 inch long) with the protective shroud over the tube to prevent damage. A schematic of the sensor is also depicted in Figure 77. The overall accuracy of the output function relative to $\sqrt{\theta}$ is 1.2%.

Test Results

Calibration test results on the inlet temperature thermistor/resistor probe from before and after engine mounted tests are tabulated below. As indicated, all data points are within the specified ±2%.

TABLE 5. T_{t2} SENSOR TEST RESULTS

Temperature (°F)	% Error in $\sqrt{\theta}$ Before	After
-63	+0.6	+0.6
-36	-0.7	-0.4
-18	-0.7	-0.2
-7	-0.1	0
42	+0.5	+1.1
76	+1.2	+1.3
83	+1.0	+1.3
108	-0.1	+0.2
133	-1.2	-0.8

RADIATION PYROMETER

The turbine blade radiation pyrometer utilizes a lens type optical sensor which resides in the hot section of the engine and views a small circular target on the suction side of the passing blades. A flexible fiber-optic cable transmits the collected radiation from the sensor to the electronic computer located in the relatively cool environment on the outside of the engine. The silicon photovoltaic detector and associated analog circuits

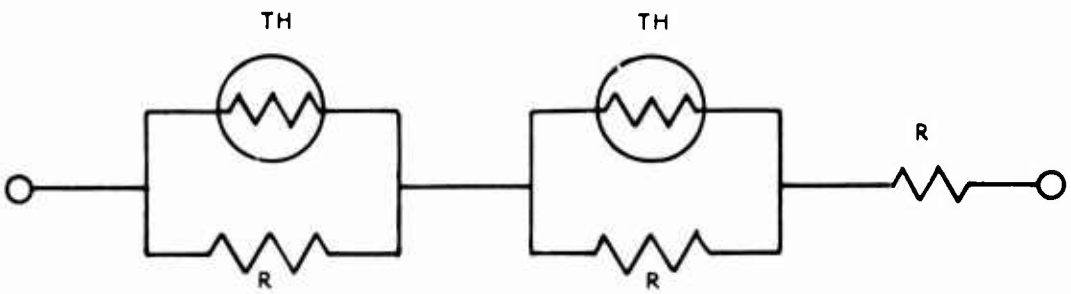

THERMISTOR RESISTOR NETWORK CONFIGURATION

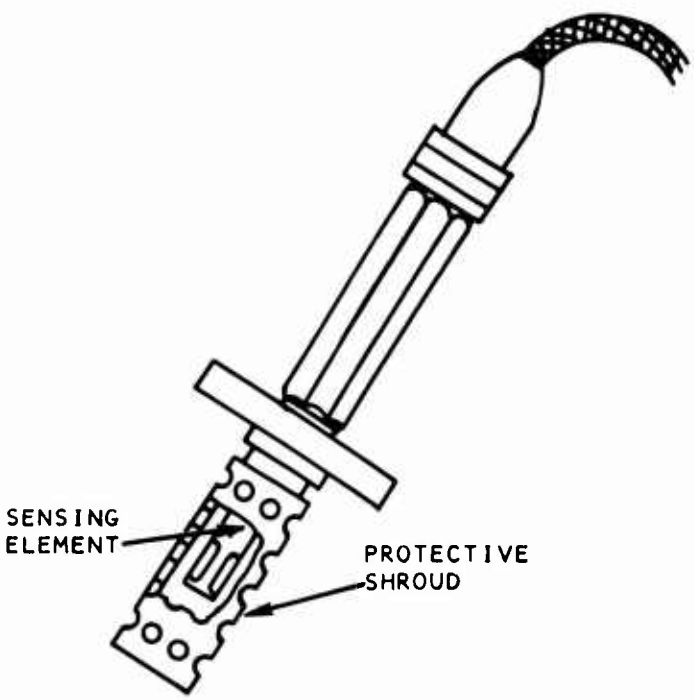

Figure 77. T_{t2} Sensor Schematic

in the computer convert the high-frequency blade profile radiation signal to a voltage which corresponds to the peak temperature of the hottest blade. This signal is then used to limit the peak blade temperature by controlling engine fuel flow.

Design Requirements

The environmental and performance requirements for the radiation pyrometer are as follows:

Sensor Environment

Maximum ambient temperature	1700°F
Maximum pressure	250 psid
Vibration	50 g's at 1050 Hz
Purge & cooling air	.003 lb/sec maximum at 100°F inlet temperature

Detector Environment

Maximum ambient temperature	200°F
Vibration	same as above

Performance

Field of view	.1 dia. target
Limiting blade temperature	1650°F, T_{4b}
Accuracy	$\pm$15°F, T_{4b}
Dynamic response	4 µsec

Design Description

Optical Sensor

The function of the optical sensor is to sight on a specific target area, to efficiently collect the radiant power emitted by the hot target, and to exclude stray radiation.

Figure 78 shows a layout of the lens type sensor. The structural elements inboard of the mounting flange are of Inconel X-750, a nickel-chromium alloy selected for its corrosion and oxidation resistance and high strength at temperatures to 1800°F. A precision-ground and polished sapphire lens, which is metallized and brazed into a nickel-plated KOVAR tube, collects target radiation and focuses it through the field stop onto the light pipe. The lens braze joint seals the light pipe and defining apertures against high-pressure purge air. A single glare stop and matte-finished sidewalls are employed to minimize internal reflection and the transmission of stray, off-target radiation.

A bent nickel-sheathed light pipe is employed in tne hot section of the pyrometer. It interfaces with the flexible fiber-optic cable on the outside of the engine. The light pipe is a fused tri-glass fiber bundle which is capable of operating at prolonged 850°F temperatures with no apparent degradation in transmission efficiency. The light pipe is supported at both ends. At the lens end, a high-temperature (3000°F) cement is used, while a close-clearance bearing is employed at the opposite end. This mounting configuration results in a light pipe natural frequency considerably removed from the engine spectrum and also provides freedom for relative thermal expansion.

Purge and cooling air is channeled through passages between the optical elements and the outer Inconel case. The annular clearances are sized to provide an airstream velocity in excess of 20 ft/sec, which, for a cooling flow of .003 lb/sec, is sufficient to keep the exposed lens below 750°F.

In addition to cooling the pyrometer, the airstream is deflected by the outermost end of the sensor shroud to form a velocity barrier to contaminants in the engine airstream. The lens is set back from the purge discharge to intentionally create a quiet zone at the lens surface, a design which has proven to be effective in preventing eddy currents from depositing contaminants onto the sapphire window.

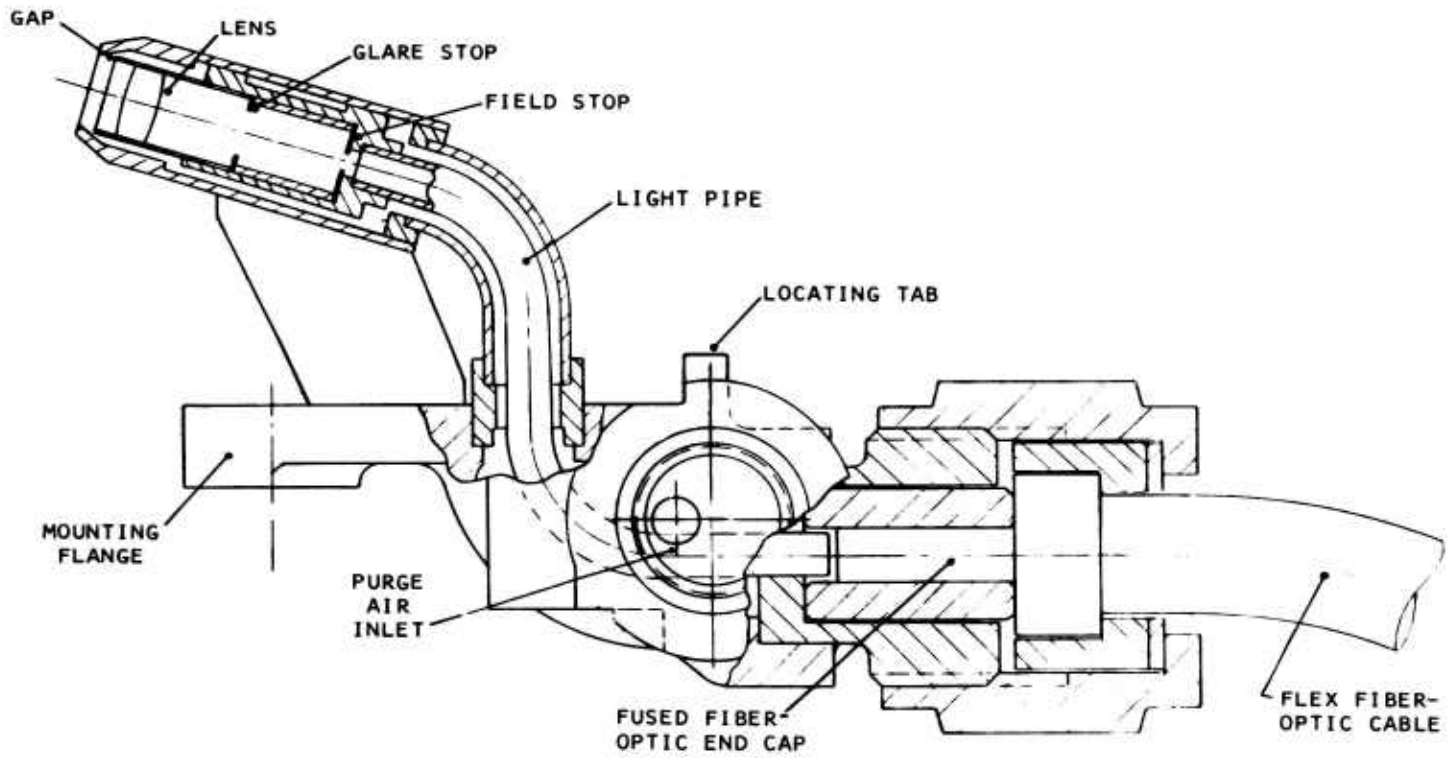

Figure 78. Radiation Pyrometer Lens Assembly

Electronic Processor

The function of the electronic processor is to convert the radiant energy transmitted through the pyrometer optical system into a voltage proportional to the peak blade temperature. This is accomplished with three basic modules: radiation detector, current-to-voltage converter, and peak detector.

The radiation detector is a silicon photovoltaic cell whose spectral response of .4 to 1.1 microns avoids the absorption and emission bands of the combustion products flowing past the optical sensor field of view. The detector is operated in the short-circuit current mode into a high-slew-rate (70 v/ second) operational amplifier to constitute a fast and relatively drift-free current to the voltage converter. The output voltage of the converter is proportional to the radiant power incident on the detector active area, and thus to approximately the 14th power of blade temperature.

A disadvantage of silicon, however, is that its output current changes with ambient temperature. To counteract this effect, a thermistor network is bonded to the detector housing and connected in the feedback path of the amplifier. As the ambient temperature in the vicinity of the detector changes, so does the magnitude of the thermistor resistance; hence, the gain of the amplifier changes to compensate for the variation in detector current.

The output of the current is a rapidly varying signal which tracks the temperature profiles of each of the 25 turbine blades passing at speeds up to 65,000 rpm. The function of the peak detector is to take this signal and to recognize and store the peak blade temperature each revolution. To accomplish this, an analog peak detecting circuit is employed. High-slew-rate FET input amplifiers are used along with a high-insulation-resistance metallized polycarbonate storage capacitor. This configuration yields a fast charging response with extremely low leakage paths to prevent the capacitor from discharging prematurely. A shunting resistor across the storage capacitor is used to

tune the discharge rate to be slightly faster than the fastest time constant associated with the heat transfer dynamics of the turbine blade. This technique allows the peak detector to follow decreasing temperature transients while resulting in only a fraction of a degree error in measured peak blade temperature in an engine steady-state condition.

Bench and Engine Test Results

The pyrometer was functionally tested in the laboratory against a blackbody radiation standard as shown in Figure 79. The electronic processor was enclosed in an environmental chamber where temperature was varied between -55°F and 220°F. The static calibration of the device shown in Figure 80 reveals that in the normal blade temperature limiting region above 1600°F, where the detector ambient temperature compensating network was optimized, the error in measured temperature is less than $\pm$7°F. Thus, the device meets the accuracy requirement for a blade temperature limiter.

The calibration of the pyrometer was extended to low blade temperatures in the vicinity of 1200° to 1300°F in order to provide the capability of checking out the blade temperature limiting control loop at less critical part-power conditions of the engine. The degraded accuracy in this region (i.e., $\pm$25°F) was of no concern since these temperatures are outside the normal blade temperature limiting region. However, the capability exists to considerably reduce these errors with a more sophisticated thermistor network.

The dynamic response of the pyrometer was tested by exciting the optical sensor with pulses of radiation from a function-driven LED. The voltage response of the current-to-voltage converter and peak detector was measured with a high frequency band-pass oscilloscope, and the traces are included in Figure 81. This data shows that the current-to-voltage converter exhibits a nearly deadbeat response with a top to bottom transit time of 4 µsec. The peak detector follows the output of the converter and decays exponentially at its preset time constant of .4 second. Thus, the device meets the dynamic requirements

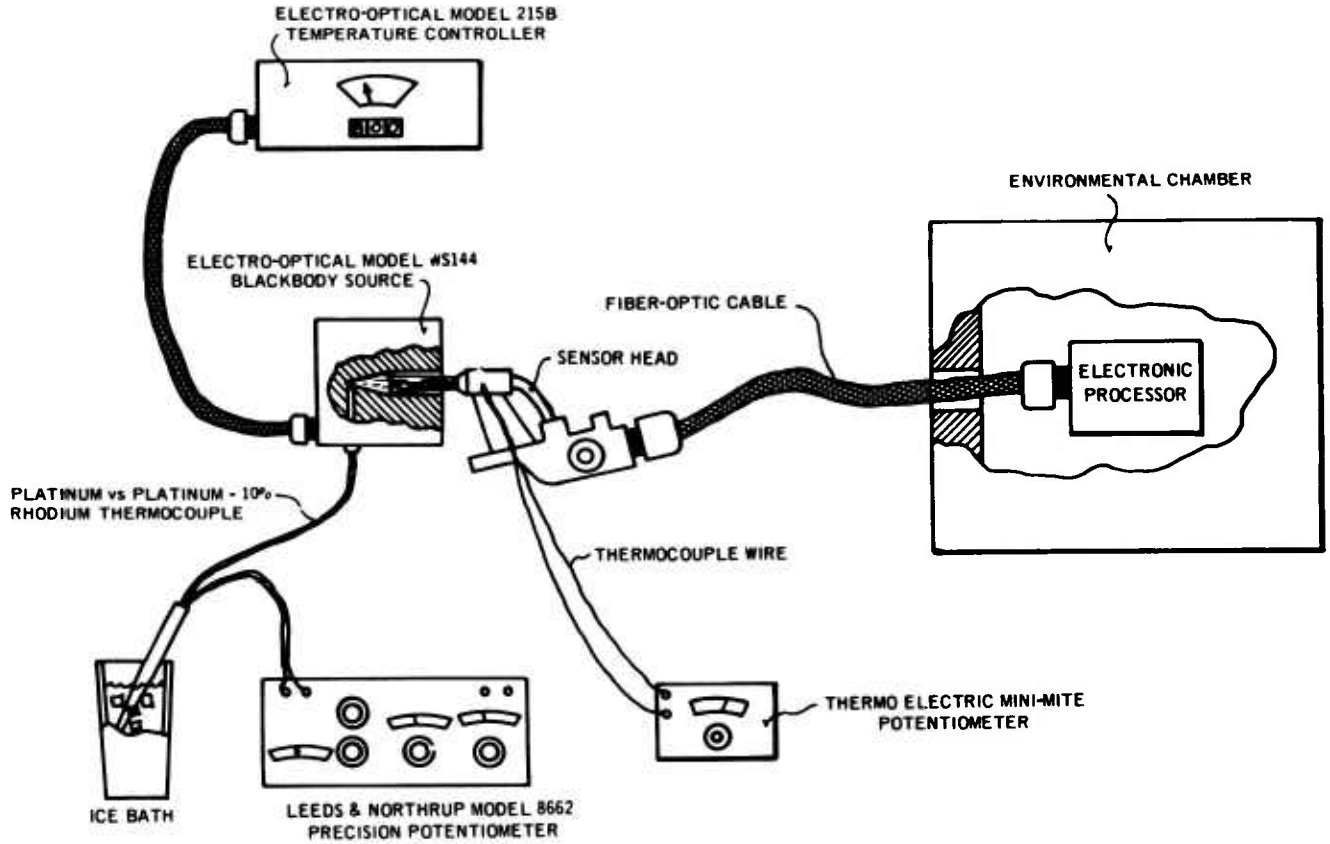

Figure 79. Test Schematic - Radiation Pyrometer Calibration

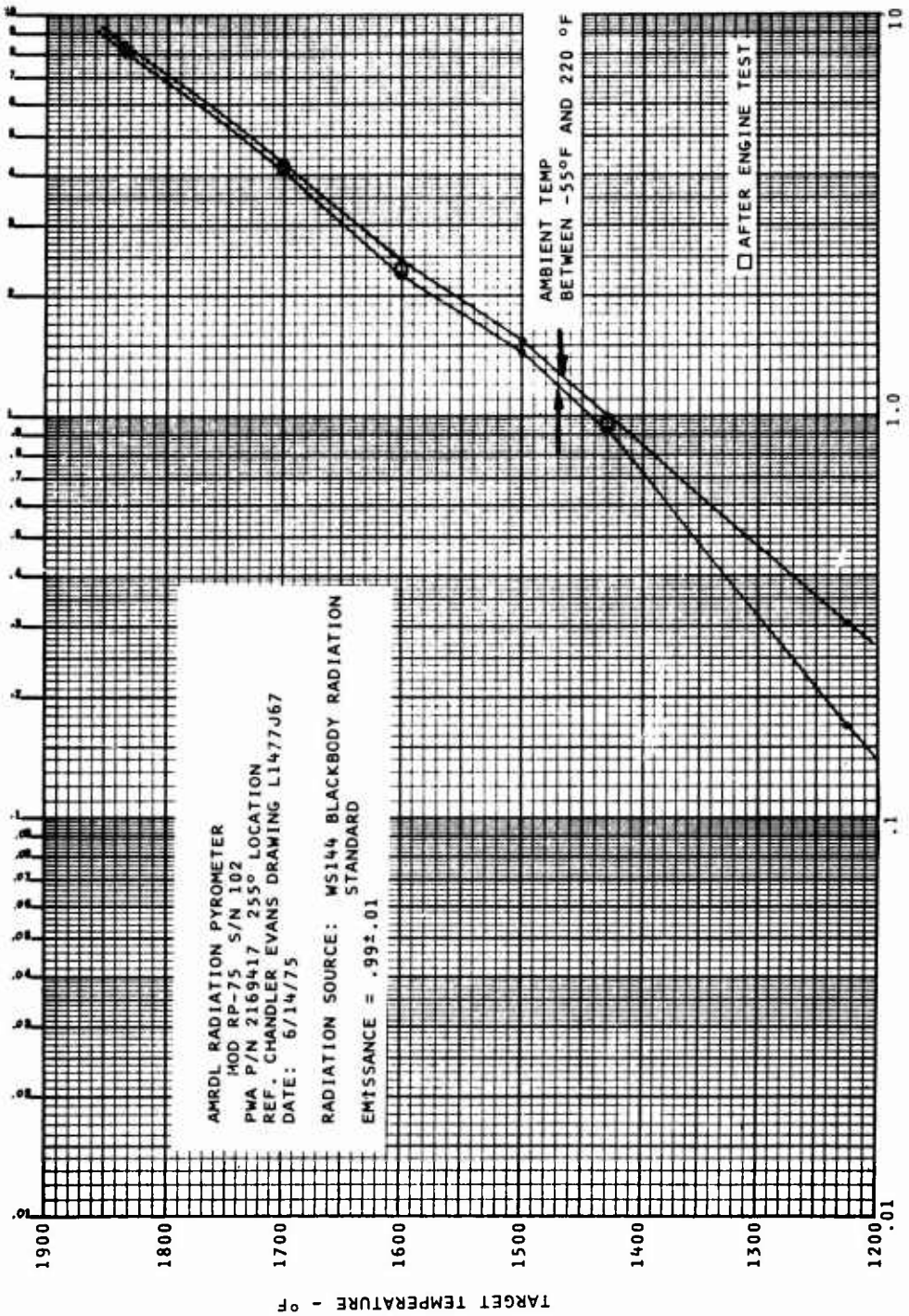

Figure 80. Pyrometer Temperature Calibration - Bench Test

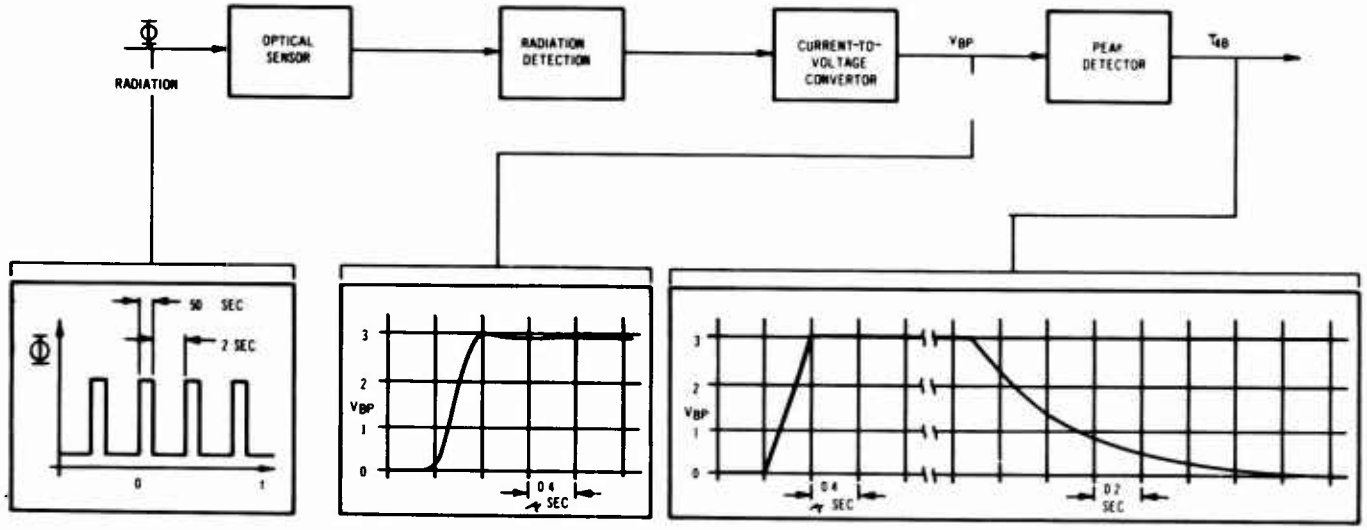

Figure 81. Pyrometer Transient Response Test - Bench Test

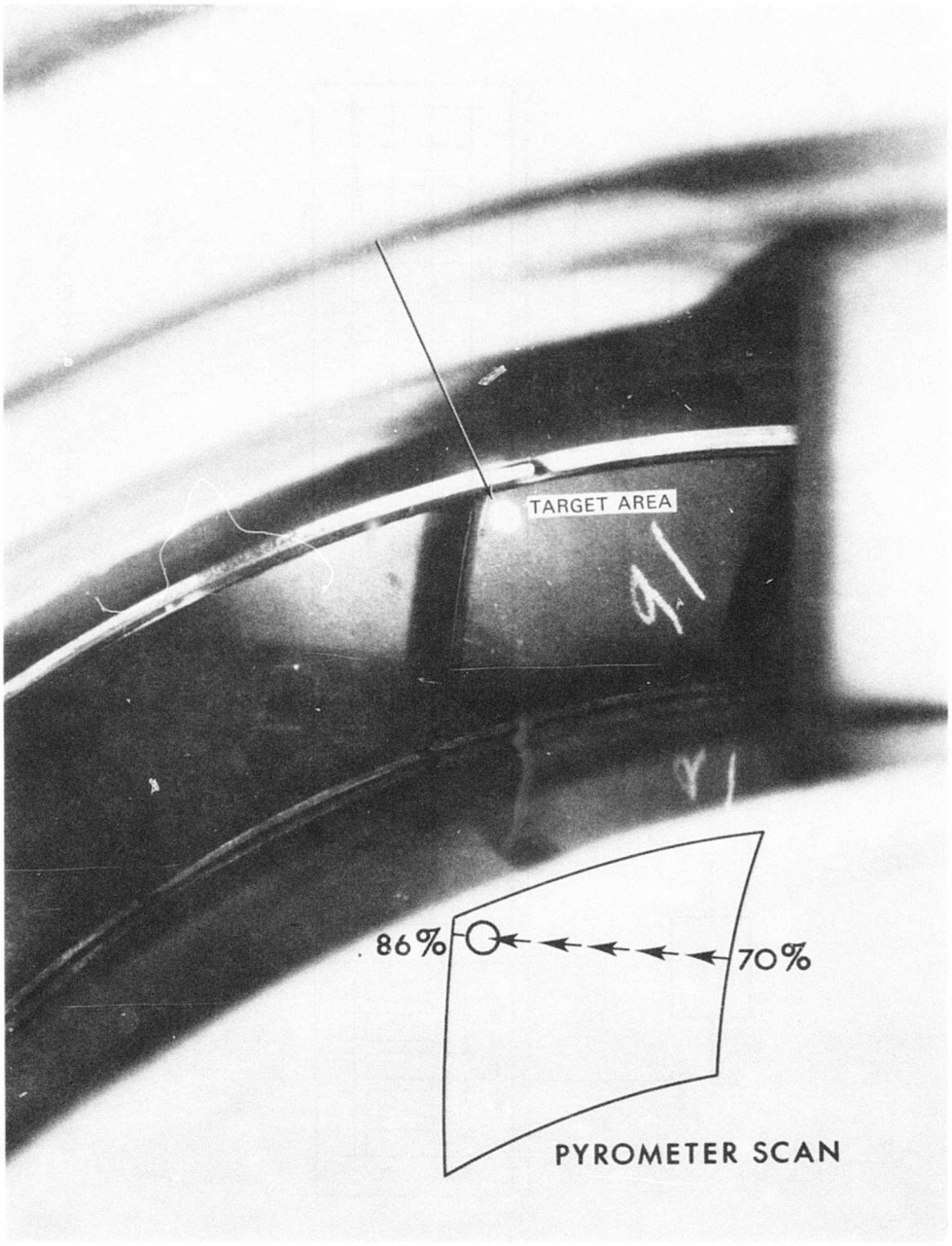

Figure 82. Pyrometer Target Area

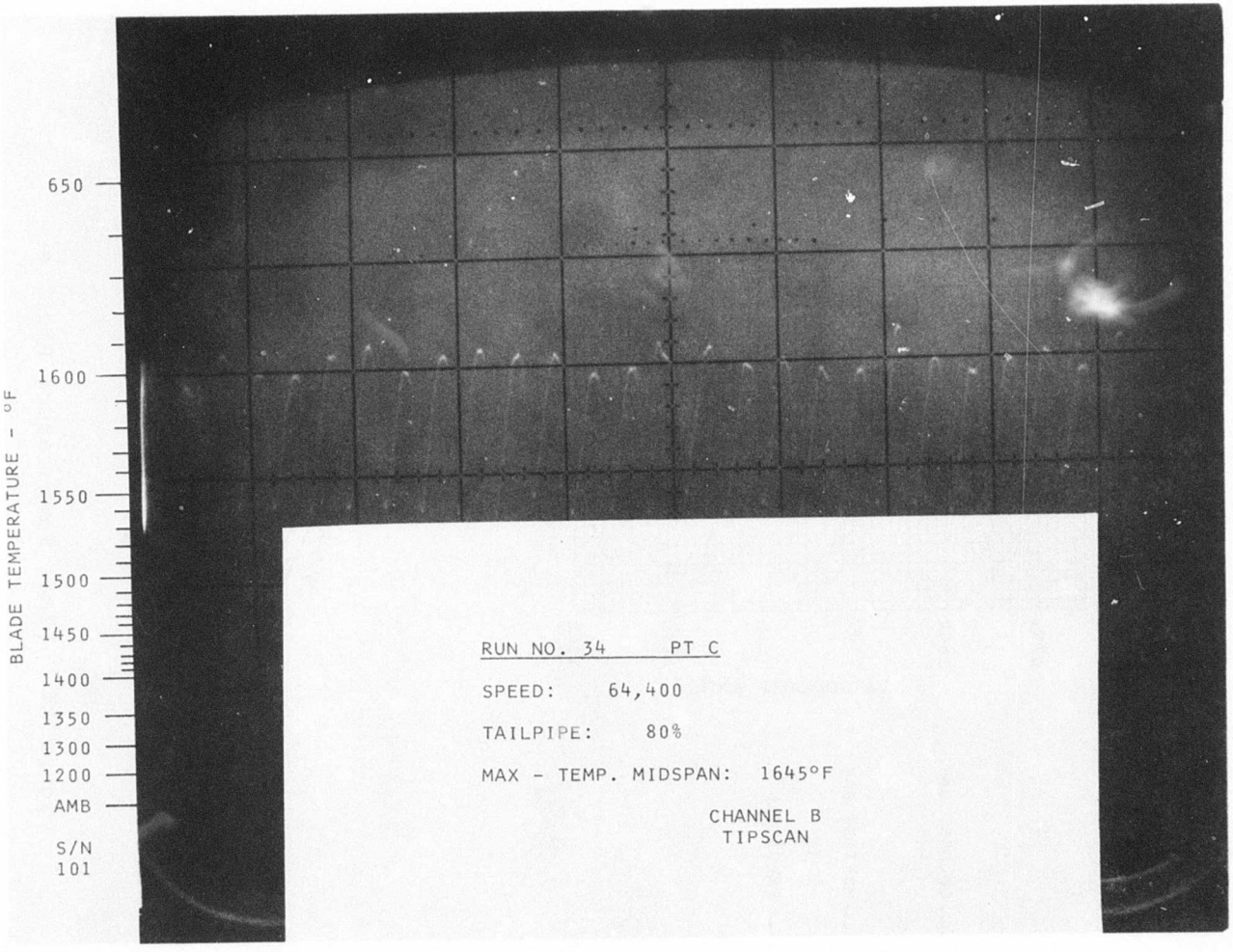

Figure 83. Blade Temperature Transient Profile - Engine Tests

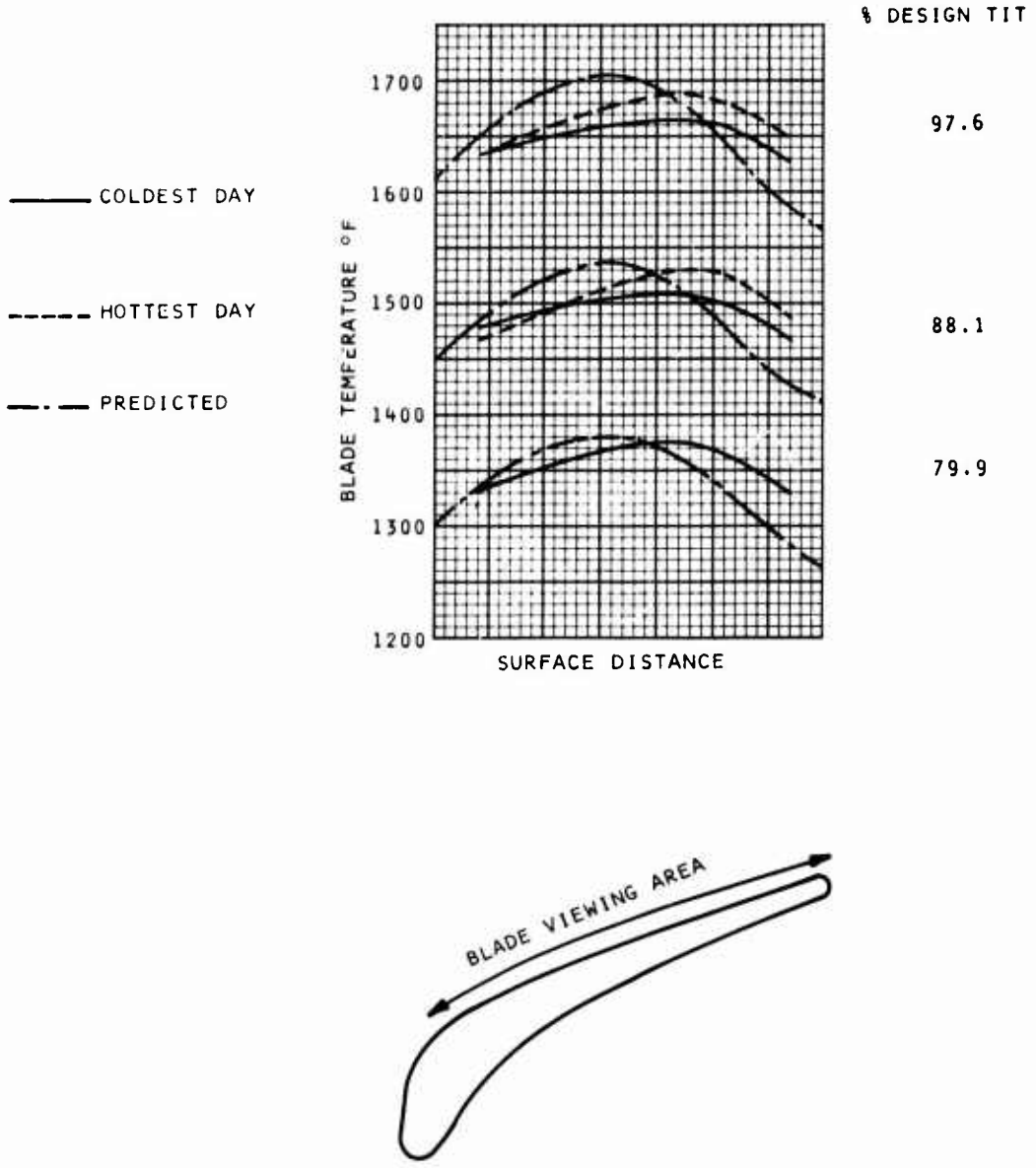

Figure 84. Blade Temperature Profiles

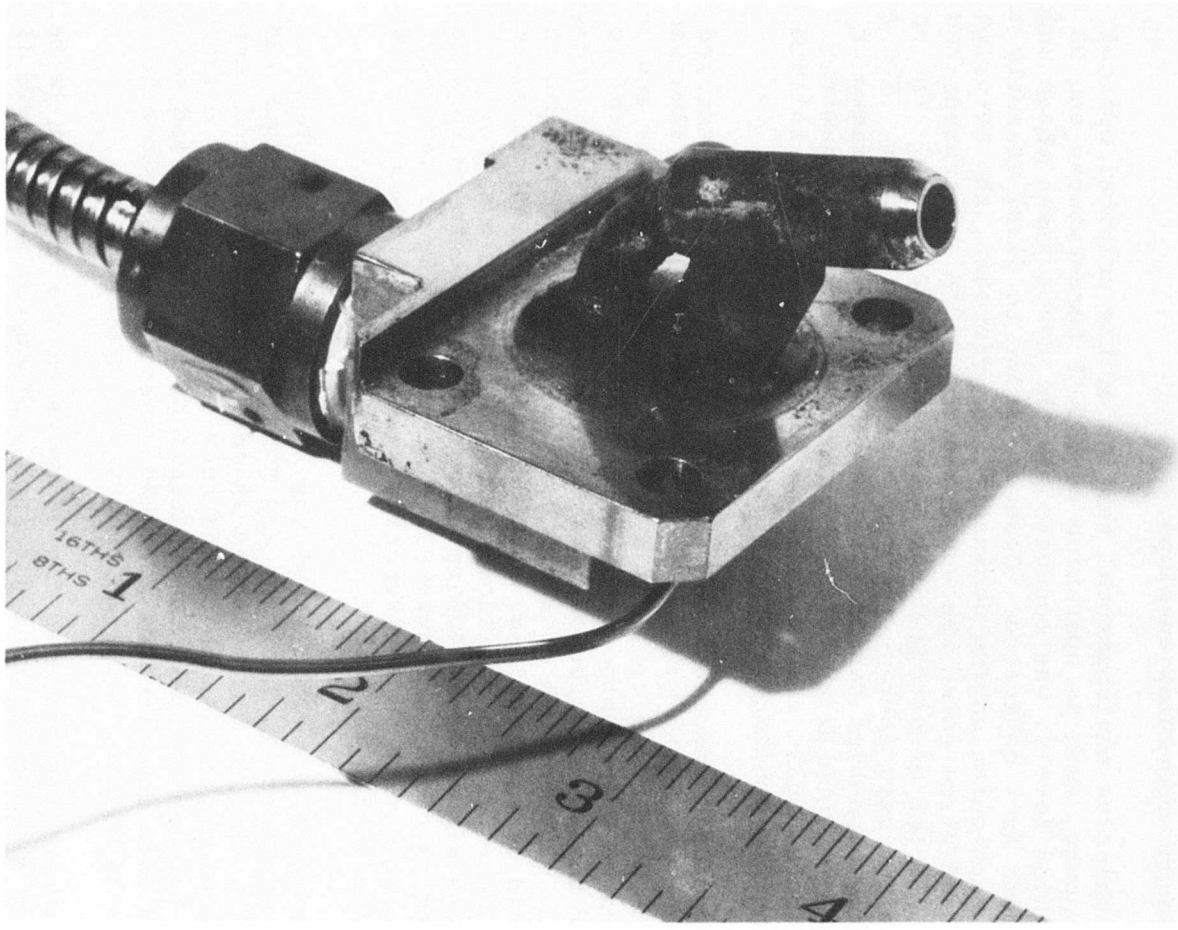

Figure 85. Pyrometer Optical Sensor After Engine Tests

to track blade temperature profiles at 65,000 rpm and to follow the fastest blade temperature transients encountered in the engine operating envelope.

Comprehensive environmental testing of the critical optical components, such as operation at 1000°F temperatures and 50 g vibration levels, was conducted in the development phase under previous Army contracts. However, prior to final assembly of this particular engine demonstration pyrometer, the metallized lens and braze joint was subjected to 1000°F and pressurized with 250 psi of nitrogen for approximately 24 hours. The unit exhibited zero leakage with no optical deterioration. The completely assembled sensor was also subjected to a maximum of 50 g's at 1000 Hz and 600°F temperatures for approximately 4-8 hours, again resulting in no visible structural failure or measurable optical deterioration.

The optical sensor was installed on the partially assembled engine, and light was passed in reverse through the flexible fiber-optic cable and lens assembly. The target size and location on the turbine blade were observed and documented to allow the calculation of blade cooling efficiency from engine data. A photograph showing the 0.1-inch-diameter target at the tip of the trailing, suction edge of the blade is given in Figure 82. An oscilloscope trace of the blade profile voltage signal at 64,400 rpm from the current to voltage converter is given in Figure 83. The profiles are relatively noise free with no adulterating spikes from products of combustion in the airstream.

The temperature profiles of the hottest and coolest blades were expanded on the scope and studied in depth. Figure 89 shows a plot of the measured vs analytically predicted temperature along the length of the turbine blade. A 15°F difference between the peak temperatures of the analysis and measured data demonstrates that the sensor operated close to, if not well within, its $\pm$ 15°F accuracy requirement.

The sensor was operated for 30 hours on the engine while being purged with an external air supply of approximately .003 lb/sec. This kept the sensor body temperature, which was monitored with a thermocouple, below 600°F at all times. Figure 85 shows photographs of the optical sensor as received at Chandler Evans upon completion of the engine test program.

Although the Inconel hood which encases the optical components was obviously handled in shipping, the photographs show the heavy deposit of coke still remaining on the sensor body. The lens, however, was free of contamination, and a room-temperature calibration after engine running shows the test points in the middle of the pre-engine test calibration band of Figure 79.

The accuracy of the lens type turbine blade radiation pyrometer in measuring the temperature gradients of high-speed blades and in maintaining this high level of performance over a period of time in an engine environment was sufficiently demonstrated by the engine test program. Due to the abrupt termination of the program, however, the closed-loop blade temperature limiting feature of the control system was not demonstrated. However, sufficient engine-mounted test results were obtained to conclude that closed-loop testing would be successful.

The ability of the optical sensor to withstand temperatures up to 850°F with the present light pipe and 1000°F with a previously developed pipe has been demonstrated. This allows purging with engine CDP which would be necessary in an airborne application. However, it is not known from this testing if CDP would require filtering to keep the lens clean.

SYSTEM BENCH TESTS

For the system bench calibration, the components were set up on the fuel stand as shown in the layout of Figure 86. The pump/alternator assembly was connected to the high-speed gearbox drive using the quill shaft designed for use in the engine installation. Thereby, a complete checkout of this drive configuration was included before engine testing. A special interface housing was designed for the quill drive. The seals of the system components were interconnected pretty much as for the engine installation except that special extended electrical cables were needed to connect to the remotely located electronics. The igniters were housed in a special explosion-proof box with a window to allow the spark to be observed. A variable-speed motor with a high-speed gearbox was used for the pump alternator drive. The engine speed signal to the

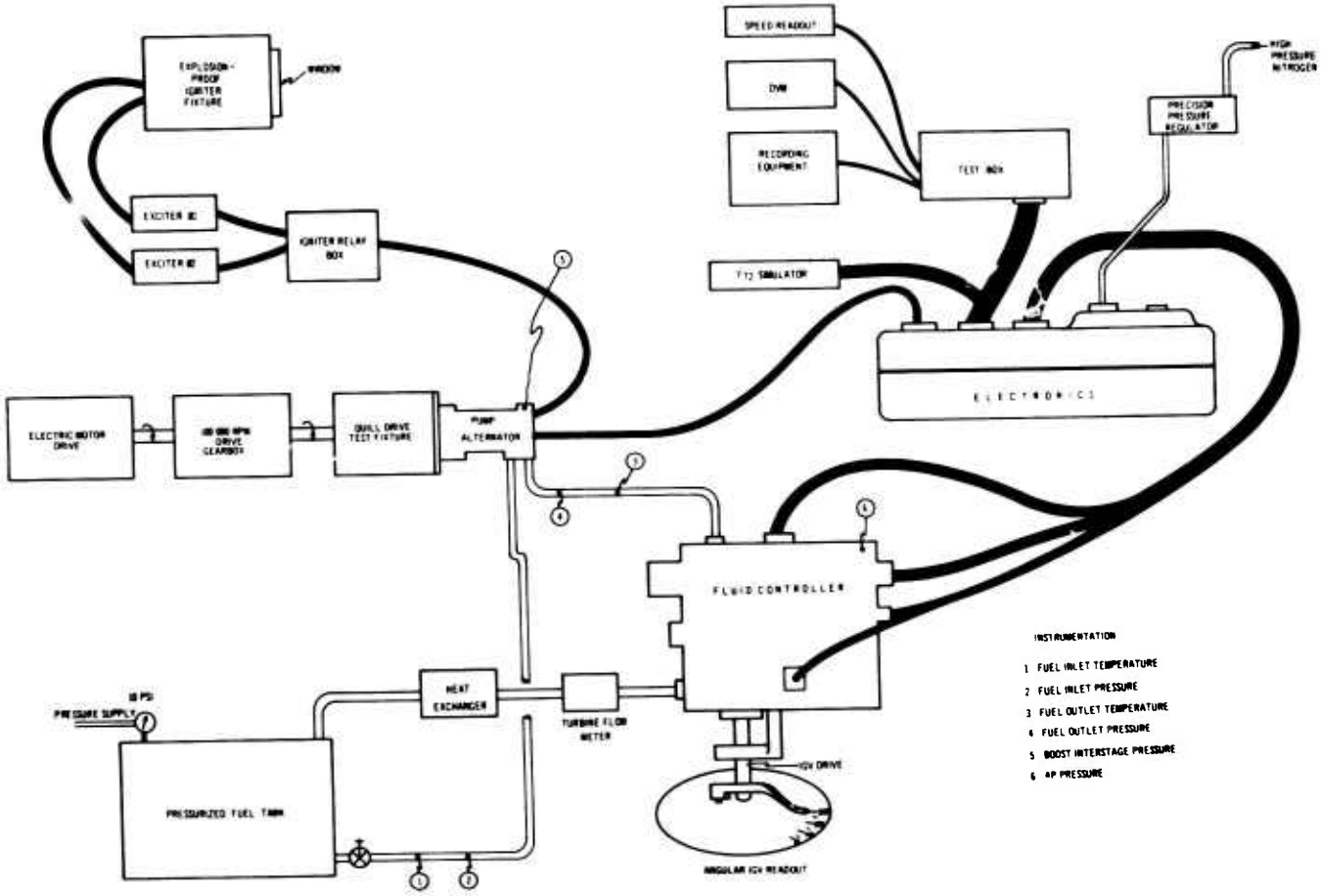

Figure 86. System Bench Test Setup

electronic computer is computer from the alternator AC input. The simulated burner pressures used in the calibration were set through a precision pressure set capable of accuracies to ±0.05 psi.

Bench calibrations were conducted prior to and following the engine test program.

Acceleration

Figure 87 shows the acceleration schedules for simulated hot, cold and standard inlet temperature. The acceleration test data shows excellent correlation with the desired schedules and all test points are within the specified ±4% accuracy requirement. It should be noted that the fuel flow errors are very small for the points that are not directly on the schedule. For example, the test point at 53,000 rpm is .04 ratio units from the desired schedule, but this represents only 2.6 pph in fuel flow at a fuel flow level of approximately 130 pph.

Figure 88 shows acceleration and governor data for military, idle and intermediate PLA speed setting. The test points at 65,000 rpm for the military speed droop is only 6 pph from the desired droop schedule, where steady-state flow is about 340 pph.

The comparable data taken after the completion of engine testing for a simulated hot, cold and standard day is shown in Figures 89, 90 and 91. The data was recorded after correcting the metering valve pressure regulator problem manifested during engine running. In comparing the calibrations taken before and after the engine testing, it was concluded that with the exception of the regulator valve, there was no noticeable deterioration in the system performance.

Deceleration

The deceleration data from the pre- and post-engine run bench calibrations are shown plotted in Figures 87 and 89 respectively. Since decelerations are not a function

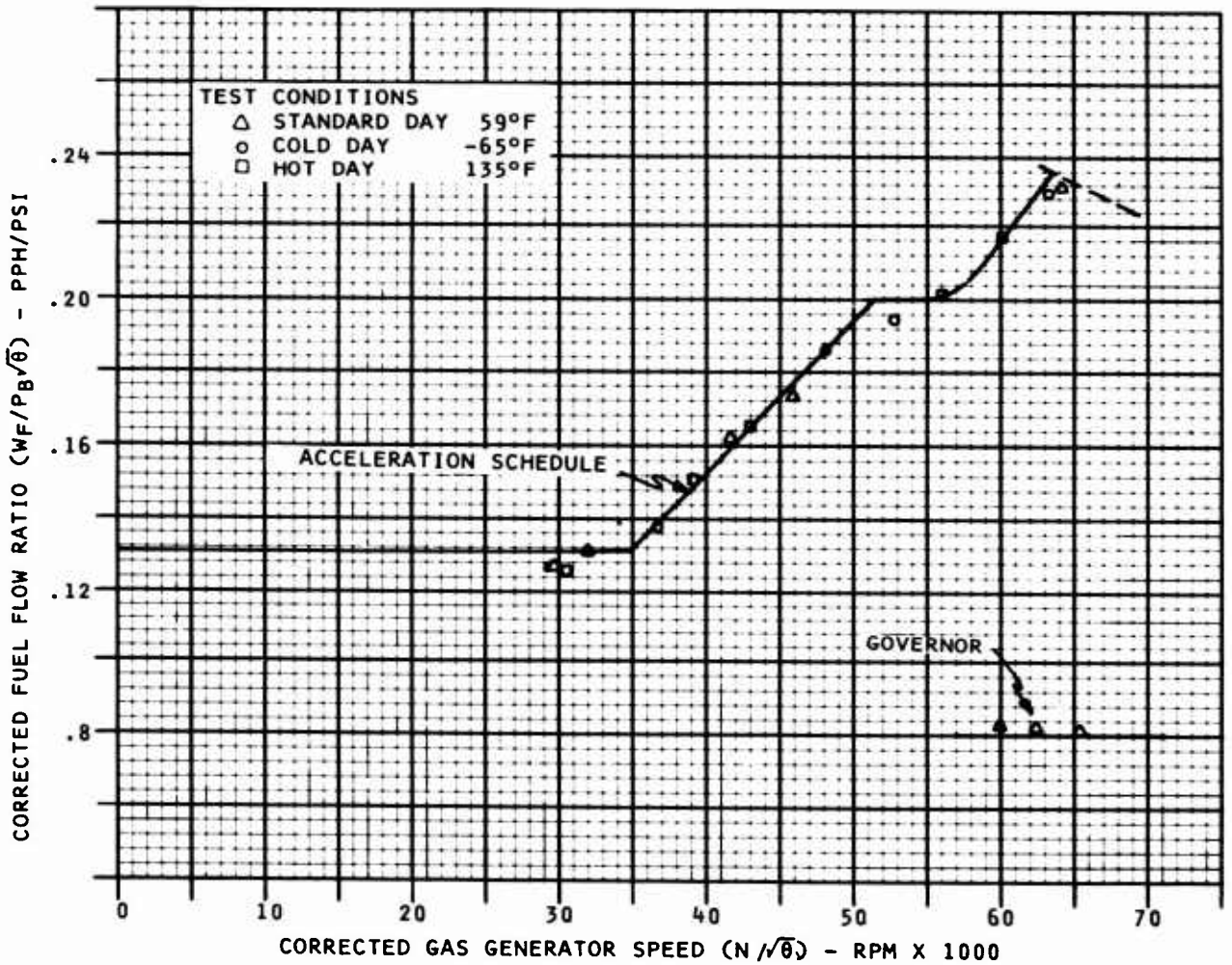

Figure 87. Acceleration Schedule - Bench Test

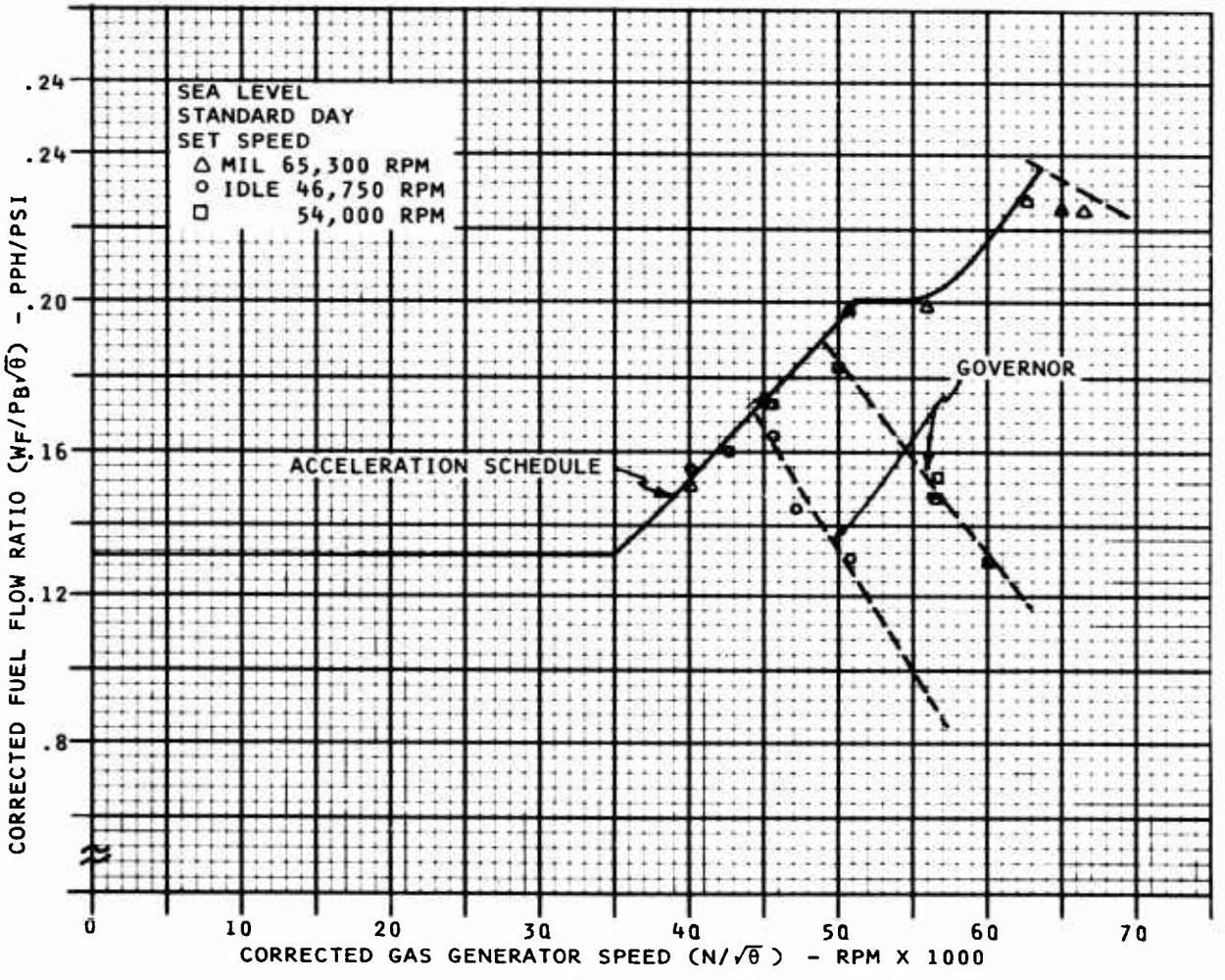

Figure 88. Acceleration and Governor Schedules - Bench Test

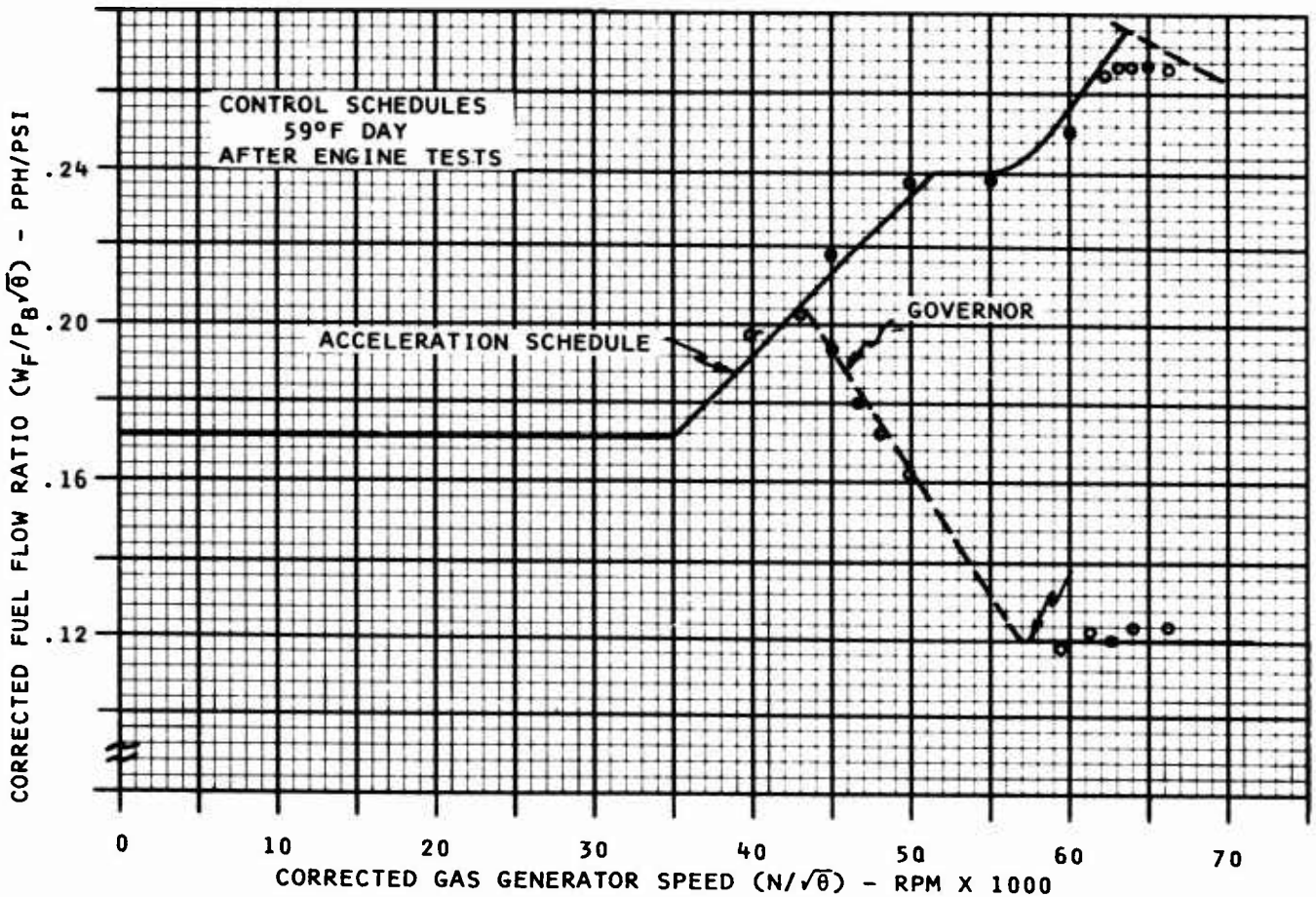

Figure 89. Control Schedules, 59°F Day - Bench Test

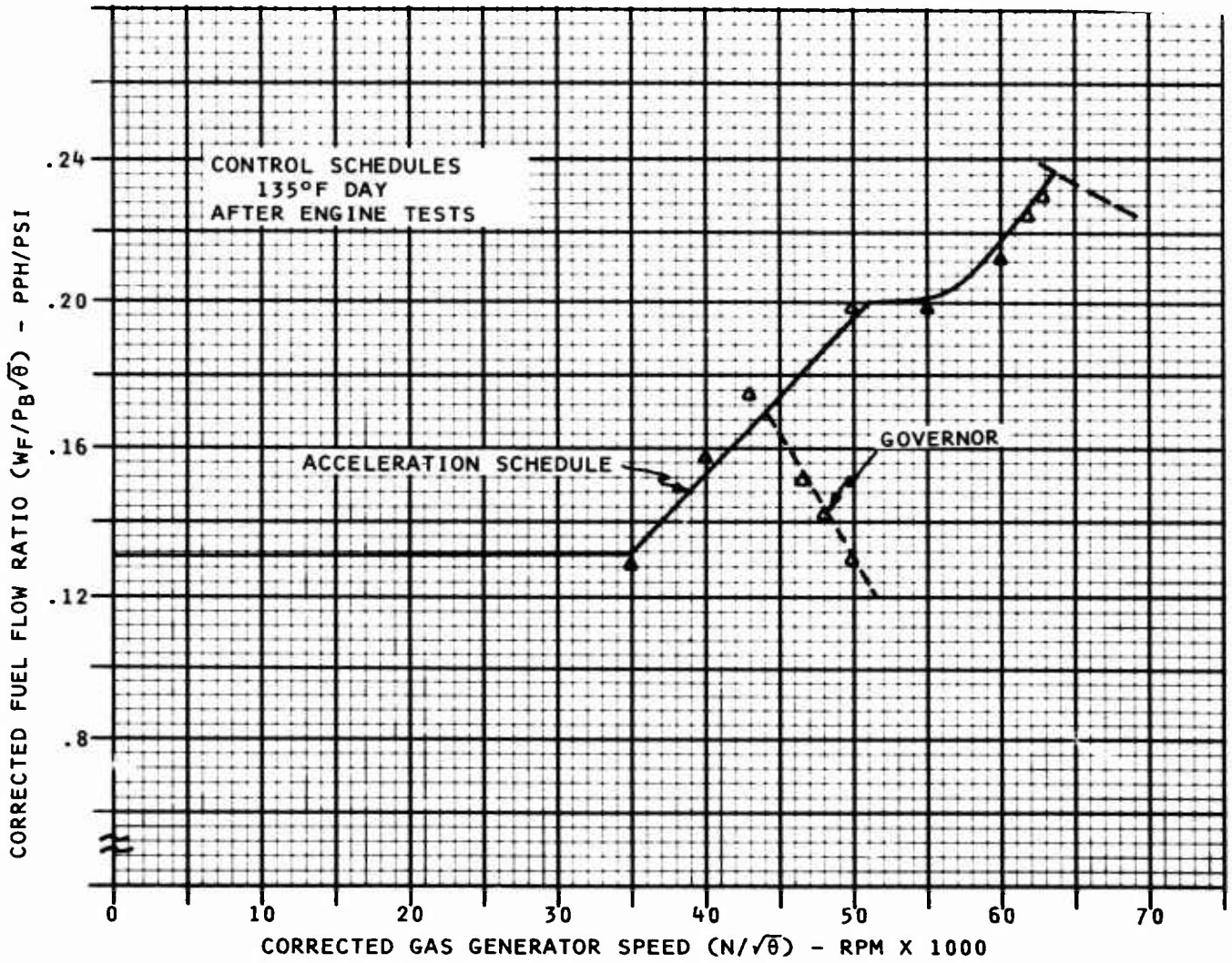

Figure 90. Control Schedules, 135°F Day - Bench Test

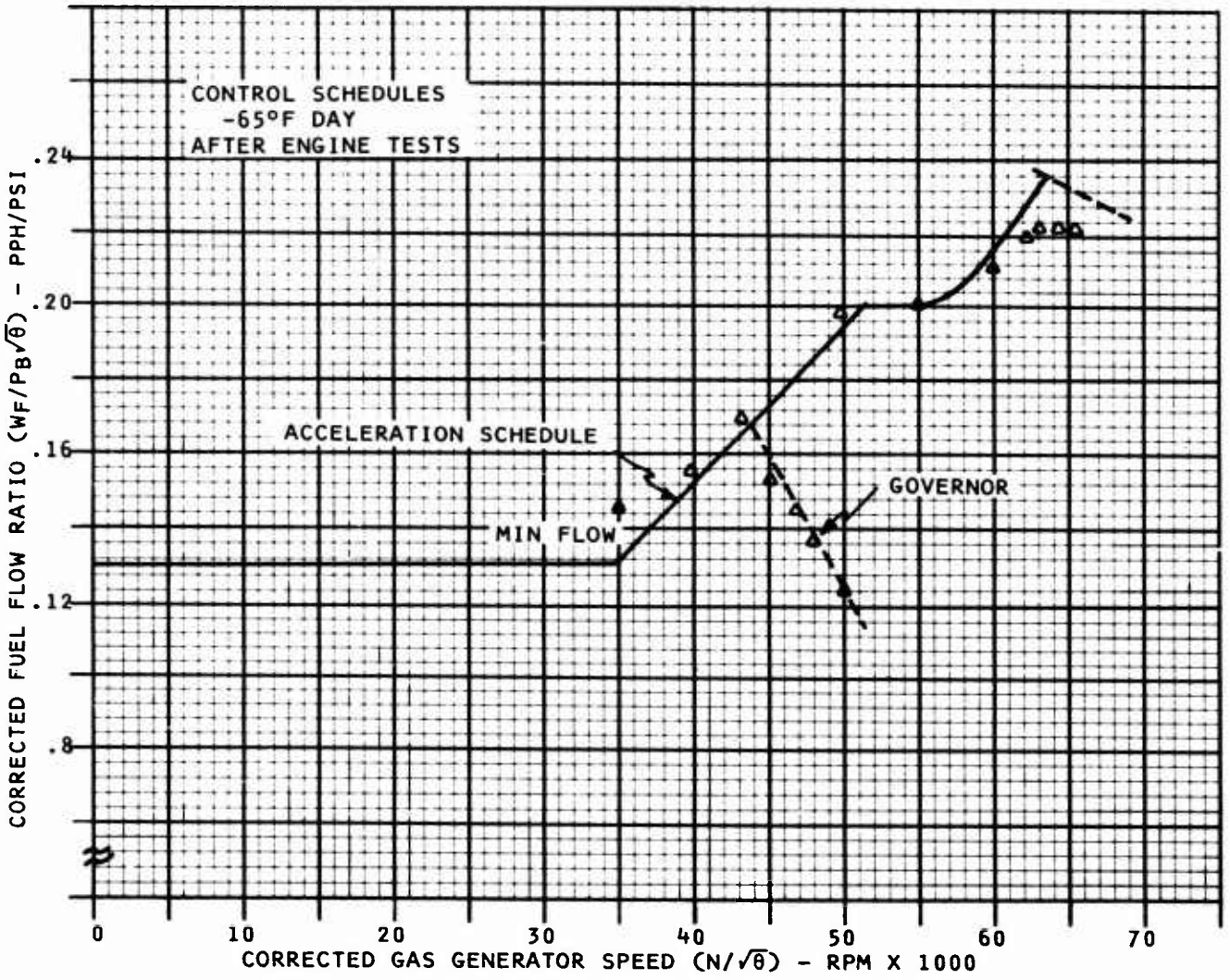

Figure 91. Control Schedule, -65°F Day - Bench Test

of inlet temperature T_{t2}, only standard-day temperatures were calibrated. The specification for scheduling decelerations is that the effor does not exceed 7.5% of point. For the constant ratio units specified for the STAGG engine, this computes to ±0.06 ratio unit. The maximum calibration error was 0.04 ratio unit at 63,500 rpm.

Governor

The calibrations included the governor droop data at idle, intermediate and maximum PLA speed settings. This data correlated with the requirements for a fanned droop schedule and is shown in Figures 88 through 91.

Temperature Limiting

Figure 92 shows the blade temperature limiting data. The original bench calibration used a steep droop slope commensurate with meeting limiting requirements of ±30°F; however, when the control was made ready for engine testing, the gain was set much lower to ensure stable operation.

The post-engine run calibration data reflects the lower gain used throughout the engine-mounted testing. Figure 92 also shows the blade temperature droop schedule at 1550°F, where it was planned to make the engine demonstration run. The nonlinearity is due to the output characteristic of the radiation pyrometer.

IGV Actuator

The calibration of the inlet guide vane actuator for hot, cold, and standard days is shown in Figures 93 and 94. Figure 93 is the data recorded prior to engine testing, and Figure 94 is the data taken after the engine test program was concluded. The specified accuracy was ± 1/2 degree, and this has been exceeded only at points where there is a sharp discontinuity in the schedule. This results from inherent interpolation errors in the electronic generation of the desired schedule.

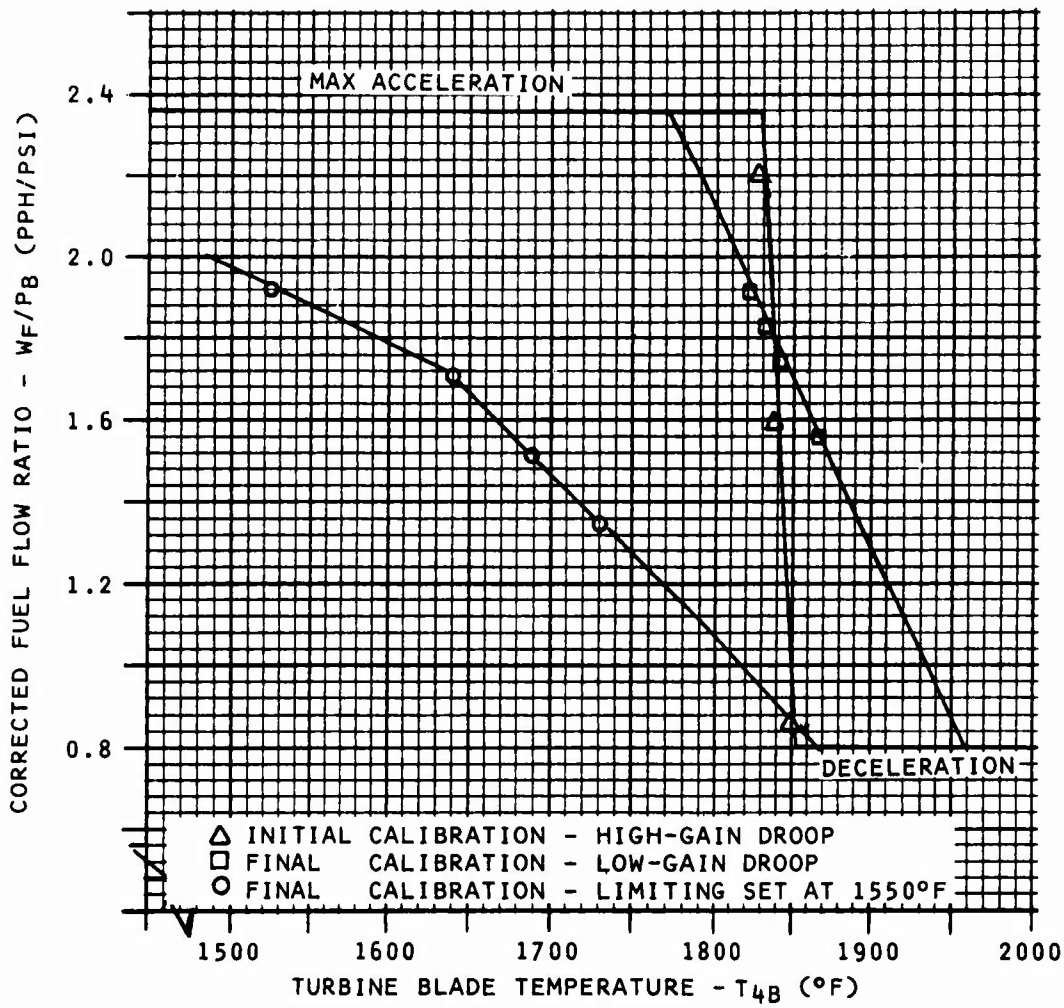

Figure 92. Temperature Limiter Test Data - Bench Test

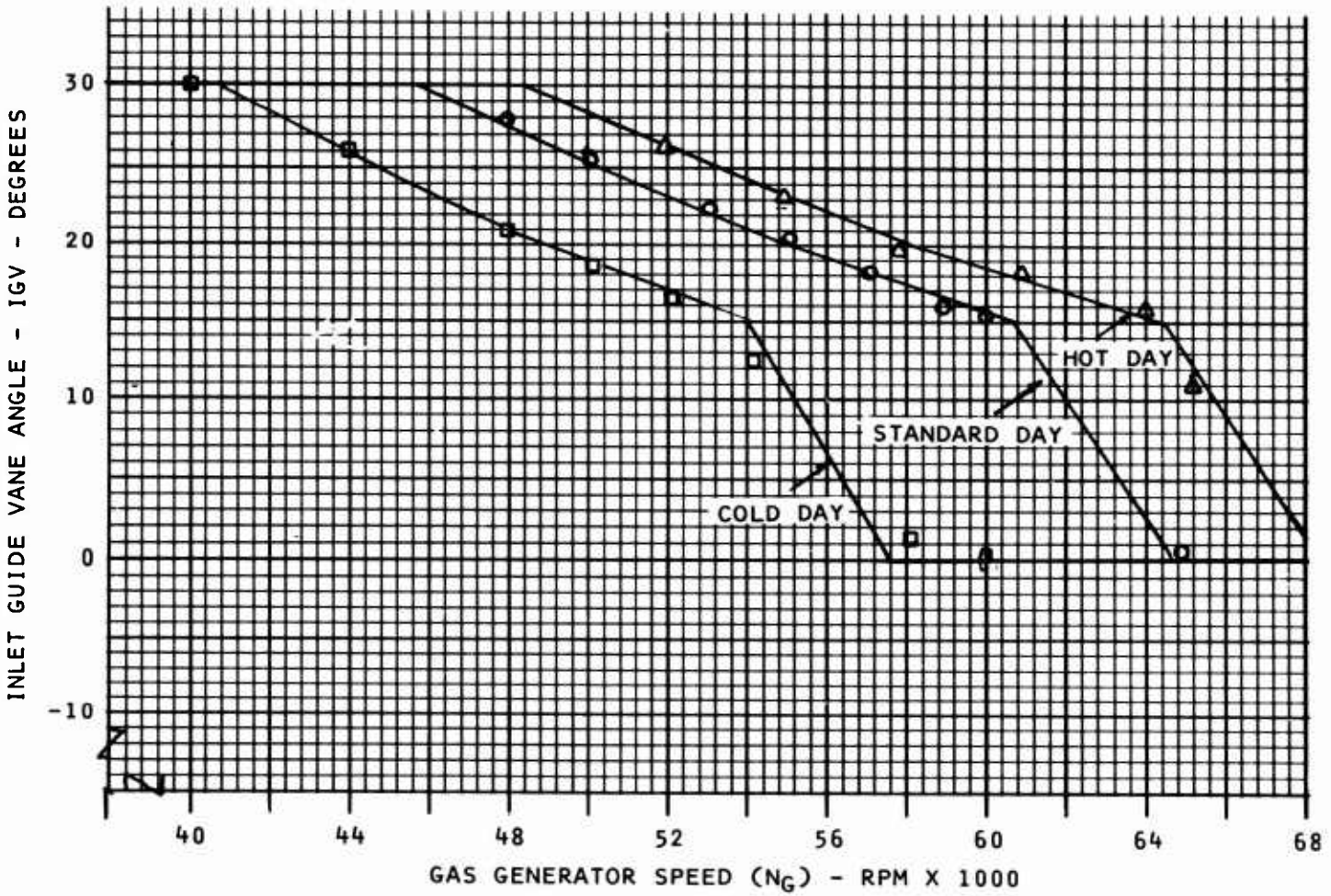

Figure 93. IGV Calibration Test - Bench Test Before Engine Test

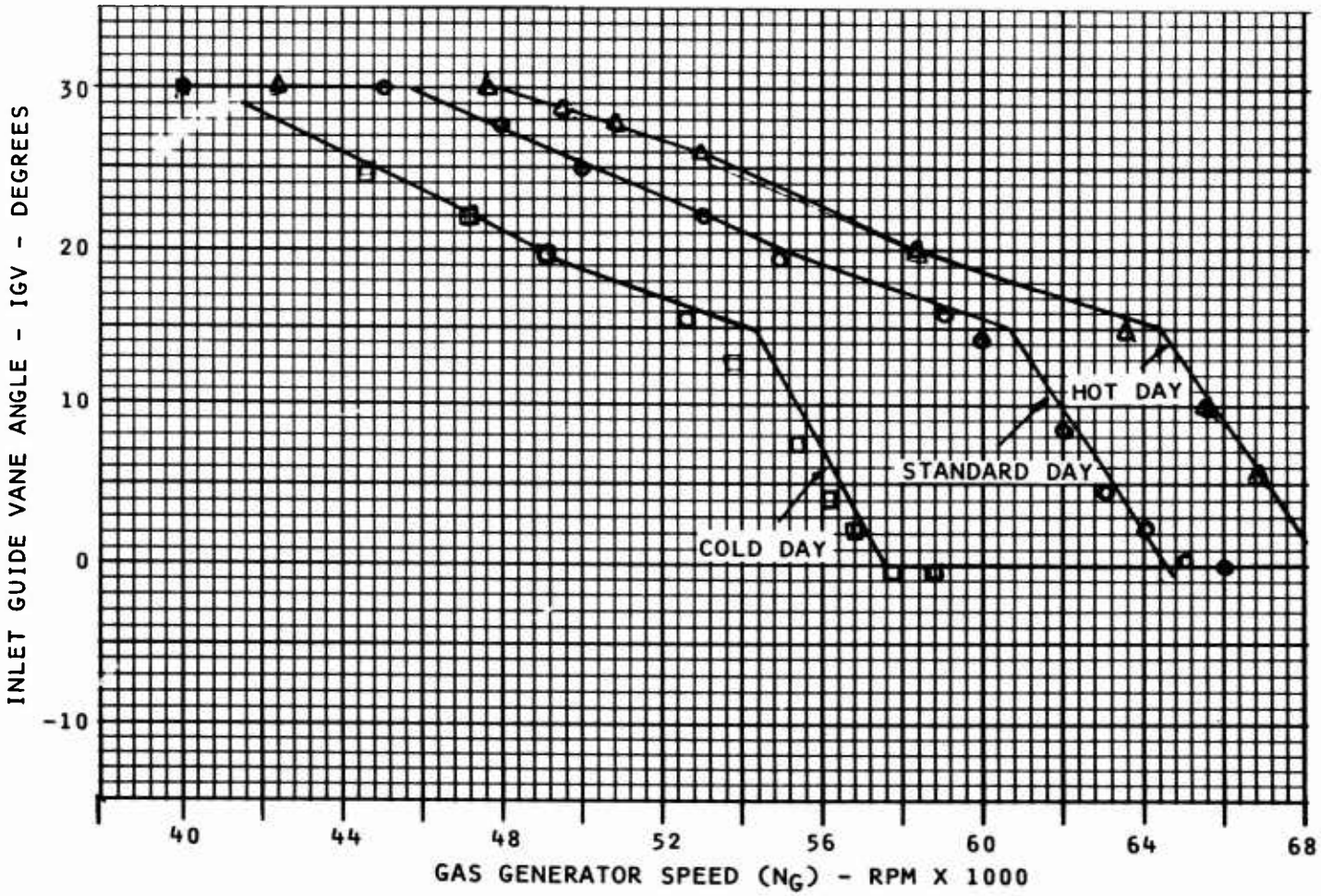

Figure 94. IGV Calibration Test - Bench Test After Engine Test

CONCLUSIONS AND RECOMMENDATIONS

This program was the continuation of work accomplished under previous Army contracts to develop advanced electronic control and fuel pumping components for future small gas turbine engines. The results of this effort have demonstrated the advantages of electronic control, including flexibility for wide application, digital programmability for rapidly changing fuel flow and IGV control schedules, low weight and size, high accuracy, and ease of including built-in self-test features. Also, high-speed (65,000 rpm) centrifugal fuel pumping technology, electro-hydromechanical fuel metering and IGV actuation, and radiation pyrometry for turbine blade temperature limiting have been successfully demonstrated.

The next logical step in the electronic computer development is to incorporate a microprocessor which will offer improved flexibility, lower cost and increased reliability based on fewer components being required and continued improvement of manufacturing techniques.

The low efficiency of the pumping system is characteristic of high-speed, high-pressure, low-flow, centrifugal pumps. Substantial improvements in efficiency have been accomplished, and continued development offers further improvement. Additionally, it is recommended that continued development and endurance testing be conducted on high-speed face seals and journal bearings for extending life.

The radiation pyrometry for blade temperature limiting requires long-term engine-mounted operating experience to solve unknown endurance problems, particularly regarding keeping the optical system clean using compressor discharge pressure for purging.

From the viewpoint of the overall control system, development has sufficiently progressed so that the final implementation of a full-authority electronic control system can now be initiated. This effort should consider requirements for redundancy and backup protection and the level of self-test features for cost effectiveness, for a comprehensive control system specification for an actual free turbine engine control application.

LITERATURE CITED

1. White, A. H., Wills, D. F., ADVANCED ENGINE CONTROL PROGRAM, Chandler Evans Inc., USAAMRDL Technical Report 72-59, Eustis Directorate, U.S. Army Air Mobility Research and Development Laboratory, Ft. Eustis, Virginia, November 1972, AD 758173.

2. Hearn, R. J., Cole, M. A., White, A. H., ADVANCED ENGINE CONTROL PROGRAM, Colt Industries Inc., USAAMRDL Technical Report 73-81, Eustis Directorate, U.S. Army Air Mobility Research and Development Laboratory, Ft. Eustis, Virginia, November 1973, AD 773660.

3. ENGINES, AIRCRAFT, TURBOSHAFT, GENERAL SPECIFICATION FOR Report AV-E-8593A, U.S. Army Aviation Systems Command, St. Louis, Missouri 63166, June 1972.

4. Miller, B. C., INTEGRATED ACCESSORY SYSTEMS FOR SMALL GAS TURBINE ENGINES, Pratt and Whitney Aircraft, United Technologies Corporation, Florida Research and Development Center, Report No. FR-6983, June 1975.

5. White, A. H., INTEGRATED ACCESSORY SYSTEMS FOR SMALL GAS TURBINE ENGINES, Chandler Evans Corporation, Report No. R-689-29, June 1975. West Hartford, Connecticut.

6. Tobey, G. E., Graeme, J. G., Hulsman, L. P., OPERATIONAL AMPLIFIERS, McGraw Hill, 1971. New York, New York.

7. NORTON HANDBOOK OF TRANSDUCERS FOR ELECTRONIC MEASUREMENT SYSTEMS, Prentice-Hall, 1969. Englewood Cliffs, New Jersey.

8. Burnell, D. G., Morrison, T. B., White, A. H., TURBINE ENGINE FUEL CONTROL RELIABILITY AND MAINTAINABILITY ANALYSIS, Chandler Evans Co., USAAMRDL Technical Report 73-60, Eustis Directorate, U. S. Army Air Mobility Research and Development Laboratory, Ft. Eustis, Virginia, August 1973.

LIST OF SYMBOLS AND ABBREVIATIONS

A/D	analog to digital converter
CMOS	complementary metal oxide semiconductor
d.a.	double amplitude
D/A	digital to analog converter
EMI	electromagnetic interference
FET	field effect transistor
FRDC	Florida Research and Development Center
g	gravitational acceleration, 32.2 ft/sec^2
I.C.	integrated circuit
I.G.V.	inlet guide vane
KΩ	kilo-ohm
LVDT	linear variable differential transformer
MMV	main metering valve
N	speed, rpm
N*	reference speed
N_g	gas generator speed, rpm
N_s	specific speed
P_b	burner pressure
PCB	printed circuit board
PLA	power level angle, deg

LIST OF SYMBOLS AND ABBREVIATIONS (Cont)

pph	pounds per hour
pps	pounds per second
PV	psi x ft/minimum
PROM	programmable read-only memory
RFI	radio frequency interference
STAGG	small turbine advanced gas generator
T_{t2}	compressor inlet total temperature, °F
T_{4b}	turbine blade temperature, °F
T_{4b}^*	turbine blade reference temperature, °F
UBL	unit bearing load, psi
V	voltage
V/L	vapor to liquid ratio
VCO	voltage - controlled oscillator
W	watts
α	proportional
ΔT	increment of temperature, °F
ΔP	increment of pressure psid
μ	micro (10^{-6})
τ	time constant
θ	corrected compressor inlet total temperature